3-2020

Development of a Small Scale Rotating Detonation Engine

Joseph R. Dechert

DEVELOPMENT OF A SMALL SCALE ROTATING DETONATION ENGINE

THESIS

Joseph R. Dechert, Captain, USAF

AFIT-ENY-MS-20-M-257

DEPARTMENT OF THE AIR FORCE
AIR UNIVERSITY

AIR FORCE INSTITUTE OF TECHNOLOGY

Wright-Patterson Air Force Base, Ohio

AFIT-ENY-MS-20-M-257

DEVELOPMENT OF A SMALL SCALE ROTATING DETONATION ENGINE

THESIS

Presented to the Faculty

Department of Aeronautics and Astronautics

Graduate School of Engineering and Management

Air Force Institute of Technology

Air University

Air Education and Training Command

in Partial Fulfillment of the Requirements for the

Degree of Master of Science in Aeronautical Engineering

Joseph R. Dechert, B.E.

Captain, USAF

March 2020

AFIT-ENY-MS-20-M-257

DEVELOPMENT OF A SMALL SCALE ROTATING DETONATION ENGINE

Joseph R. Dechert, B.E.
Captain, USAF

Committee Membership:

Fred R. Schauer, Ph.D.
Chairman

Marc D. Polanka, Ph.D.
Member

S. Alex Schumaker, Ph.D.
Member

SIGNATURE PAGE HERE

Abstract

The Rotating Detonation Engine (RDE) has been researched extensively in recent years, but the minimum size limits of an RDE have not been well investigated. The goal of this research was to build an RDE small enough to produce a detonation frequency above 20 kHz with a single detonation wave while also reducing the engine's total mass flow rate. The engine's small physical size and reduced mass flow rates would offer a more benign alternative for RDE research when compared to a typical, 150 mm diameter RDE in terms of safety, acoustic output, and vibration. If an RDE could be built with these operating characteristics, it would enable the use of sensitive diagnostic equipment in a more common lab setting for future RDE research.

This research objective resulted in the design of an RDE with an outer diameter sized at 28 mm using ethylene and nitrous oxide as a fuel and oxidizer. The engine was tested over a range of equivalence ratios between 0.5-1.5 and mass flow rates 0.025-0.075 to characterize its operation. Key design parameters were the injection hole diameter, detonation channel gap, detonation channel length, detonation channel diameter, and the ratio between the detonation channel area and the exit area. These parameters effected the rate at which the reactants could be refreshed in the detonation channel as well as the detonation's stability. High speed imaging in conjunction with a microphone were used to monitor engine operation and evaluate detonation wave behavior.

Current research has revealed that detonation is achievable in an RDE of this diameter. However, the detonation wave exhibited unstable behavior during all test cases that achieved detonation. The minimum mass flow rates were recorded over the range of equivalence ratios tested to build an operating map for the engine,

where the lowest flow rate achieved was 0.025 kg/s at an equivalence ratio of 1.2. Increased detonation channel pressure increased the probability that a detonation would occur, which also corresponded with minimizing the mass flow rate required to achieve a detonation. The detonation wave speed was approximately 30-40% lower than expected, which resulted in an operating frequency than ranged between 11.7-14 kHz.

Acknowledgements

I would like to thank the entire D-Bay team for their assistance and patience throughout my research efforts. I would especially like to thank Brian Sell and Curtis Rice for their countless hours spent helping me with design, testing, rigging equipment, and troubleshooting. Matt Petersen also provided great support in developing the control and data acquisitions system for this research. I also greatly appreciated the guidance from John Hoke, Matt Fotia, and Chris Stevens during this effort. Finally, I would like to thank my committee members, Dr. Fred Schauer, Dr. Marc Polanka, and Dr. Alex Schumaker. Under their mentorship, I was provided with a first-rate educational and professional development experience as well as engineering expertise that will be invaluable to me through the rest of my career.

Joseph R. Dechert

Table of Contents

Page

List of Figures

List of Tables

List of Abbreviations

Abbreviation		Page
RDE	Rotating Detonation Engine	2
AFRL	Air Force Research Laboratory	4
DERF	Detonation Engine Research Facility	4
CJ	Chapman-Jouguet	8
FJ	Fickett-Jacobs	11
DDT	Deflagration to Detonation	15
NASA	National Aeronautic and Space Administration	24
CEA	Chemical Equilibrium with Applications	24
JIC	Jets in Crossflow	27
SIJ	Semi-Impinging Jets	27
CTAP	Capillary Tube Averaged Pressure	30
ITP	Infinite Tube Pressure	30
FFT	Fast Fourier Transform	37
DAQ	Data Acquisition System	66
SPL	Sound Pressure Level	111

List of Symbols

Symbol		Page
ϵ	Area Ratio	77
A_t	Throat Area	77
A_c	Channel Area	77
$P_{c,min}$	Minimum Channel Pressure	92

DEVELOPMENT OF A SMALL SCALE ROTATING DETONATION ENGINE

I. Introduction

In recent decades, research in detonation combustion has continued to gain interest due to the potential efficiency gains in propulsive systems. Additionally, combustors associated with detonation engines are typically smaller than their jet engine counterparts which enable the use of smaller turbomachinery. However, harnessing this potential has been challenged with overcoming the extreme conditions associated with a detonation. A detonation wave can produce temperatures in excess of 2000 K and a 15-30 fold increase in pressure [1]. Additionally, a detonation wave can produce acoustics that could be harmful to nearby observers. These conditions impose difficulties for both detonation engine design and testing.

A detonation is characterized by a flame front travelling at or above sonic velocities, whereas the more commonly known deflagration flame travels at speeds orders of magnitudes less than this. In a detonation, the combustion zone is preceded by a shock wave that significantly increases the pressure and temperature of the reactants, which provide favorable conditions for combustion. The following combustion wave provides the energy to push the shock wave forward. The coupled shock wave and combustion wave enables the propagation of the detonation [2].

The sharp rise in pressure and temperature prior to combustion are the key reasons why a detonation has the potential to extract more work than a deflagration. When comparing a Brayton cycle to a Humphrey cycle, the potential advantages of detonation become more visible. As shown in Figure 1, the Brayton cycle, which is common in current jet engines, utilizes deflagration under constant pressure (points

0, 1, 4, 5, 0). Alternatively, the Humphrey cycle models a detonation cycle, where detonation/combustion occurs at constant volume (points 0, 1, 2, 3, 0). Additionally, the Brayton cycle relies on turbomachinery for the compression process, whereas the Humphrey cycle compresses the fluid simply through the preceding shock wave. The overarching result is that the Humphrey cycle is able to extract more work as depicted by the larger area under the P-v and T-s curves [3].

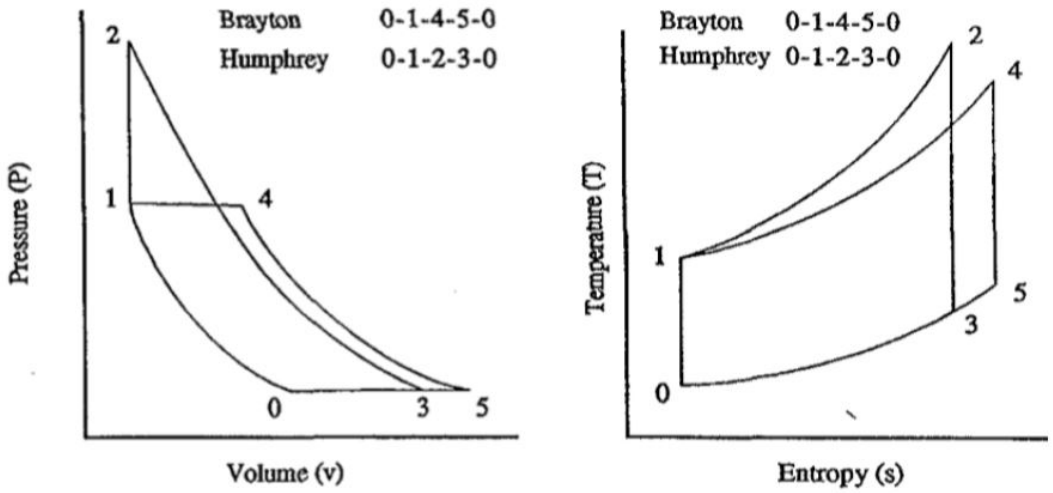

Figure 1. Comparison of Brayton and Humphrey cycles [3]

At the forefront of detonation research has been the Rotating Detonation Engine (RDE). An RDE provides a relatively simple means to translate the work available from a detonation cycle into a propulsive system. In addition the efficiency benefits, RDE's are mechanically simple devices with no moving parts, as shown in Figure 2. Fuel and oxidizer supplies enter into individual plenums and are then distributed into their respective injection holes. The fuel and oxidizer is then injected and mixed in a detonation channel as reactants. A detonation wave travels around the circumference of the channel consuming the reactants. This wave can travel on the order of 2000-2500 m/s. The reactants must be supplied into the detonation channel at a rate fast enough so that they are refreshed prior to each passing wave. As the reactants

are consumed the product gases travel down the remaining channel length and are exhausted from the engine.

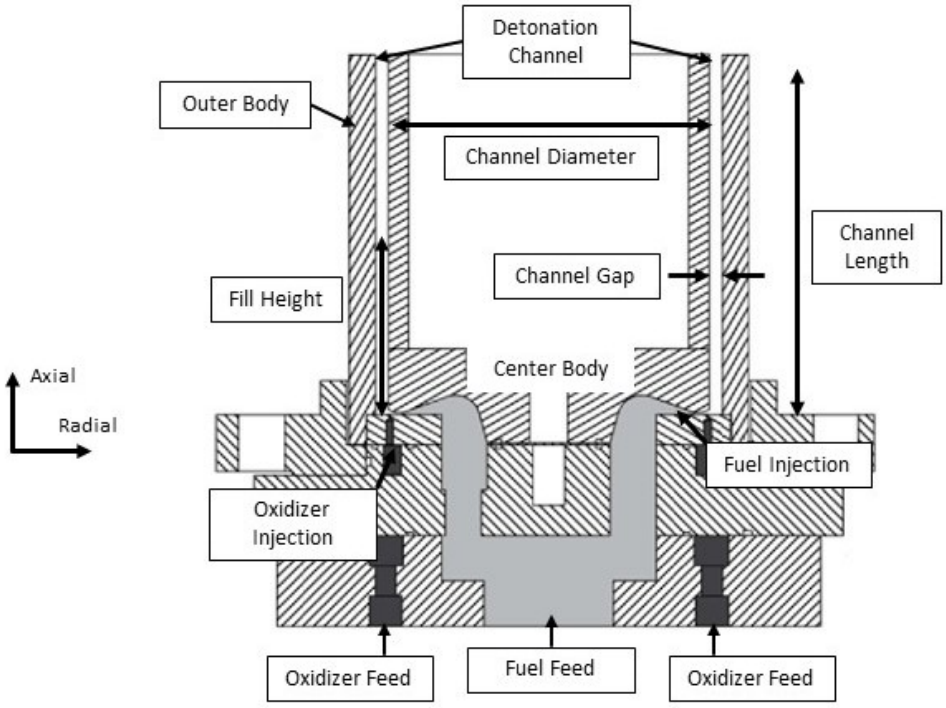

Figure 2. Key dimensions and components of an RDE [modified from [4]]

RDE operating mechanisms may be straightforward, however flow conditions, chemical processes, and specific geometric parameters actually make successful RDE operation quite complex. Bykovskii et al. extensively researched RDE geometries and found that there were limits to detonation channel length, channel gap, and reactant fill height that needed to be considered in order to achieve stable detonation [5]. Achieving the required fill height is also a significant challenge since fresh reactants must be supplied in the detonation channel in less than 200 μs for a typical 150 mm diameter RDE. The actual amount of time available can be even shorter since the high pressure associated with a passing detonation wave can temporarily block the flow of fuel and oxidizer into the detonation channel [6]. The reactants must

also be properly mixed in this time frame. Experiments by Duval et al. found that the injection scheme can have a significant effect on reactant mixing and detonation stability [7]. Making RDE design even more onerous is the fact that each of these factors are interdependent on each other.

RDE testing can involve numerous hazards to include explosive gases and high levels of noise. RDE research facilities, such as the Air Force Research Laboratory's (AFRL) Detonation Engine Research Facility (DERF) must be able to safely house large quantities of highly reactive fuels and/or oxidizers. Additionally, due to high engine temperatures and pressures experienced during testing, facilities need reinforced walls or strong physical barriers in the event of a catastrophic engine failure. Finally, RDE's produce extreme acoustic levels that can easily damage the hearing of a nearby observer, which require test facilities to be in remote locations and/or have acoustic dampening mechanisms. These facility requirements could inhibit the number of institutions that can perform RDE testing as well as locations where it can occur.

The RDE discussed in this research was designed to reduce the hazards associated with typical/150 mm diameter RDE experimentation rigs and to also develop an understanding of RDE operating characteristics in small diameter channels. The engine was designed to be physically small in size and also scaled to minimize reactant mass flow rate requirements. These design goals would lessen the amount of hazardous materials needed to conduct testing as well as alleviate some of the facility requirements in terms of protection in the event of catastrophic engine failure due to its small physical size. A reduction in engine size, particularly the engine's detonation channel diameter, would also increase the engine's operating frequency and decrease vibration. In addition to reducing physical hazards, these operating characteristics could enhance the use of sensitive lab equipment, such as laser diagnostics, in RDE

research . The engine's small size and reduced need for fuel and oxidizer would also make it more portable and could be moved to various lab environments that may have been previously inaccessible to typical RDE's.

These considerations led to the research objective of designing an RDE that was approximately 25-30 mm in diameter, with a channel gap of 2 mm, that could operate at a mass flow rate of approximately 0.05 kg/s. The engine was also designed to produce a detonation frequency at or above 20 kHz on a single detonation wave. Following the engine design process, the engine would be tested at mass flow rates between 0.025-0.075 kg/s and at equivalence ratios between 0.5-1.5 to evaluate if a detonation was even possible with these engine geometries and operating regimes. If detonation was achieved, an operating map for the engine would be developed over the span of test points. The test data would then be analyzed to determine what factors affected the detonability of the engine to include detonation channel pressure, injection pressures, and momentum flux ratios. Finally, high-speed imagery of the detonation wave would be analyzed for detonation wave behavior and conditions that influenced wave stability.

A small scale RDE would have uniquely difficult requirements over a typical, 150 mm diameter RDE. The primary challenge of a small scale RDE was achieving proper refresh rates with good reactant mixing. At an operating frequency of 20 kHz, the reactants would need to be refreshed and mixed in the detonation channel in as little as 50 μs; four times shorter than a common RDE. Additionally, the small detonation channel radius of this engine could cause detonation stability issues as researched by Kudo et al. [8]. The small channel volume in comparison to the large channel surface area would also allow for high heat loss. These heat losses could reduce the detonation wave's strength and stability [9]

Detonation was achieved in the engine designed for this research. Detonation was

observed at equivalence ratios between 0.8-1.5 and at mass flow rates as low as 0.025 kg/s. Chamber pressure had a significant effect on the conditions that allowed the engine to produce a detonation, and modifications to the engine's centerbody were required to raise the chamber's static pressure. The analysis of the detonation wave revealed that wave speeds were 30-40% lower than expected, which resulted in an operating frequency between 12-14 kHz. Although the engine produced a detonation at numerous test points, the detonation wave exhibited unstable behavior. Research opportunities still remain, but progress thus far has proven that detonation is possible in an engine of this scale.

II. Background

The Rotating Detonation Engine (RDE) has been researched extensively in recent years, but the minimum size limits of an RDE have not been well investigated. The goal of this research was to build an RDE that produced a detonation frequency above 20 kHz with a single detonation wave while also reducing the engine's mass flow rate. To design an engine that operated under these conditions would require an engine size was physically smaller than common RDE's that typically range in size from 100-200 mm in diameter. To effectively design a small scale RDE, an understanding of detonation dynamics and key geometries needed to be considered. Additionally, a look at previous engine design research and methods used to instrument RDE's also needed to be investigated. Section 2.1, introduces detonation background and general concepts. Second 2.4 examines detonation cell size, which was a critical critical design parameter for correctly sizing many aspects of an RDE. Section 2.6 investigated various injection schemes for RDE operation. Section 2.5 analyzes the previous research for build-up and design requirements, and lastly Section 2.7 introduces measurement techniques used to characterize the RDE's operating envelope.

2.1 Detonation Concepts

Combustion can be broken-up into two categories: deflagration and detonation. Deflagration is the most commonly known type of combustion and is what is currently used in most jet engine and rocket applications. Deflagrative combustion can also be characterized by two different types of flames: laminar and turbulent. Laminar flames have the lowest flames speed and are normally less that 1.0 m/s. Turbulent flame speeds are faster than laminar flames and commonly range between 1-30 m/s [2]. Although turbulent flame speeds are relatively high, they are still subsonic flame

fronts and are orders of magnitude slower than a detonation wave front. A detonation wave travels at or above sonic velocities which can typically range between 2000-3000 m/s [10].

The scientific measurement of detonation waves was first performed by Frederick Abel in 1869 using explosive charges of gun cotton. However, it was not until Donald Chapman and Ehrile Jouguet's research in the late 1800's and early 1900's that detonation characteristics could be quantitatively predicted. Their research was based on previous work by Raleigh, Rankine, and Hugoniot. Specifically, Chapman and Jouguet noted relationships between Rayleigh lines and Rankine-Hugoniot curves [10]. Rayleigh lines, as shown in Figure 3, represent possible solutions to the continuity and momentum equations between two states for a given mass flow rate, $\dot{m}$. These lines are defined by Eq. 1, where P_1 and v_1 are pressure and specific volume upstream of the detonation wave and P_2 and v_2 are conditions downstream of the detonation wave. The slope of the line becomes more negative as mass flow rate increases, becoming vertical as mass flow rate is increased to infinity. Solutions in sectors A and B are not possible as this would require a negative mass flow rate [2].

$$-\dot{m}^2 = \frac{P_2 - P_1}{1/v_2 - 1/v_1} \tag{1}$$

Rankine and Hugoniot built on Rayleigh's work by noting that the energy equation must also be satisfied (shown in Eq. 2 below), where γ is the ratio of specific heats and h is the heat released during the reaction. Possible solutions to this equation form Rankine-Hugoniot curves as shown in Figure 4. In Chapman and Jouguet's study of thermodynamic properties of detonations, they observed that there is a minimum entropy and velocity solution to these equations which correspond to a point where the Rayleigh line is tangent to the Rankine-Hugoniot curve. These tangency locations are known as Chapman-Jouguet (CJ) points. At the upper CJ point, burned gas

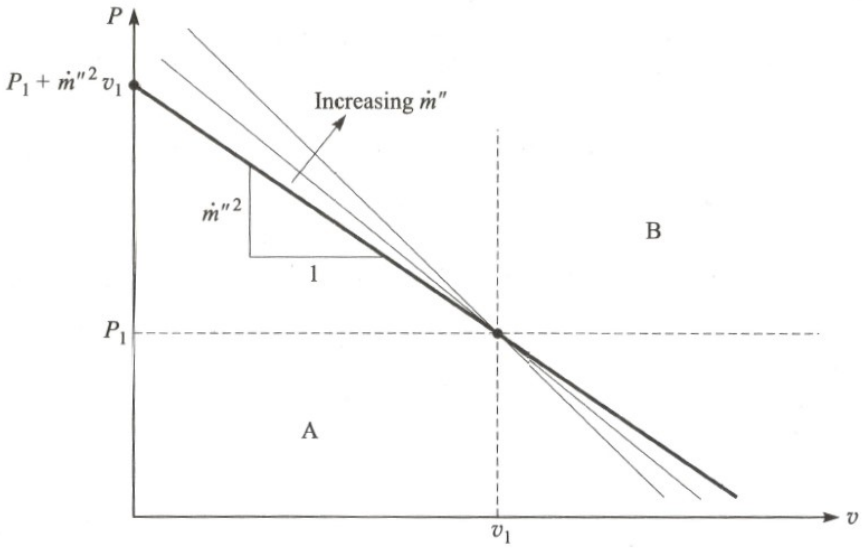

Figure 3. Rayleigh Line for flow defined by $\dot{m}$ [2]

relative to the detonation wave is at sonic velocity. States above and below the upper CJ point are associated with strong and weak detonations, respectively, where the burned gas velocity is subsonic behind a strong detonation and supersonic behind a weak detonation. However, to achieve these states, special conditions must exist. Chapman and Jouguet's analysis was for a 1D model, however the the upper CJ point provides a reasonable approximation actual detonation properties [2].

$$\frac{\gamma}{\gamma - 1}(P_2 v_2 - P_1 v_1) - \frac{1}{2}(P_2 - P_1)(v_1 + v_2) - h = 0 \tag{2}$$

Within a detonation wave, there are three sub-components: a compression wave, reaction zone, and expansion wave [10]. A one dimensional model of this structure, as shown in Figure 5, was proposed by Zeldovich, von Neumann, and Doring, known as the ZND model. Across the compression wave (state 2') there is a sharp rise in temperature, pressure, and density. Immediately following the compression wave is

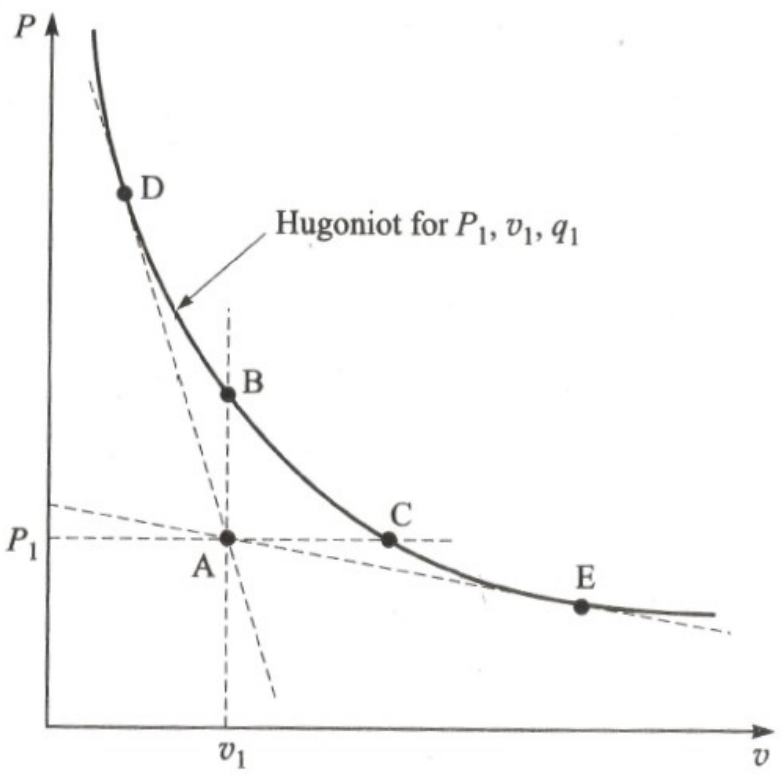

Figure 4. Rankine-Hugoniot curve for given q [2]

the reaction zone where energy from the combustion event is released. Behind the reaction zone (state 2), temperature is increased, and pressure and density decrease as the product gases are allowed to expand behind the compression wave [2]. For freely propagating detonations, the expansion of gases in the reaction zone drives the compression wave and the compression wave provides the activation energy to propagate the reaction. The interaction of these three components drive the velocity of a freely propagating detonation to CJ velocity associated with the upper CJ point [10].

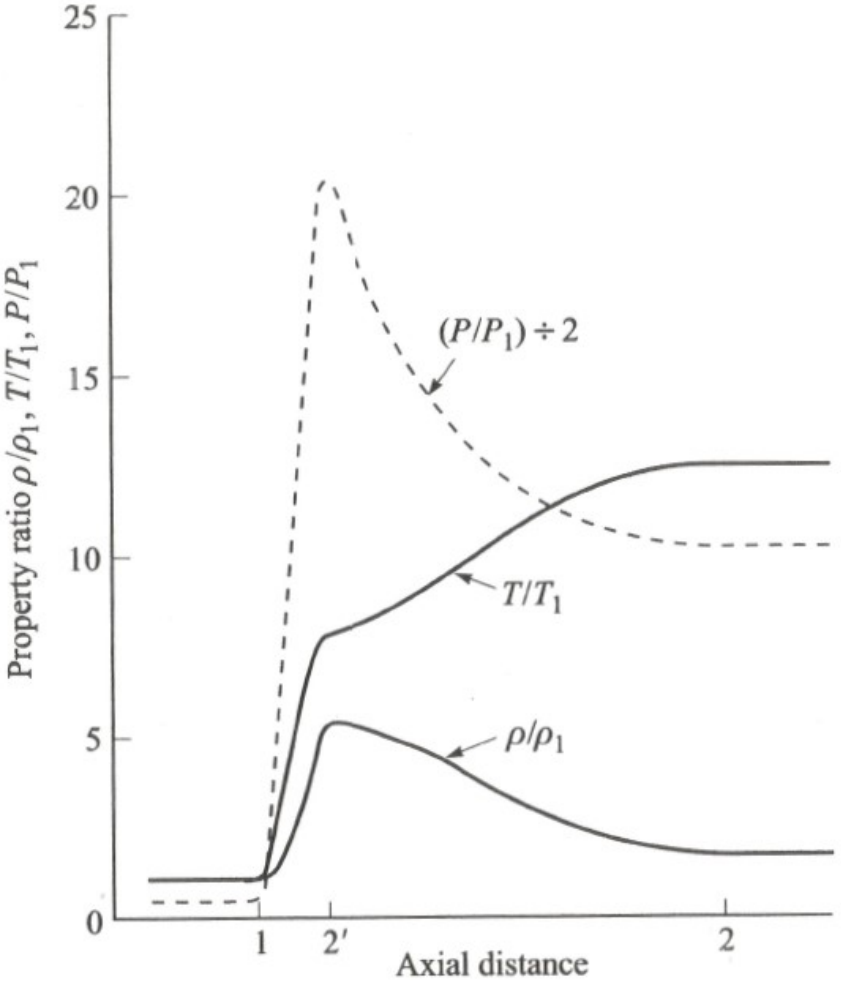

Figure 5. Representation of ZND detonation structure [2]

2.2 Rotating Detonation Engine Concepts

Harnessing the power of a detonation in an engine has been receiving increasingly more attention from researchers due to the potential 15-30x pressure increase associated with a detonation [1]. The large pressure rise offers higher potential for more work to be extracted than that of an equivalent deflagration reaction. The potential for more work can be seen in a comparison between Fickett-Jacobs (FJ), Humphrey, and Brayton cycles as shown in Figure 6. The defining difference between

the Humphrey and the Brayton cycle is that the Humphrey cycle is a constant volume cycle (when combustion occurs) and the Brayton cycle is a constant pressure cycle. The Brayton curve represents the cycle typically used in turbine and rocket engines where gas compressed and pressure is increased (Points 1-2), the volume is increased at constant pressure via heat addition/combustion (horizontal line at Point 2), work is then extracted (right hand portion of curve), and finally the excess heat is exhausted from the system to complete the cycle (lower horizontal line).

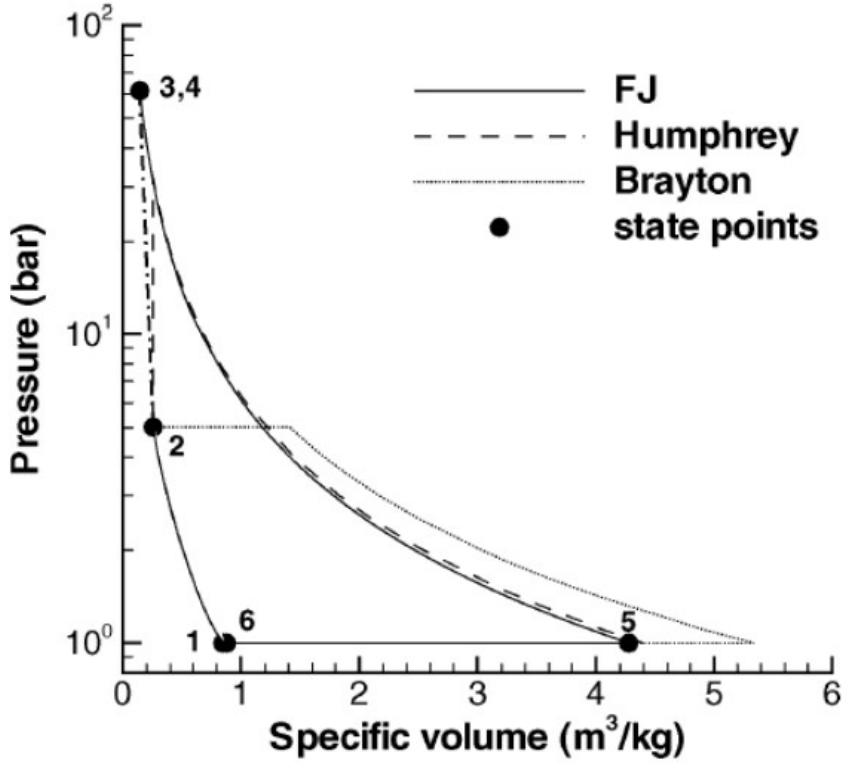

Figure 6. Pressure-specific volume diagram for cycle comparison [11]

Alternatively, the Humphrey cycle can be used to model a detonation engine cycle, where the gas is pressurized via shockwave initiating a detonation, which further increases pressure (represented by Points 1-4). Work is then extracted from the system (Points 4-5), and then excess heat is exhausted from the system. The FJ cycle

takes the Humphrey cycle one step further by considering Rayleigh heat addition in the heat addition process, instead of simple heat addition under constant volume. The slight difference in the two cycles is shown between Points 2-3. The FJ cycle is a more accurate representation of a propagating detonation [12]. For all three cases, the most notable differences between the Fickett-Jacobs, Humphrey and the Brayton cycles is the larger area under the curve for the Fickett-Jacobs and Humphrey cycles, which is representative of the amount of work that can be extracted from each cycle [11].

At the forefront of harnessing a detonation cycle for use in propulsive system is the RDE. They have grown in popularity due to their simplistic design. As shown in Figure 2, an RDE consists of three main parts: a center body, outer body, and the fuel/oxidizer feed and injection system. The annular gap between the center body and outer body form the detonation channel. The detonation channel contains the detonation wave as is travels circumferentially around the annulus. To feed the detonation, reactants are injected at the base of the detonation channel. In this diagram, oxidizer is injected axially and fuel is injected radially outward at a 90° angle to the oxidizer injection holes. The reactants are mixed in the detonation channel prior to being consumed by the detonation wave. After the reactants are consumed, the products travel axially down the channel and are exhausted from the engine [1].

As the detonation wave travels around the circumference of the RDE, it forms the wave structure seen in Figure 7. A normal shock wave is formed in front of the detonation wave as a result of expanding gases from the combustion event, which leaves product gases behind the detonation wave. As the product gases immediately behind the detonation wave expand and transit axially due to the presence of a side-relief, they collide with product gases from a previous detonation wave forming an

oblique shock. As part of this interaction, a slip-line is established where the new and old product gases meet. Prandtl-Meyer expansion fans are formed at the top and bottom of the normal shock wave. The upper expansion fans are formed due to the expansion of the product gases as they move from the high pressure immediately behind the normal shock wave to the relatively low pressure behind the oblique shock. Where normal shock, oblique shock and the upper expansion fans meet is known as the triple point [1]. An additional expansion fan is formed at the base of the detonation wave where the high pressure gas associated with the normal shock meets the lower pressure reactants at the injector interface. The high pressure of the normal shock wave can also momentarily block the flow of reactants into the combustion chamber, which affects reactant mixing, fill height, and can adversely impact RDE operation. [6].

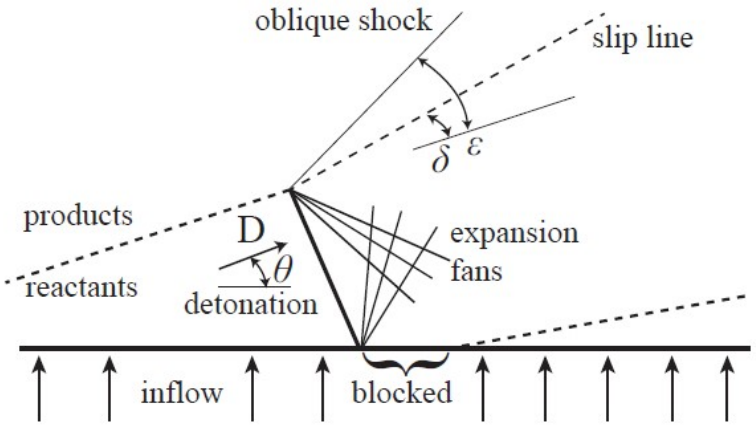

Figure 7. RDE wave structure [6]

2.3 Deflagration to Detonation Transition

Detonation and deflagration are characterized as separate types of combustion. However, detonations are typically initiated from a deflagration then transitioned to a detonation. This initiation is known as deflagration to detonation transition (DDT). During DDT, deflagration in a confined space continues to accelerate to approximately the CJ deflagration speed (lower CJ point). At this point, the system is in a quasi deflagration-detonation state. The onset of turbulence in the flow creates localized hot spots. These localized hot spots cause the gas in the flow to expand rapidly forming shock waves and ensuing detonation fronts that are initially spherical in shape. The detonation fronts collide with the walls of the chamber forming what are known as transverse waves (shown in Figure 8). The transverse waves travel perpendicularly to the detonation wave front. The collision of the transverse waves form a high pressure Mach Stem that pushes the detonation front forward and propagates the detonation wave [10].

Experiments by Meyers et al. demonstrated the importance of turbulence on DDT. A Shchelkin spiral, as shown in Figure 9b, was used to induce turbulence in the flow and shorten the time and distance required for DDT. This data was compared to DDT in a smooth walled tube (annotated "clean" configuration in Figure 9a), with the assumption that the smooth walled tube would maintain laminar flow to a greater extent than the Shchelkin spiral configuration. Figure 10 shows that in the clean configuration, detonation was not achieved until the second most upstream pressure probe, P_6, at 15.24 cm downstream and that it took approximately 185.0 ms to reach the end of the tube. Comparing these results to the Shchelkin spiral, detonation was achieved by the first pressure probe, P_7, approximately 7.62 cm downstream and reached the end of the tube in less than 137.5 ms. Their results revealed that the Shchelkin spiral resulted in a DDT event that occurred in less time and distance

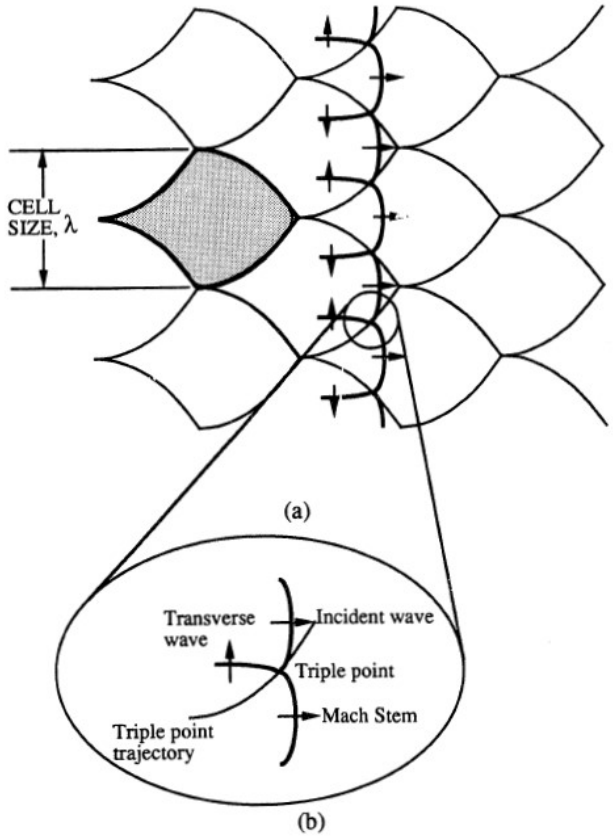

Figure 8. Detonation structure and "fish scale" pattern [13]

thus supporting the conclusion that DDT is coupled with the presence of turbulent flow. However, even in a smooth walled tube, the flow will eventually transition to turbulent and can experience DDT [14].

2.4 Detonation Cell Size

Once the detonation has been established, the detonation wave takes on the form shown in Figure 8, consisting of three components: the incident wave, transverse wave, and Mach stem. The incident wave is formed as part of the original shock wave

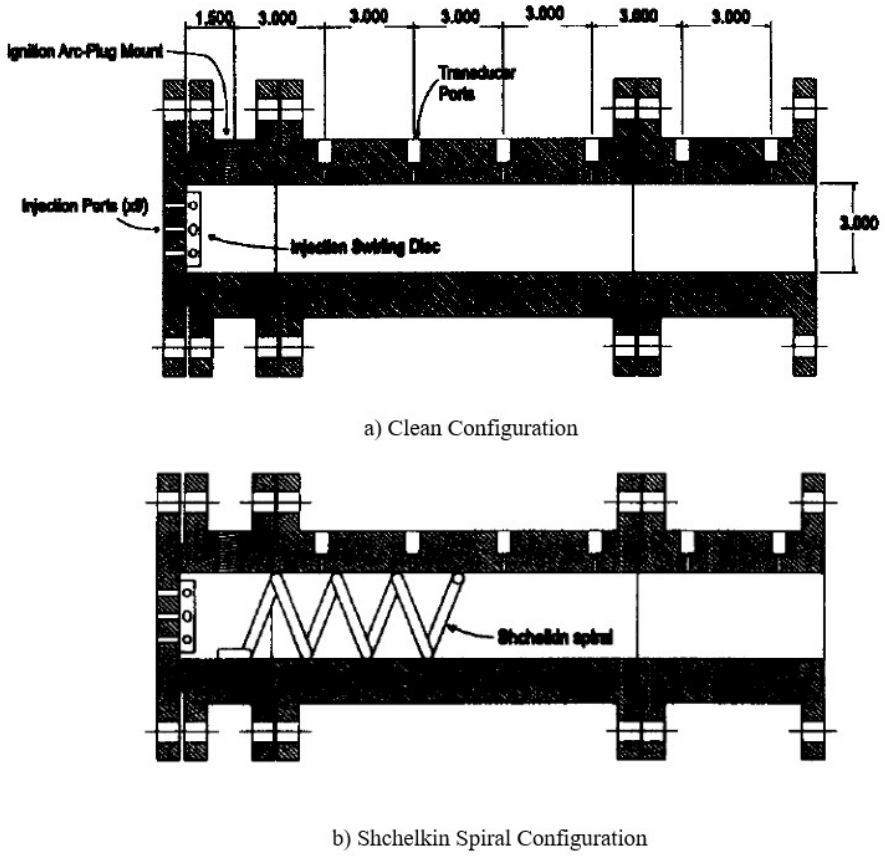

Figure 9. Experimental setup of a detonation tube in clean and Shchelkin Spiral configurations [14]

resulting from the DDT event and travels in the direction of the overall detonation wave. The transverse wave travels perpendicularly to the incident wave as shown in Figure 8b. When transverse waves collide with other transverse waves, a Mach stem is formed. The Mach stem is initially stronger than the incident wave, but dissipates as it travels downstream. The point at which the incident wave, transverse wave, and Mach stem all meet is also known as the triple point. The unsteady nature of these three wave structures cause the triple point(s) to move as the detonation wave travels downstream forming what is known as the triple point trajectory. The resulting contour left by the passing detonation creates the "fish scale" pattern shown

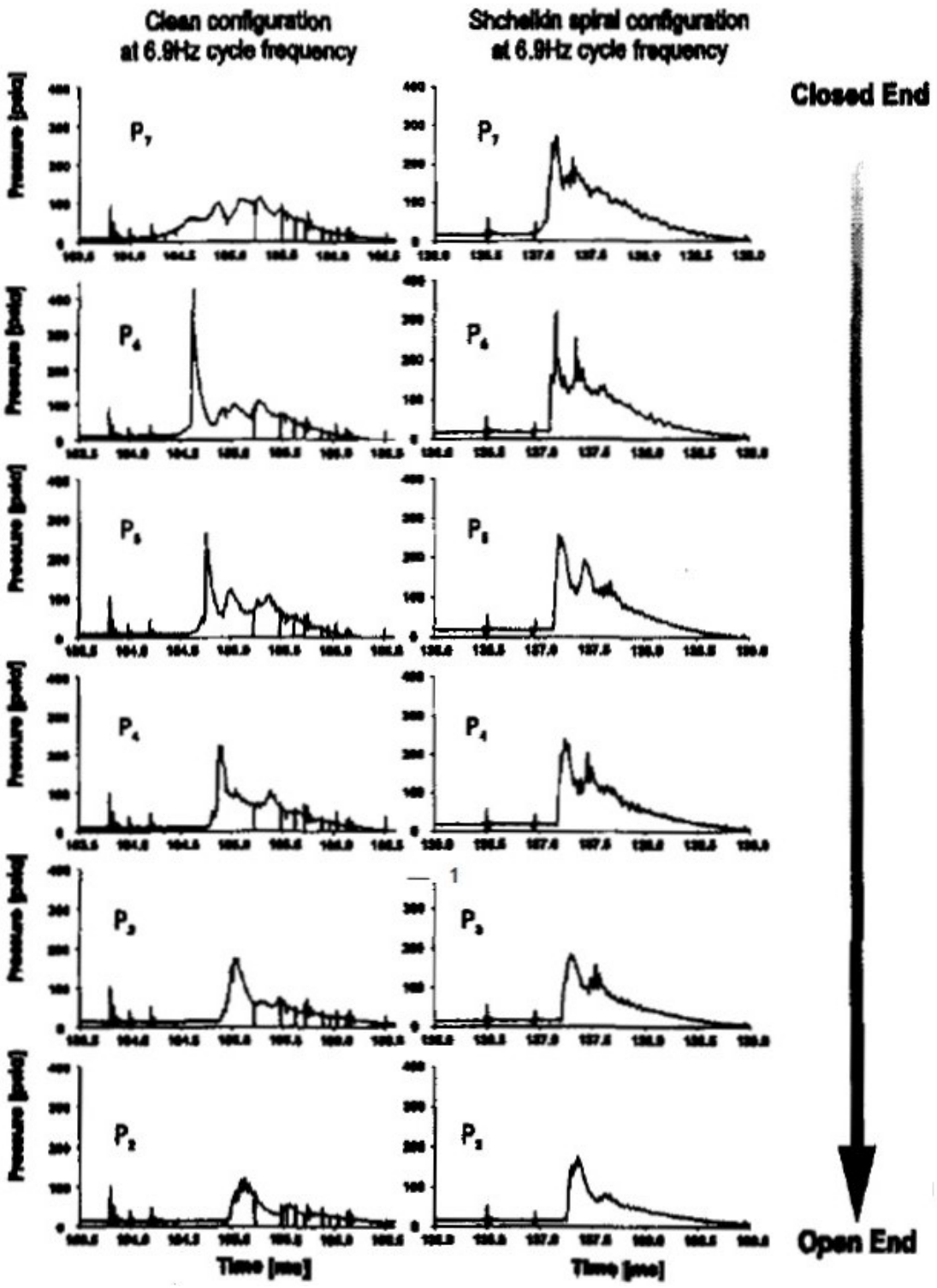

Figure 10. DDT time and distance comparison between clean and Shchelkin Spiral configurations [14]

in Figure 8a below.

The fish scale pattern is of great significance to detonations. From the fish scale pattern, a cell size, λ, can be determined. The width of a single scale is what defines the cell size for a set of reactants. Cell size is a key parameter for the propagation of a detonation and is a critical dimension for in RDE design. Cell size can determine the RDE's geometry and can ultimately impact the RDE's physical size [5]. Therefore, minimizing cell size was key for the design of a small scale RDE and ensuring successful operation.

To the find cell size for a set of reactants, it is common to use what is known as a soot foil technique. In this method, a thin piece of metal or "foil" is placed inside a detonation tube. When the mixture is detonated, a shear layer is formed as a result of flow interaction at the triple point(s). The shear layer deposits soot from the combustion products on the foil leaving behind an imprint of the triple point trajectories from the the detonation wave [13]. An example soot foil courtesy of Sell at the Air Force Research Laboratory's (AFRL) Detonation Engine Research Facility (DERF) is shown in Figure 11 where the triple point trajectories have formed the classic fish scale pattern.

Cell size can be affected by pressure, temperature, equivalence ratio, ϕ, and reactant type. Babbie et al. performed experiments with H_2 and air to determine pressure and equivalence ratio effects on cell size. It is generally agreed upon that pressure can have an effect on cell size, but their work was the first to perform a sweep of both pressure and equivalence ratio [15]. In their experiments, equivalence ratio was varied from 0.65 to 1.0 and pressure from 2 atmospheres to 10 atmospheres as shown in Figure 12. In agreement with previous work done by Kaneshige et al., as equivalence ratio decreased from 1.0, cell size increased [16]. Additionally, as pressure was increased, cell size decreased by approximately a factor of two. Babbie et

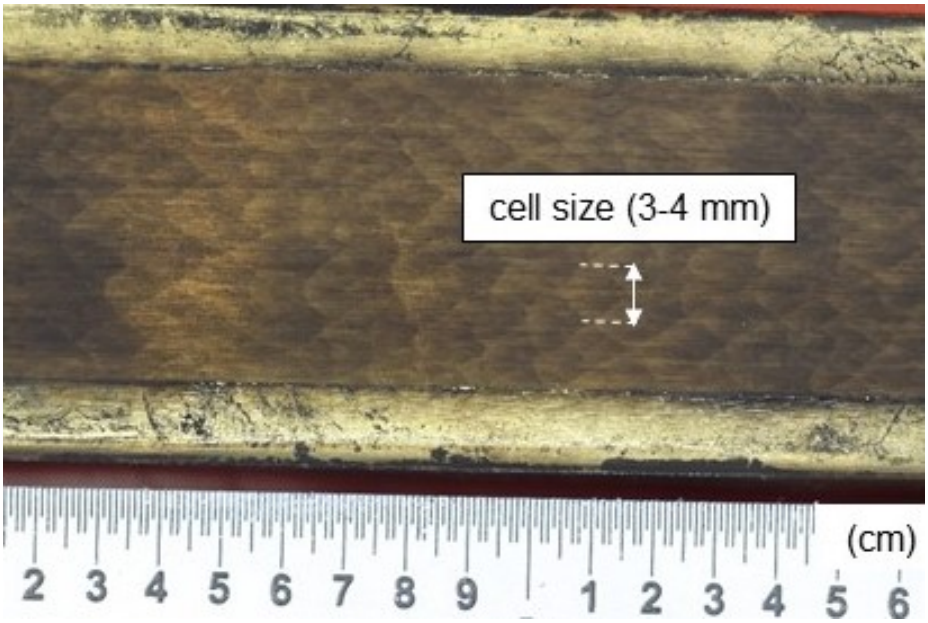

Figure 11. Soot foil of C_3H_8 and N_2O at ϕ=1.0 courtesy of B. Sell

al. concluded that equivalence ratio had the strongest affect on cell size. However, their work revealed that pressure had a stronger effect on cell size than what was previously thought among detonation researchers [15].

In addition to pressure, temperature can have a significant effect on cell size. Ciccarelli et al. completed extensive work testing temperature and equivalence ratio effects in a H_2 and air mixture. They varied reactant temperature from 350 K to 650 K while also introducing steam as a dilutent (as a percentage of the air in the mixture). As show in Figure 13, when temperature was increased from 400 K to 650 K, cell size decreased from 16 cm to 3 cm at 15% steam dilution. They concluded that an increase in temperature decreases cell size for these reactants and the effect became more pronounced as the dilution percentage was increased. This was all while pressure remained constant at 1 MPa. [17].

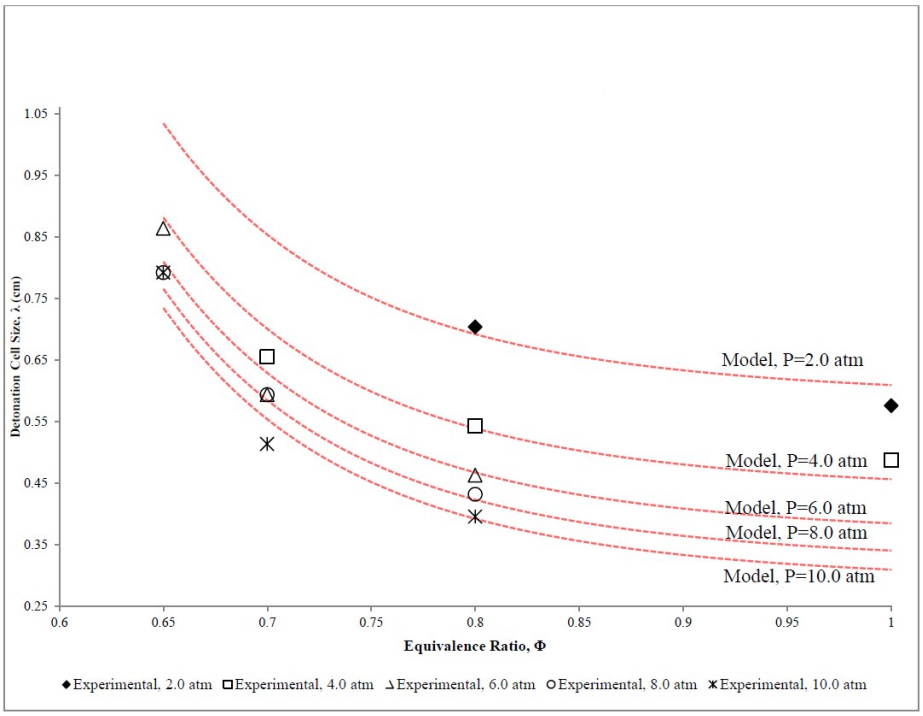

Figure 12. H_2 and air cell size with varying pressure and equivalence ratio [15]

2.5 Design Considerations

The ability of a detonation wave to propagate can be directly tied to cell size. There must be enough volume in the detonation channel for wave structures to form and interact allowing new cells can form. Lee theorized that if the space is too small, the rarefaction wave can penetrate into the detonation wave and cause the detonation to become unstable [10]. Mitrofanov et al. experimented with detonation tubes and found that the tube diameter must be at least 13λ in order for the detonation to propagate [18]. Their experiments were completed in a tube and may not fully represent of the conditions inside of an RDE. However, this work was essential to the foundation of detonation geometries and defining a relationship between cell size and stability.

Bykovskii et al. later completed a comprehensive study of RDE detonation channel

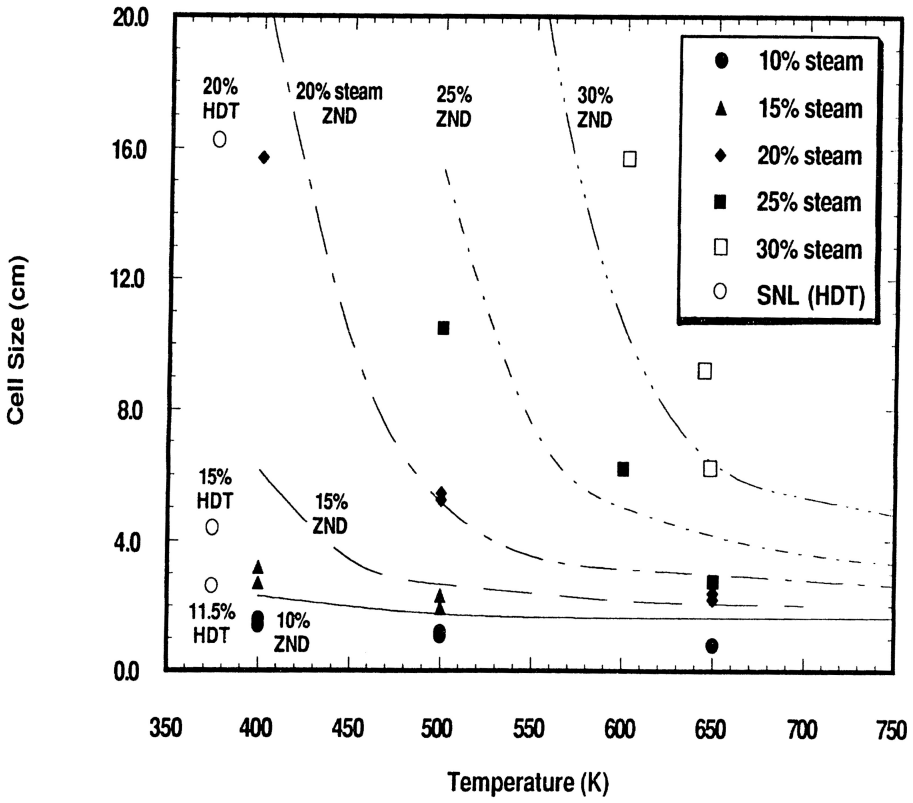

Figure 13. H_2 and air cell size with varying temperature [17]

geometry and its effect on detonation stability. Their research revealed critical dimensions necessary to sustain a detonation wave in an RDE, which included reactant fill height, h, detonation channel gap, Δ, channel length, l_c, and channel diameter, d_c as shown in Figure 14. The study found that these parameters are rooted in the detonation's cell size. In order to sustain the detonation, reactants must be propagated a certain distance in to the detonation channel before the detonation wave consumes them. This distance is known as the fill height, and Bykovskii et al. fount that this value must be at least $(12\pm5)\lambda$. From fill height, the minimum distance between the walls of the center body and outer body, also known as channel gap, can be determined. The minimum channel gap was found to be $0.2h$ [5].

Based on cell size and fill height the overall detonation channel length can be

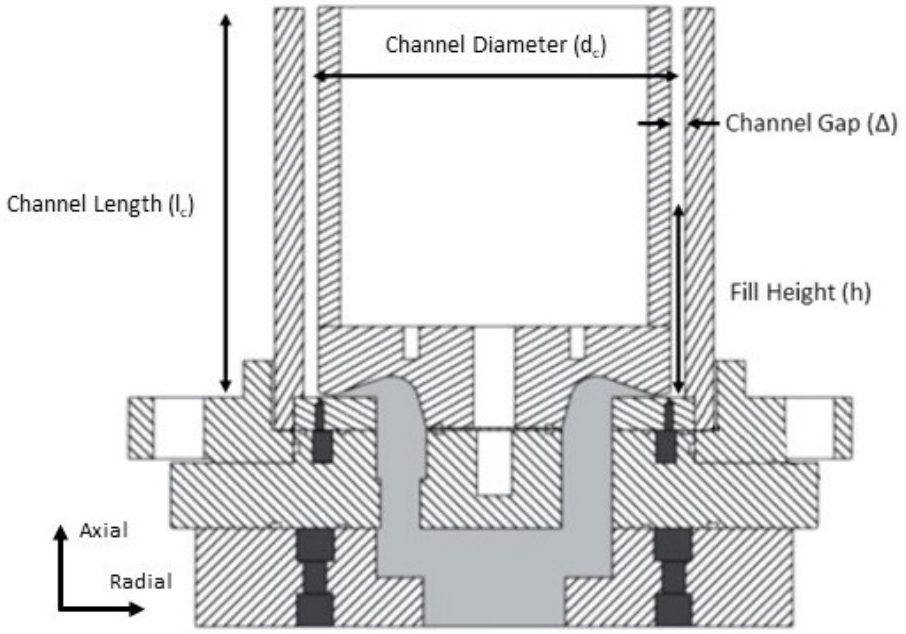

Figure 14. RDE design criteria as researched by Bykovskii et al. [5]

calculated. The minimum chamber length, was found to be $2h$, with an optimal length of $4h$. The length of the combustion chamber can effect the pressure inside the combustion chamber. If the chamber is too short, there may not be enough pressure ahead of the detonation wave to sustain it. Alternatively if the chamber is too long, the building boundary layer thickness can reduce the effective channel gap and cause the detonation wave to become unstable. Additionally, with increasing length there will be added heat and momentum losses to the walls, negatively impacting detonation stability [5].

Bykovskii et al. also investigated the minimum channel diameter and found that it is based on the length of the reaction zone, l_r, where the length of the reaction zone is defined by $l_r = 0.7\lambda$. From the reaction zone length, the minimum channel diameter, $d_{c,min}$, could be found, where $d_{c,min} = 40l_r$. With a known channel diameter, the detonation frequency can be calculated in Eq. 3, where f is the detonation frequency, D is the detonation velocity, n is the number of detonation waves [5].

$$f = \frac{Dn}{\pi d_c} \tag{3}$$

To determine the detonation frequency for a given RDE, the detonation velocity must be known. Detonation velocity can be a function of many factors to include fuel/oxidizer type and equivalence ratio. Experiments by Fernelius et al. investigated detonation velocities for methane, ethylene, ethane, propane and hydrogen when mixed with nitrous-oxide. For each mixture, equivalence ratio was varied from 0.6 to 1.4. Their experiments used a water cooled detonation tube to ensure that temperature was consistent for each case. Ion probes (discussed in Section 2.7) were used to calculate detonation velocity [19].

As shown in Figure 15, their results revealed that as equivalence ratio increased, detonation velocity increased. In the case of ethylene, detonation velocity increased from 2077 m/s at $\phi = 0.6$ to 2303 m/s at $\phi = 1.4$ with 100% N_2O as the oxidizer. Methane, ethane, and propane all had very similar increases across the same range of ϕ. In all cases, the experimental results matched theoretical CJ detonation velocities calculated by the National Aeronautic and Space Administration's (NASA) Chemical Equilibrium with Applications (CEA) tool within five percent [19]. Their validation of CEA calculations allowed for estimation of detonation velocities for different fuel/oxidizer combinations and initial conditions that were not presented in their research.

Fernelius et al's. experiments also included the introduction of air into the mixture as a percent of the oxidizer. For ethylene and N_2O, detonation velocity decreased by 40-50 m/s at 80% N_2O (20% air) across the same range of ϕ. This same trend was seen for all fuels tested. Not only did detonation velocity decrease, the mixture also became less detonable as more air was introduced. This effect was more pronounced as ϕ was either increased or decreased from 1.0 [19].

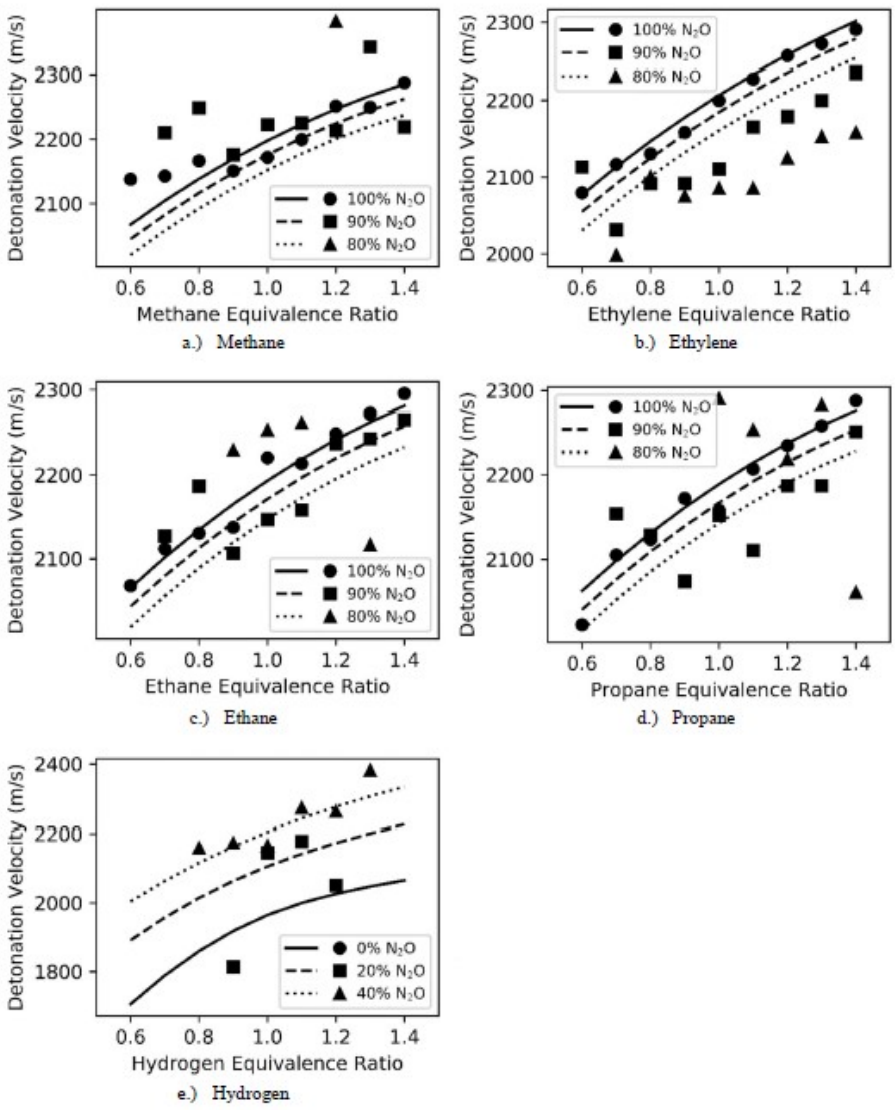

Figure 15. Detonation velocity vs. equivalence ratio for various fuel types [19]

A concern associated with a small scale RDE was detonation stability associated with a small channel radius. Kudo et al.'s work investigated rectangular tubes that curved 90° with inner radii varying from 5 mm to 60 mm. As the detonation wave travelled around the curve, the detonation speed was compared to the CJ velocity. For wave speeds at or above 80% of CJ speed, the detonation was to be considered stable. Between 60% and 80%, the detonation was considered critically stable, and

below 60% the detonation was unstable. They found that as the inner channel radius decreased, there was a point at which the detonation wave became either critically stable or unstable. Their results for detonation stability for different inner channel radii, r_i, are shown in Figure 16. They found that if r_i/λ was less than 14, the detonation was unstable [8]. Because an RDE does offer the same level of detonation confinement as an enclosed tube, these results cannot be used as a direct correlation for RDE wave behavior, but it does provide insight into possible issues associated with a small channel radius.

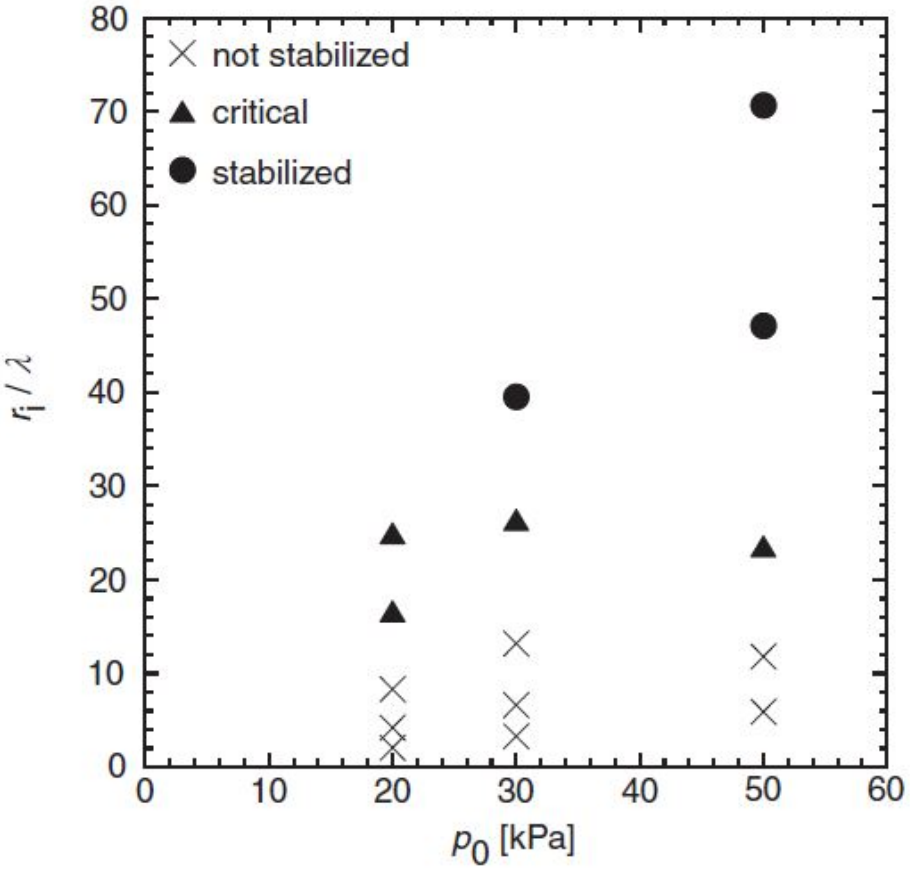

Figure 16. Detonation stability as a function of inner radius and pressure [8]

2.6 Injection Analysis

Duval et al. studied three injection schemes in an effort to quantify the parameters that make them most effective. Their experiments found that the detonability of the mixture could be significantly affected by the extent of how well the reactants were mixed. If the reactants were not mixed properly, the detonation wave could become unstable or even be terminated. The three schemes studied were pintle injectors, jets in crossflow (JIC), and semi-impinging jets (SIJ) as shown in Figure 17 [7].

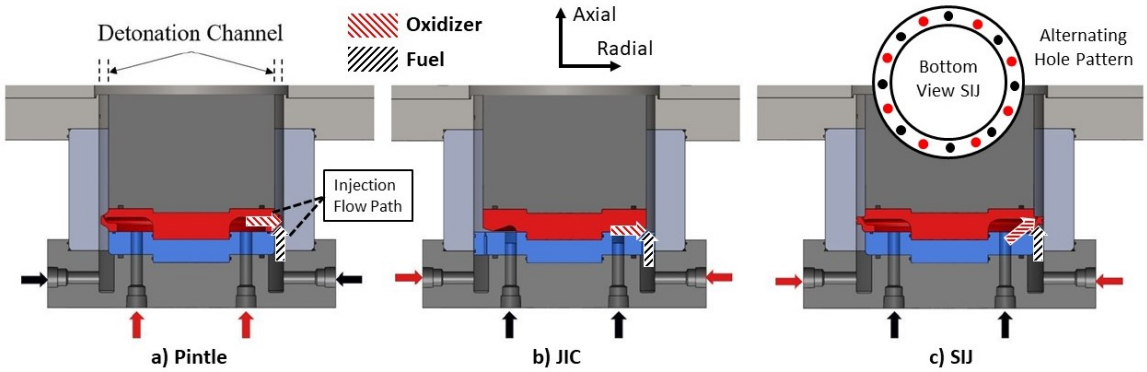

Figure 17. Configuration of a) pintle, b) jets in crossflow, and c) semi-impinging injection schemes [modified from [7]].

As shown in Figure 17a, pintle injectors inject fuel axially and oxidizer radially into the annulus (this arrangement could be swapped in all configurations discussed). The channel gap is reduced axially where the oxidizer is injected forming a protrusion or "pintle" [7]. This type of injection scheme is common in conventional rockets and can be used as a throttling mechanism by moving the pintle in and out [20]. The moving parts associated with a pintle injector can add complexity to the design.

The second scheme analyzed was jets in crossflow, where the fuel is injected axially and the oxidizer is injected perpendicularly to the fuel (radially) as shown in Figure 17b. The impinging fuel and oxidizer flows create turbulence and enhances mixing. This configuration is very similar to pintle injectors, however there is no protrusion

into the annulus offering a simple manufacturing process [7]. JIC are commonly used instead of Pintle injectors in RDE research since throttling and flow control are often done in locations upstream of the injectors [21].

The last scheme investigated was SIJ, where a protrusion is formed by the oxidizer injectors as shown in Figure 17c. It is injected at a more axial angle ($\approx 45°$) when compared to pintle or JIC injectors. Additionally, SIJ injectors are not aligned azimuthally. They are aligned so that the fuel is injected between the oxidizer injection holes [7]. This type of injection scheme is currently being researched by Gaillard et al. at the French National Aerospace Lab, ONERA, where the semi-impinging jets attempt to combine the mixing benefits of both flow impingement and the shear layer between the two jets [22]. Although this method may be effective, the angled injection holes combined with the pintle could make this configuration difficult to implement in a small scale RDE.

Duval et al. found that successful mixing can be achieved by two different factors depending on which injection scheme was being used. For pintle and JIC, mixing and subsequent stable detonation was achieved with a momentum flux ratio, J, near 0.5-0.6 using Eqs. 4 and 5

$$J = \frac{q_{fuel}}{q_{oxidizer}} \tag{4}$$

$$q = \gamma p_s M^2 \tag{5}$$

where, q, is momentum flux, P_s is the static pressure, and M is the Mach number. [7].

Conversely, the SIJ scheme was dependent on matching choking conditions between the fuel and oxidizer injectors. In other words, there must be high enough

mass flow rate for a given injector area, a_{inj}, so that Mach 1.0 flow could be achieved through the injector, which can be calculated using Eq. 6

$$p_t = \frac{\dot{m}}{\left[\frac{a_{inj}}{\sqrt{T_t}}\sqrt{\frac{\gamma}{R}}\frac{\gamma+1}{2}\right]^{\frac{-\gamma+1}{2(\gamma-1)}}} \tag{6}$$

where P_t is the total pressure, T_t is the total temperature, and R is the specific gas constant [7]. In this case, the injection hole area or flow rate could be adjusted to change the static pressure, Mach number, and resulting momentum flux.

Achieving a choking condition in the injectors is required to counteract the pressure rise associated with the passing detonation wave. As the detonation wave passes, the high pressure momentarily blocks off the injector flow. In some cases, the high pressure can force exhaust products back into the fuel and/or oxidizer plenum and affect the equivalence ratio of the reactants, which could potentially change the velocity and the stability of the detonation wave [7].

In addition to their study of RDE geometries, Bykovskii et al. analyzed detonation pressure characteristics, injection pressure requirements, and their impact on detonation stability in an RDE. They found that the pressure before the detonation wave compared to the pressure behind the detonation wave was typically 10 ± 4 times higher. Additionally, pressure before the detonation wave could be 4 ± 1 times higher than the average detonation channel pressure. This relationship tended to be on the higher end of this range as detonation frequency increased. As detonation frequency rose, there was less time for exhaust products to exit the channel before the next detonation wave passed, resulting in an increased channel pressure [5].

The amount of pressure in the detonation channel drives requirements for injection pressure. Bykovskii et al's. experiments indicated that fuel injector pressures needed to be twice that of the chamber pressure, and oxidizer pressure needed to be three times as much as the chamber pressure to maintain stable detonation [5].

If the injection scheme is not able to achieve proper mixing, equivalence ratios could vary within the detonation channel and impact detonation behavior [5]. For an RDE, the amount of time to achieve the desired fill height and mix the reactants is very short. For typical RDE's operating at 1-10 kHz [1], the reactants must be refreshed and mixed every 0.1-0.0001 s. For a 20 kHz RDE, this equates to an even shorter time of 50 μs making injection pressures, mixing, and achieving the proper fill height extremely challenging to achieve stable detonation.

2.7 Instrumentation Techniques

In order to characterize the operating characteristics of a small scale RDE, instrumentation to capture, temperature, pressure, and detonation frequency data was needed. Taking direct measurements of temperature and pressure inside the detonation channel of an RDE can be challenging due to the extreme environment the instrumentation can be exposed to. Additionally, high sampling rates were required to capture data associated with the detonation wave since it could travel around the RDE at a frequency of up to 20 kHz. Therefore, robust, accurate, and high-speed instrumentation was required to gather data from a small scale RDE.

Stephens et al. completed a study for taking pressure measurements inside the annulus of an RDE using various instrumentation methods. The following techniques were considered for the study: Capillary Tube Averaged Pressure (CTAP), Infinite Tube Pressure (ITP), Kiel Probe, and a PCB (brand) piezo-electric pressure transducer. Using the same experimental set-up, each probe's data was compared against each other to better understand possible inaccuracies of each device as well as the advantages and disadvantages of each technique [23].

As shown in Figure 18 below, a CTAP is designed to capture average static pressure. By using a long slender tube between the pressure source and the pressure

transducer, the viscous losses attenuate pressure fluctuations and allow the transducer to capture a clean average pressure signal. An additional benefit to the CTAP technique is that the transducer is placed a distance away from the heat associated with detonation which reduces the possibility of damage [23].

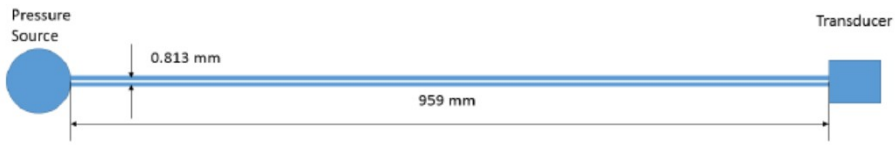

Figure 18. CTAP schematic [23]

ITP devices, as shown in Figure 19, are used to measure transient pressure fluctuations. This method is useful for gathering detonation wave data and to also extract detonation wave frequency. The layout of an ITP is similar to a CTAP, but the pressure transducer is placed near the pressure source and the "infinite tube" is exhausted to the atmosphere. The transducer is able to measure the transient pressures since it is located near the pressure source, while the infinite tube dampens out reflected shocks that could distort the pressure measurements. Because it is mounted on a "T", it is protected from shock waves and temperature damage. When using this technique, the pressure measure measurements must be corrected based on how far the pressure transducer is placed away from the pressure source [23].

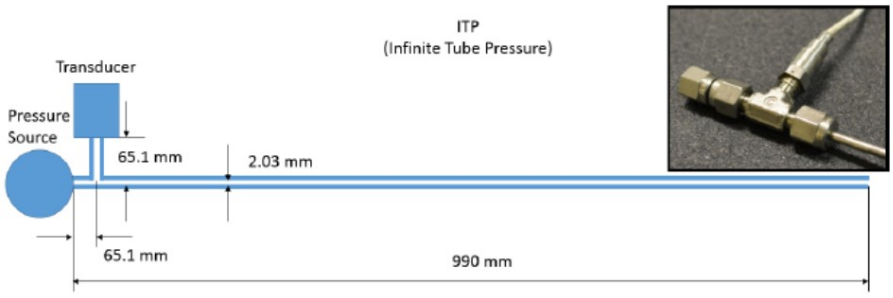

Figure 19. ITP schematic [23]

Kiel Probes, shown in Figure 20, are used to measure stagnation pressure. They operate in the same manner as a pitot probe. However, a shroud surrounds the probe to direct the airflow and minimize possible inaccuracies caused the "angle of attack" of the probe. Unlike CTAP's and ITP's, Kiel probes must be placed directly in the annulus of an RDE, and therefore have a very short lifespan (matter of seconds) since they are exposed directly to extreme temperatures and pressures. Kiel probes are capable of capturing the pressure data associated with the lead shock since it is travelling axially/in-line with the flow. However, Kiel probes may not be able to detect transverse wave pressure since they travel perpendicular to the flow [23].

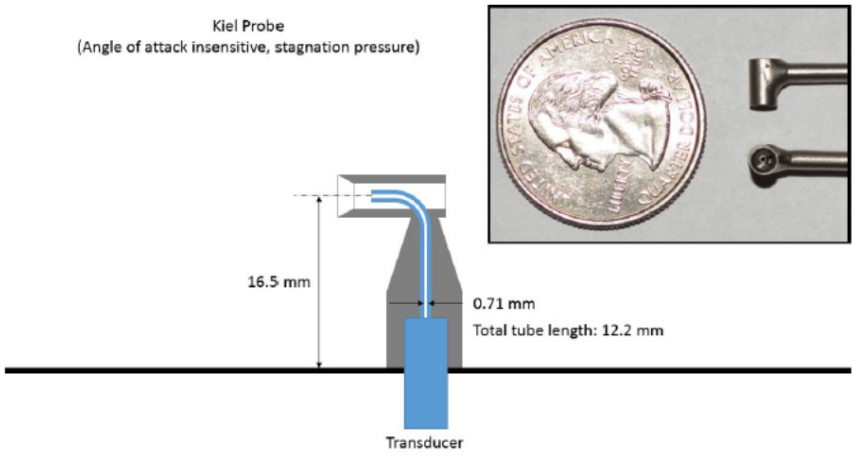

Figure 20. Kiel schematic [23]

All of the probes examined in Stephens et al.'s research recorded data with some noise to varying degrees. The CTAP eventually captured an accurate average pressure, but initially indicated an erroneous pressure spike stemming vibration caused by the initial detonation. The ITP experienced "ringing" from Hemholtz resonance as the flow inside the annulus passed over instrumentation tap. Detonation wave pressure spikes could be seen from the ITP, but the ringing created too much noise to be able to decipher the transverse detonation wave pressures. The Kiel probes

also suffered from Hemholtz resonance as the flow passed through the instrument's shroud. Additionally, the length of the Kiel probe's shroud caused an undesired lag in pressure rise/measurement (much like the CTAP is designed to do). The error can be clearly seen in Figure 21b, where the total pressure of Kiel probe was less than the static pressure measured by the ITP, which could obviously not exist [23]. Understanding these potential errors were critical to gathering data in an RDE.

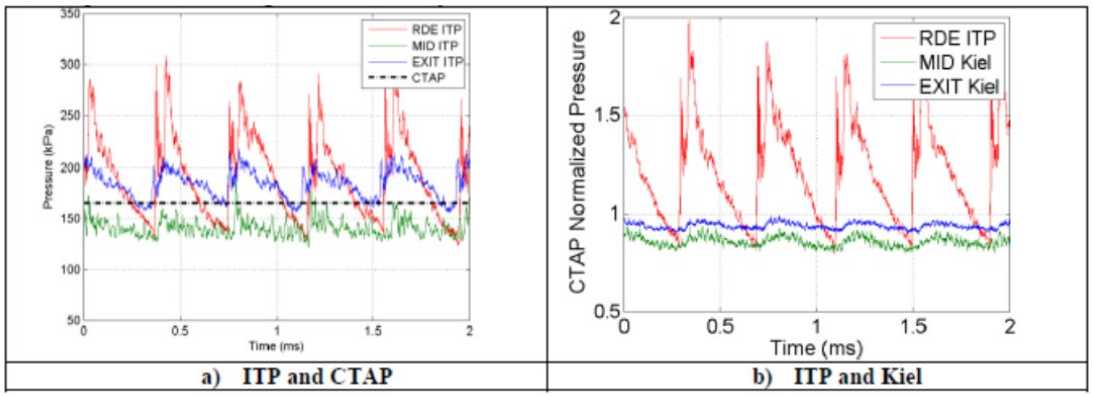

Figure 21. Comparison of CTAP, ITP, and Kiel probe pressure histories [23]

Pressure measurement was an important aspect for understanding the operating characteristics of an RDE, but an important goal of this research was to be able to achieve RDE detonation frequencies above 20 kHz. This operating parameter could be measured by pressure spikes from an ITP, but alternatives to this method have also been researched. Kowalkowski et al. investigated different measurement techniques to see how well they agreed on the timing of a passing detonation wave in a detonation tube. Their experimental set-up is shown in Figure 22 where a mixture was ignited, then a Schelkin Spiral initiated a deflagration to detonation event. The timing of deflagration/detonation wave was measured at four points as it progressed down the detonation tube. Ion probes, photo diodes, and pressure transducers were compared during this experiment [24].

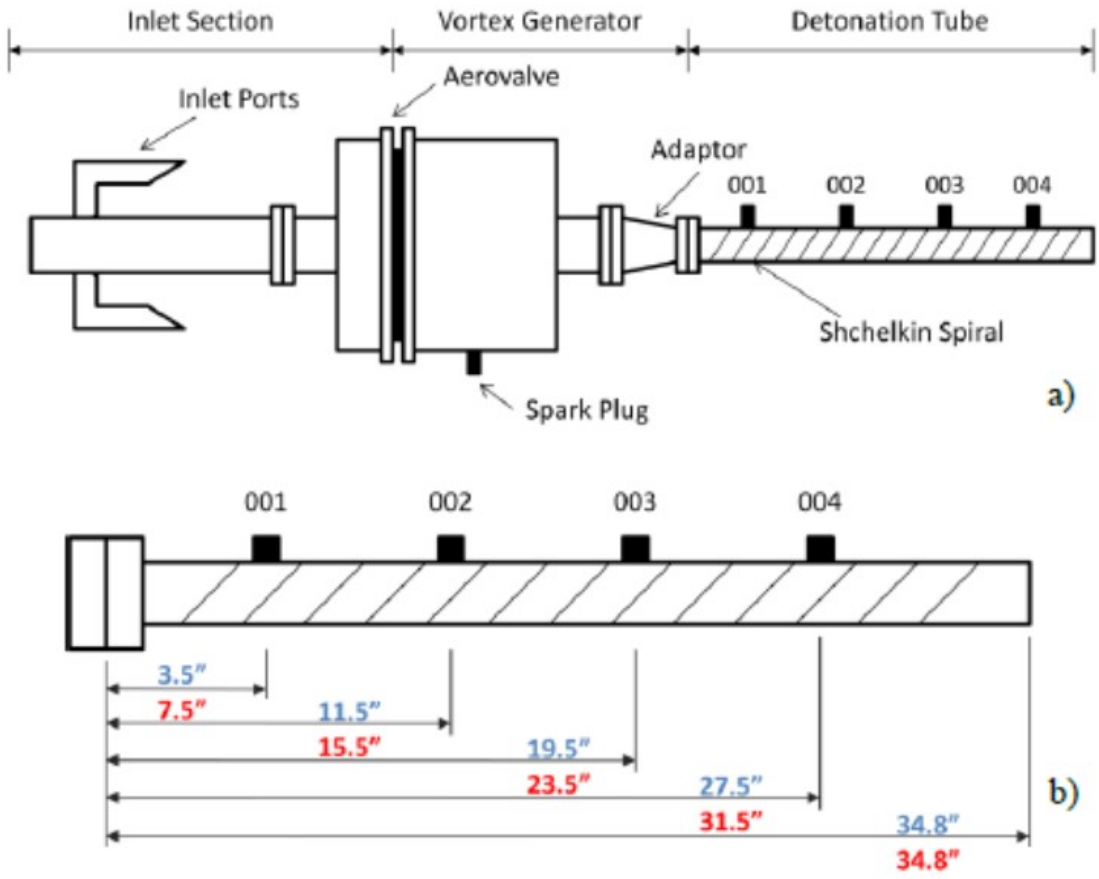

Figure 22. Detonation tube set-up for comparing flame sensing techniques [24]

Ion probes take advantage of the ions that form during a chemical reaction. During a combustion event there is a "global" or overall chemical reaction as shown in Eq. 7 below. However, within the global reaction there can be hundreds of intermediate or "elementary" reactions. For example, O_2 and H_2 may first break apart into atomic O and H, then combine to form an OH^- radical before finally combining with another H to form H_2O. When the OH^- is present the ion probe is able to detect the negatively charged molecule, thereby detecting the presence of an active chemical reaction [24].

Ion probes look and operate similar to an automotive spark plug, but instead of producing an arc, the cathode and anode detects the voltage potential within the mixture. If a voltage potential is detected, this indicates the passing of a detonation

wave [24].

$$2H_2 + O_2 \rightarrow 2H_2O \tag{7}$$

Similar to ion probes, photo diodes also utilize properties associated with elementary reactions. However, instead of detecting voltage potential, photo diodes detect specific wavelengths of light associated with ions in the elementary reactions. For example, when CH^* and C_2^* ions are excited, they produce 432 and 474 nm wavelengths respectively. The advantage of photo diodes when compared to ion probes, is that photo diodes can be tuned to detect specific wavelengths of light and therefore specific ions of interest. Alternatively, ion probes can only detect the presence of an electric field, not specific ion types [24].

Figure 23 compares measurements between ion probes, photo diodes, and pressure transducers (PCB brand) at four axial locations along the detonation tube. The pressure transducer detected a signal prior to the ion probe and photo diode in the first (top) plot which indicated that the reaction was still in a deflagration mode. As the reaction transitioned from deflagration to detonation, the pressure rise and/or voltage rise associated with the reaction began to match more closely in time (second, third, and fourth plots). This indicated that high pressure was in the immediate vicinity of the reaction zone, typical of a detonation shock, induction, and reaction zone structure. In Figure 23, on the second and third plots, the ion probe data did not match the photo diode data. This was believed to be a result of the turbulent nature of deflagration to detonation transition. During this time the ion probe may not have been in the local area of the reaction and therefore had fewer ionized radicals. Despite this shortcoming, ion probes had the greatest durability of the three measurement devices (survived 10 minutes of testing) and provided accurate readings once the detonation had been established [24].

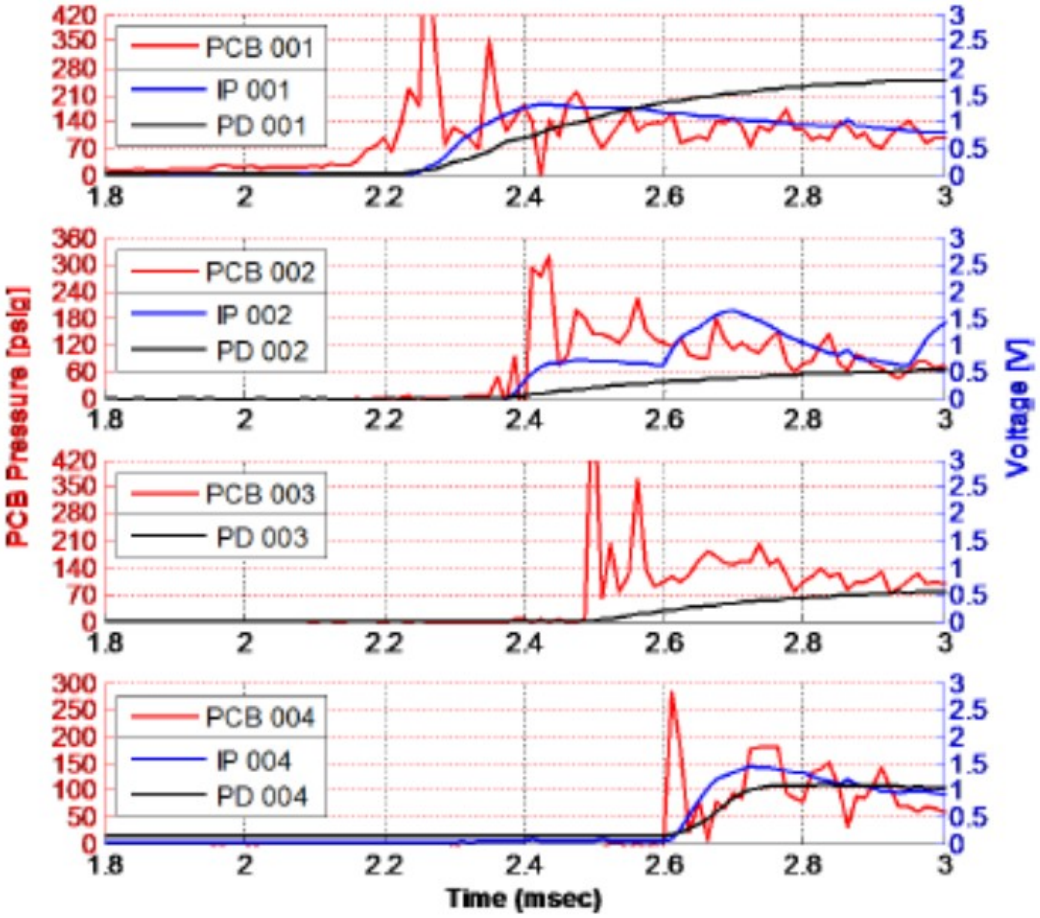

Figure 23. Pressure and ionization response during detonation [24]

Traditional detonation frequency measurement devices such as pressure transducers or ion probes require an instrumentation port in the RDE channel. Typically, the diameter of the port is relatively small in comparison to the total surface area of the inner or outer channel wall. However, in a small scale RDE, an instrumentation port could be large enough relative to the channel wall to cause interference to the detonation wave. Pandiya et al. researched the use of microphones as a non-invasive method to determine the detonation frequency of the an RDE. In their research, two microphones were placed 1.7 m away from the RDE to capture the engine's acous-

tics. Additionally, three PCB pressure transducers were installed in the detonation channel, which were equally spaced around the circumference of the channel. As shown in Figure 24, a Fast Fourier Transform (FFT) was performed on the data collected from both instrumentation methods to determine an operating frequency for the RDE. Both measurement techniques provided nearly identical results, where the primary operating frequency was found to be approximately 3800 Hz [25]. Their research demonstrated that microphones were a viable method to capture detonation frequency in RDE research.

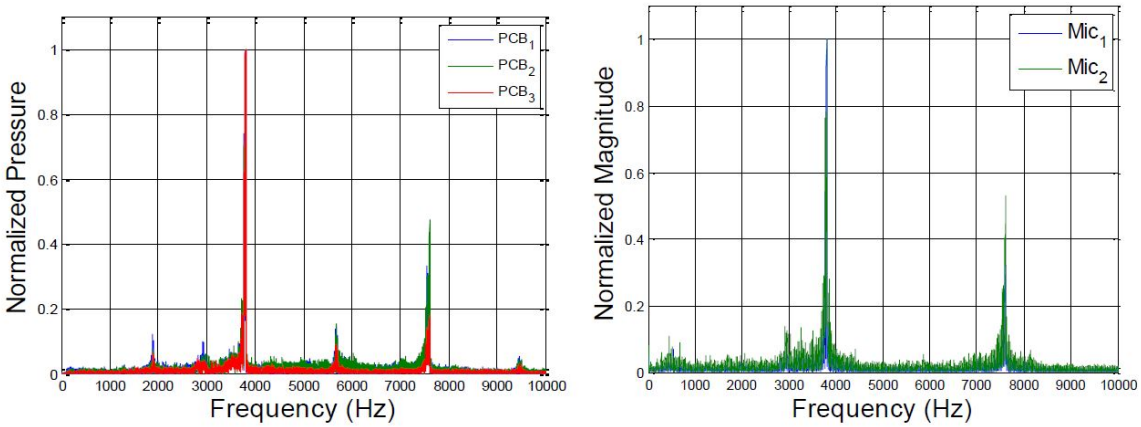

Figure 24. Comparison of PCB probes (left) vs. microphones (right) to determine detonation frequency [25]

III. Methodology

The intent of this research was to design and build an RDE that operated at or above a 20 kHz detonation frequency on a single detonation wave while also minimizing mass flow rates through the engine. These requirements drove many of the engine's design aspects. The design and build-up resulted in an RDE that was 28 mm in diameter with a channel gap of 2 mm and is discussed in Section 3.1. In addition to designing an RDE, a control system for the engine needed to be incorporated which included: fuel/oxidizer flow rate control, valve timing, plumbing, and ignition systems and is discussed in Section 3.2. The engine needed to be instrumented with pressure, temperature, and high speed imaging in order to capture pertinent data from the experiment, which is discussed in Section 3.3. Finally, an uncertainty analysis was completed in Section 3.4.

3.1 Build-Up and Design

AFRL's DERF was an ideal location for accomplishing this research's objectives. The DERF was a large, explosion proof bay that can be easily adapted for many testing requirements. Various fuels and oxidizers can be supplied to multiple locations throughout the bay, which enabled a wide variety of research work. Testing safety was enhanced by bay door interlocks that turn off all electrical control to valves that open fuel and oxidizer supply lines as well as any method to initiate a spark when the doors were opened.

Adjacent to the bay was a control room where the engine could be operated and observed remotely. Data acquisition systems used to monitor various testing parameters such as temperature, pressure, and high speed imaging were housed here. A detailed description of the the data acquisition system is discussed in Section 3.2.

The design of the RDE was largely driven by criteria developed by Bykovskii et al. As shown in Figure 25, their research developed equations for required fill height, h, channel length, l_c, channel gap, Δ, and channel diameter, d_c [5]. These dimensions are rooted in cell size for a given set of reactants. The initial dimension, fill height, which is the distance into the channel the reactants need to travel prior to the arrival each detonation wave can be found by Eq. 8 [5].

$$h = (12 \pm 5)\lambda \tag{8}$$

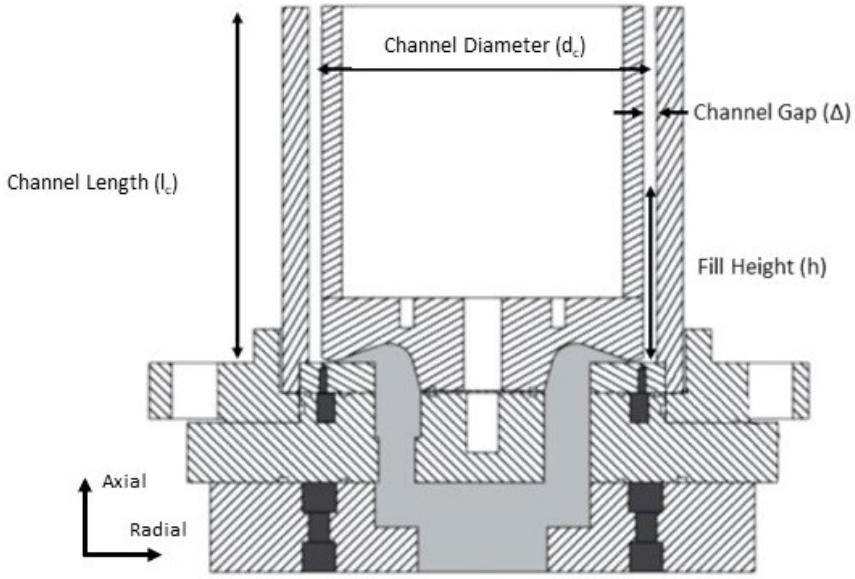

Figure 25. Key dimensions for RDE design [modified from [4]]

Prior to calculating a value for fill height, a set of reactants needed to be selected. The engine's geometry was likely going to create a difficult environment to achieve a detonation. To help overcome these challenges, the fuel and oxidizer needed to be highly reactive. Therefore, the fuel and oxidizer selected for this research was ethylene and nitrous-oxide. Work by Fernelius et al. found that ethylene and nitrous-oxide detonated over a larger range of equivalence ratios when compared to methane,

ethane, and propane fuels used with nitrous-oxide and air oxidizers [19]. No published cell size data was available for these reactants. However, soot foil testing courtesy of Sell et al. at AFRL found that the cell size for nitrous-oxide and ethane to be between 1.5-2.5 mm at an equivalence ratio of 1.0 as shown in Figure 26. Assuming that the cell size for nitrous-oxide and ethylene would be approximately 35-70% smaller than that of ethane and nitrous-oxide [16], the cell size was estimated to be between 0.5-1.75 mm. Using this range, h was calculated to be between 3.5-24 mm. However, to reduce mass flow rates as part of the current research, the lower end of this fill height range was used for the design ($h = 7\lambda$, for $\lambda = 0.5 - 1.75$ mm) which yielded a fill height of 3.5-12 mm.

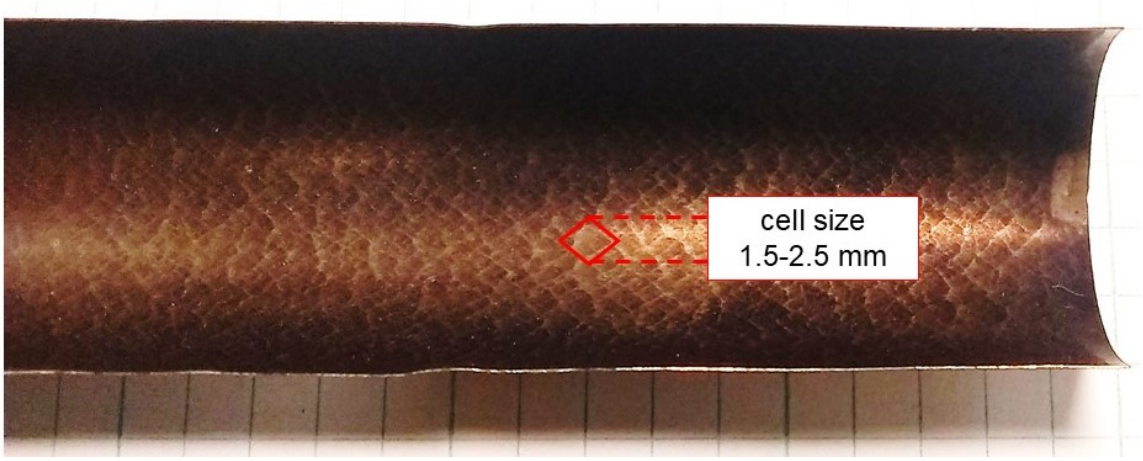

Figure 26. Soot foil used to determine cell size of C_2H_6 and N_2O at $\phi = 1.0$ courtesy of Sell et al.

The detonation channel length, l_d, is the length of the annulus formed between walls of the center body and outer body of the RDE. The detonation channel length must be sufficiently long to contain the detonation wave in the channel. Per Bykovskii et al., the detonation channel length should be at least twice the length of the reactant fill height as shown in Eq. 9 [5]. Using the values for h calculated previously, the detonation channel length would need to be at least 7-24 mm. Therefore, the engine

was designed to have a channel length of 30 mm so that there was a 20% margin above the minimum range.

$$l_d = 2h \tag{9}$$

The detonation channel gap, Δ, is defined as the radial distance between the walls of center body and outer body. Bykovskii et al. found this dimension to be a function of h, as calculated in Eq. 10 [5]. Again, with nitrous-oxide and ethylene, the channel gap would need to be between 0.7-2.4 mm. Therefore, the engine was designed to have a 2 mm channel gap.

$$\Delta = 0.2h \tag{10}$$

These equations defined key aspects for containing and sustaining the detonation process, but the desired detonation frequency of 20 kHz was critical to sizing the detonation channel diameter. The detonation channel diameter, d_c, can be found by using Bykovskii et al.'s equation for detonation frequency, f, in Eq. 3, where D is the detonation velocity [5]. Experiments by Fernelius et al. revealed that nitrous-oxide and ethylene has a detonation velocity of 2080-2291 m/s between equivalence ratios of 0.6-1.4 in a detonation tube [19].

Detonation wave speeds in an RDE typically range between 60-85% of the theoretical CJ velocity which can often be matched by the detonation velocities observed in a detonation tube [9]. Sizing the RDE based on the upper end of this wave speed range to achieve a 20 kHz detonation frequency was ambitious based on the small channel radius associated with an RDE of this scale. Alternatively, sizing the RDE based on the lower end of this range would require a reduced channel radius which would increase the possibility of detonation instability as researched by Kudo et al.

[8]. Therefore, an optimistic, 80% of the velocities observed by Fernelius et al. in a detonation tube were used to calculate the channel diameter of the RDE in an effort to maximize the channel radius and help overcome anticipated detonation wave instability. Using this percentage, the detonation wave speed could range between 1664-1833 m/s, which resulted in channel diameters between 26-29 mm using Eq. 11. Therefore, the RDE built for the current research had a diameter of 28 mm.

$$d_c = \frac{0.8D}{\pi f} \tag{11}$$

As shown in Figure 27, these dimensions guided the design of the RDE used in the current research. The engine was constructed with five individual pieces: a plumbing connection plate (red), oxidizer manifold (orange), fuel manifold (green), outer body (dark blue), and a center body (teal). Fuel and oxidizer supply lines were connected to the plumbing connection plate. When fuel and oxidizer entered the engine, they were routed into each of their respective plenum sections to allow for even distribution into injection orifices. The injection orifices were oriented 90° to each other to enhance reactant mixing in the detonation channel. Once the fuel and oxidizer were mixed in the detonation channel, the detonation wave consumed them and converted them into products. The product gases then traveled through the remaining length of the channel and were exhausted through the exit plane of the engine.

The arrangement of the components were designed with modularity in mind, since experimentation was anticipated to reveal required changes to the engine's geometry. The components were designed so that changes to the channel length, channel height, channel gap, channel diameter, and injection scheme could be modified with impact to as few parts as possible. Testing would later reveal that changes to the centerbody were required to achieve a detonation, as discussed in Section 4.2.

The plumbing connection plate consisted of one fitting for fuel, three fittings for

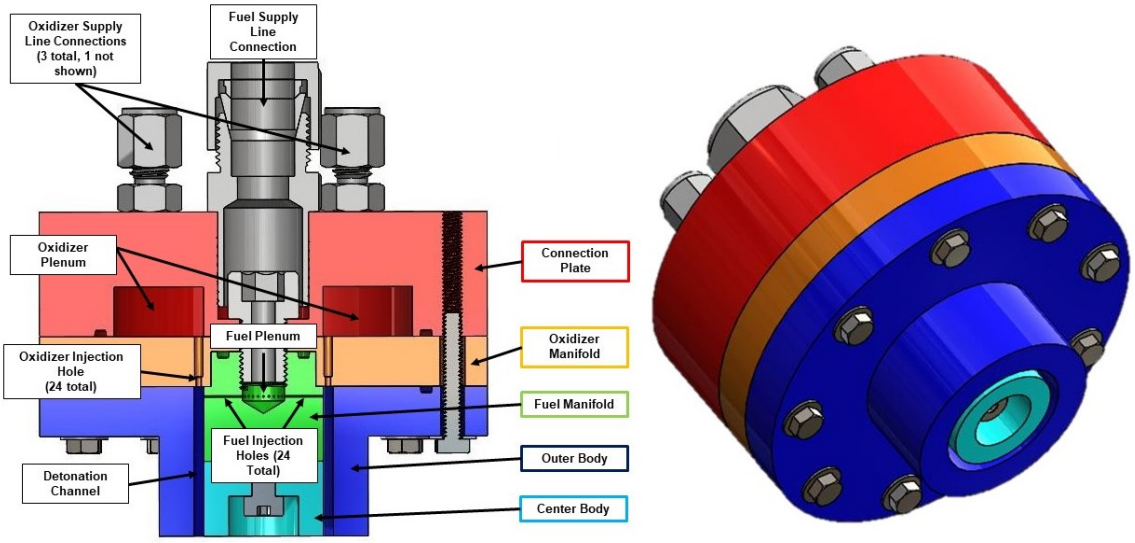

Figure 27. Cross section and perspective view of RDE

oxidizer, and a plenum to distribute oxidizer to the oxidizer manifold mated below as shown in Figure 27. Multiple fittings were used for the oxidizer to help evenly distribute nitrous-oxide to the injection holes below. Additionally, using three connections reduced the possibility of choking the flow in the fittings or tubing immediately upstream. Using a single 1/4" tube, the Mach number, M, was calculated to be between 0.29-1.0 for the mass flow rates, $\dot{m}$, of 0.022-0.071 kg/s used during testing as calculated by Eq. 12 (where T_t is total temperature, A is area, P_t is the total pressure, R is the specific gas constant, and γ is the ratio of specific heats). Choking the flow at the higher range of the anticipated mass flow rates would cause a pressure loss of approximately 50% before entering the oxidizer plenum. By implementing three 1/4" tube connections, the Mach number was reduced to 0.32 at the maximum flow rate of 0.071 kg/s.

$$M = \dot{m}\frac{\sqrt{T_t}}{AP_t}\sqrt{\frac{R}{\gamma}}(1+\frac{\gamma-1}{2}M^2)^{\frac{\gamma+1}{2(\gamma-1)}} \tag{12}$$

More connection ports or a larger diameter line for the oxidizer could have been

used to alleviate choking concerns, but space on the connection plate was limited as shown in Figure 28. With three engine mounts, four connection ports, and the associated tubing, this area was congested with hardware. Attempting to use a larger diameter tube would have made routing and bending the tubing more challenging. Other design configurations likely exist, but three, 1/4" diameter tubes allowed for the operating objectives to be met for this research.

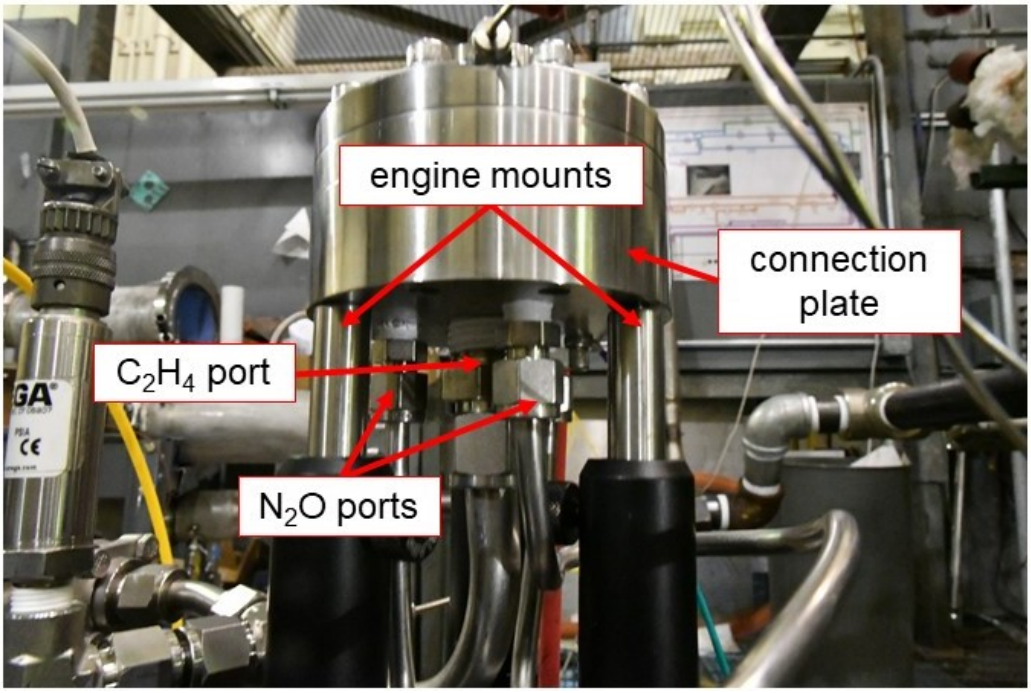

Figure 28. RDE connection plate and associated hardware

Multiple oxidizer connection ports also offered provisions for future research on thrust vectoring via equivalence ratio manipulation. The oxidizer plenum could be partitioned into three sections, segregating the injection holes below into three independent sections. With this partitioning, the equivalence ratio could be altered in one section of the injection system. The change in equivalence ratio in one section could result in asymmetric thrust (discussed in Section 5.3). However, this idea was not explored during the current research.

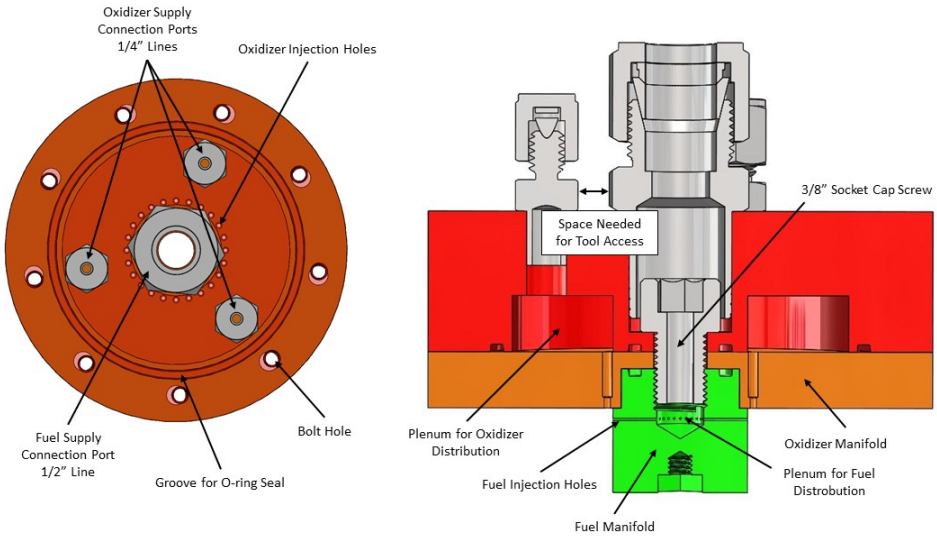

Figure 29. Cross section view of the plumbing connection plate

As seen in Figure 29, flowing fuel to the connection plate was straightforward in comparison to the oxidizer. The mass flow rate for the fuel was an order of magnitude lower than the oxidizer, therefore flow choking was not a concern. However a larger, 1/2" diameter tube was required to allow access for a 3/8" socket cap screw to be mounted inside of the plumbing connection plate. The socket cap screw was needed to secure the fuel manifold to the center of the engine. The screw was bored out in the center to 4.76 mm to allow ethylene to flow from the plumbing connection plate to the fuel manifold.

From the connection plate, fuel and oxidizer was fed into their respective injection manifolds. The oxidizer injection manifold consisted of a 90 mm diameter, 10 mm thick disk with 24 oxidizer injector holes oriented axially. The diameter of the injector holes are sized using Eq. 13 to achieve choked flow. Assuming a mass flow rate of 0.045 kg/s, temperature of 300 K, $\gamma = 1.27$, $R = 188.9$, and a $C_d = 0.65$ (discharge coefficient for a sharp edged orifice [20]), the individual injector area was found to

be 9.37*10^{-7} m^2, resulting in an injector diameter of 1.09 mm and a total pressure of 1.30 MPa. This injection pressure was under the 2.07 MPa pressure limit of the flow controller, which allowed for a 37% margin from any pressure losses between the flow controller and the injection hole. As shown in Figure 30, the injection holes are counterbored to a slightly larger diameter (1.7mm) at the top end of the injection plate to relieve some of the pressure loss through the injection holes. The diameter of the counterbored holes was limited by the adjacent connection plate.

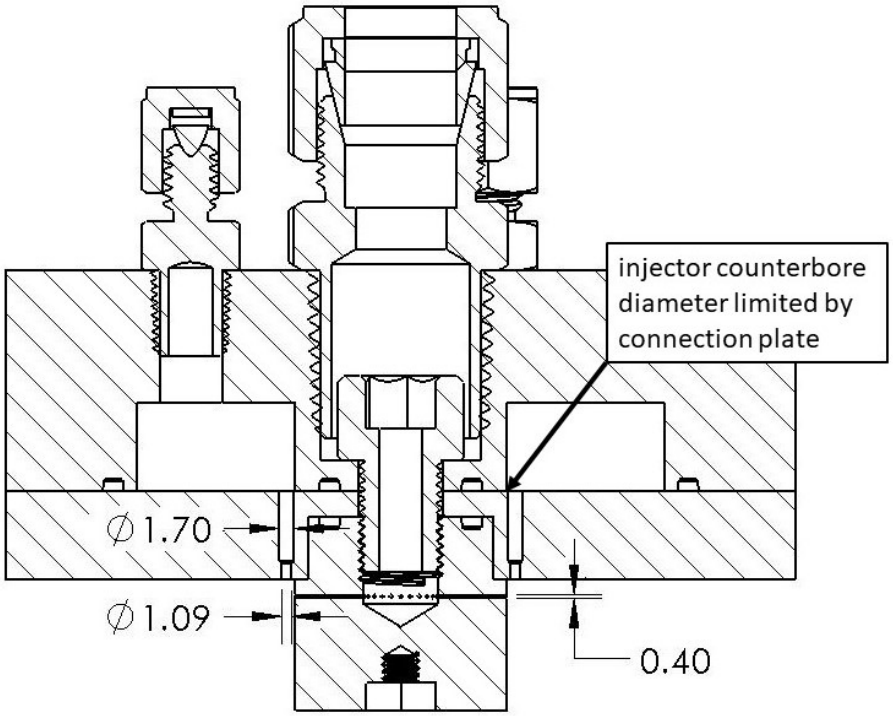

Figure 30. Cross-section view of fuel and oxidizer manifold assembly (mm)

As seen in Figure 30, the fuel injection manifold was designed in the same manner as the oxidizer manifold. Using Eq. 13, an injector diameter sized at 0.40 mm resulted in a total pressure of 1.25 MPa, assuming a mass flow rate of 0.005 kg/s, total temperature of 300 K, $\gamma = 1.24$, $R = 296.4$, and a $C_d = 0.65$ for a sharp edged orifice [20]. The fuel injection holes were not able to be counterbored like the

oxidizer holes due to the limited access to the inner portion of the manifold. The fuel injection holes were oriented radially, at a 90° angle to the oxidizer injection flow. This orientation is known as Jets in Crossflow (JIC), as discussed in Section 2.6, where the two impinging flows enhance reactant mixing in the detonation channel [7]. Other injection schemes such as pintle or semi-impinging jets could be used, but their complex geometry would be difficult to implement on an RDE of this scale.

$$P_t = \frac{\dot{m}}{\left[\frac{A}{\sqrt{T_t}}\sqrt{\frac{\gamma}{R}}\frac{\gamma+1}{2}\right]^{\frac{-\gamma+1}{2(\gamma-1)}}} \tag{13}$$

As seen in Figure 31, the fuel manifold, in combination with the center body and outer body pieces formed the detonation channel. The length and diameter of these three parts were driven by the criteria developed by Bykovskii et al. as discussed previously. The diameter of the outer body was sized at 28 mm as calculated by Eq. 11. The diameter of the fuel manifold and center body was sized at 24 mm to allow for the necessary channel gap of 2 mm as calculated by Eq. 10. Finally, the length of the outer body was sized at 30 mm as determined by Eq. 9. The fuel manifold protruded 15 mm into the detonation channel, which resulted in a center body length of 15 mm to complete the remaining length of the channel.

The engine was built in a modular form, assuming that adjustments would need to be made to component geometry. The fuel and oxidizer injection manifolds were constructed as separate parts so that fuel and oxidizer injection hole sizing could be altered independently. This would allow for adjustments to injection pressures and resulting momentum fluxes (as discussed in Section 2.6). Additionally, the inner and outer detonation channel wall pieces could be interchanged so that the length of the detonation channel altered. An altered length would change extent of boundary layer development inside the detonation channel, which could change the pressure inside of the detonation channel [5]. The diameter of the center body and outer body may

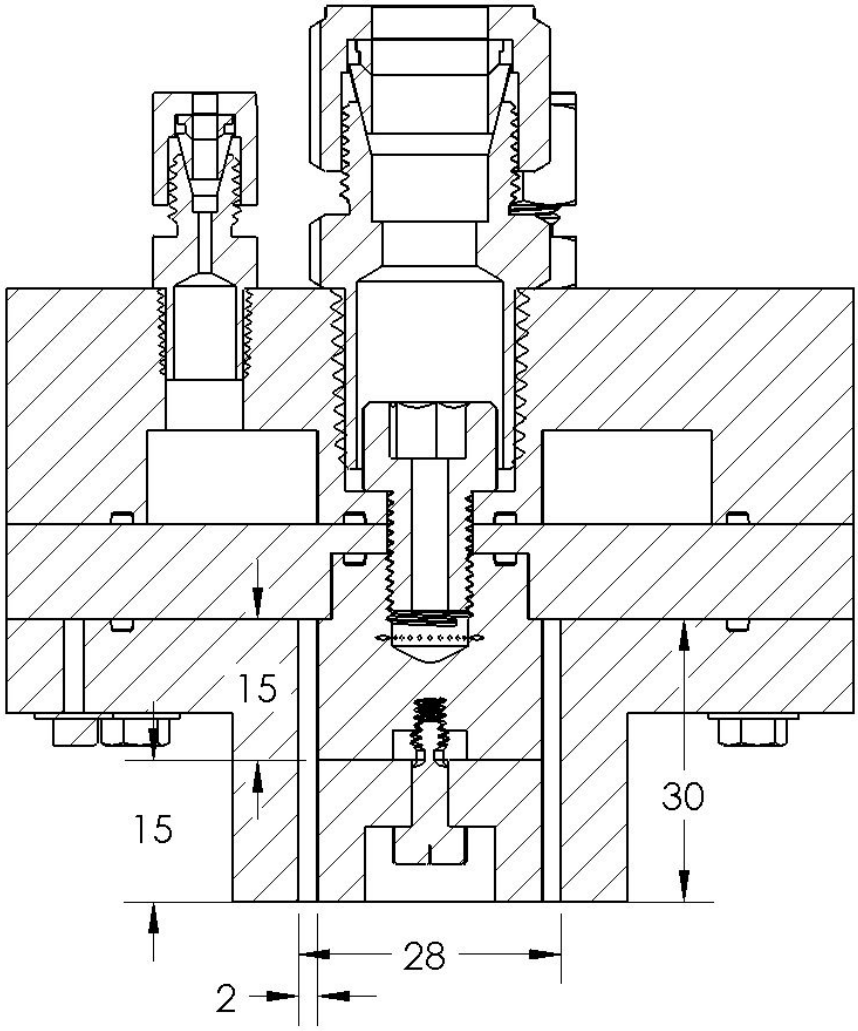

Figure 31. Detonation channel dimensions (mm)

also need to be adjusted. The engine was designed to operate at 20 kHz assuming that 80% of the wave speed observed in a detonation tube by Fernelius et al. [19] was achievable in an RDE. Testing later revealed that only 47-56% of wave speeds observed in a detonation tube were possible in the small scale RDE, which would require a reduction in the channel diameter to 16-20 mm in order to achieve a 20 kHz detonation frequency in future testing (discussed in Section 4.5). Finally, the engine was designed using an estimated cell size of 0.5-1.75 mm, but the actual cell

size may differ from this. The channel gap could be adjusted by resizing the diameter of the inner or outer channel walls, which could enhance the detonability range of the engine.

3.2 Control System

The control system for the RDE needed to complete the following tasks: establish the flow of fuel and oxidizer to the engine, control the mass flow rate of fuel and oxidizer, initiate a detonation, and shut-off fuel and oxidizer to the engine once the test sequence was complete. The layout of the control system and a simplified schematic is shown in Figures 32 and 33. Fuel and oxidizer flow from their respective supply tanks until they encounter mass flow controllers which meter the desired amount of fuel and oxidizer into the engine during testing. Downstream of the flow controllers were two isolation valves that open to allow fuel and oxidizer to flow into the engine, known as "last-chance" valves. Finally, to initiate a detonation, a spark plug was placed at the exit plane of the engine to ignite the reactants (repositioned in later testing). Signals to control the valves and spark were accomplished using LabView® software and National Instruments® controller and data acquisition hardware. As a measure of safety, a bay door interlock switch turned off the ability to initiate a spark and closed two additional valves near the fuel and oxidizer supply when the bay door was opened, rendering the RDE incapable of igniting.

A simple, yet critical part of operating the engine was the supply of fuel and oxidizer. The DERF had supplies of nitrous-oxide and ethylene available in the form of 56.8 L "K" bottles at 5.5 MPa. Delivering the required amount of oxidizer to the RDE proved to be an unexpected challenge during the build-up of the test stand. To deliver oxidizer to the engine, the pressure needed to be regulated down from 5.5 MPa to 2.2 MPa to be within the maximum allowable pressure of the mass flow

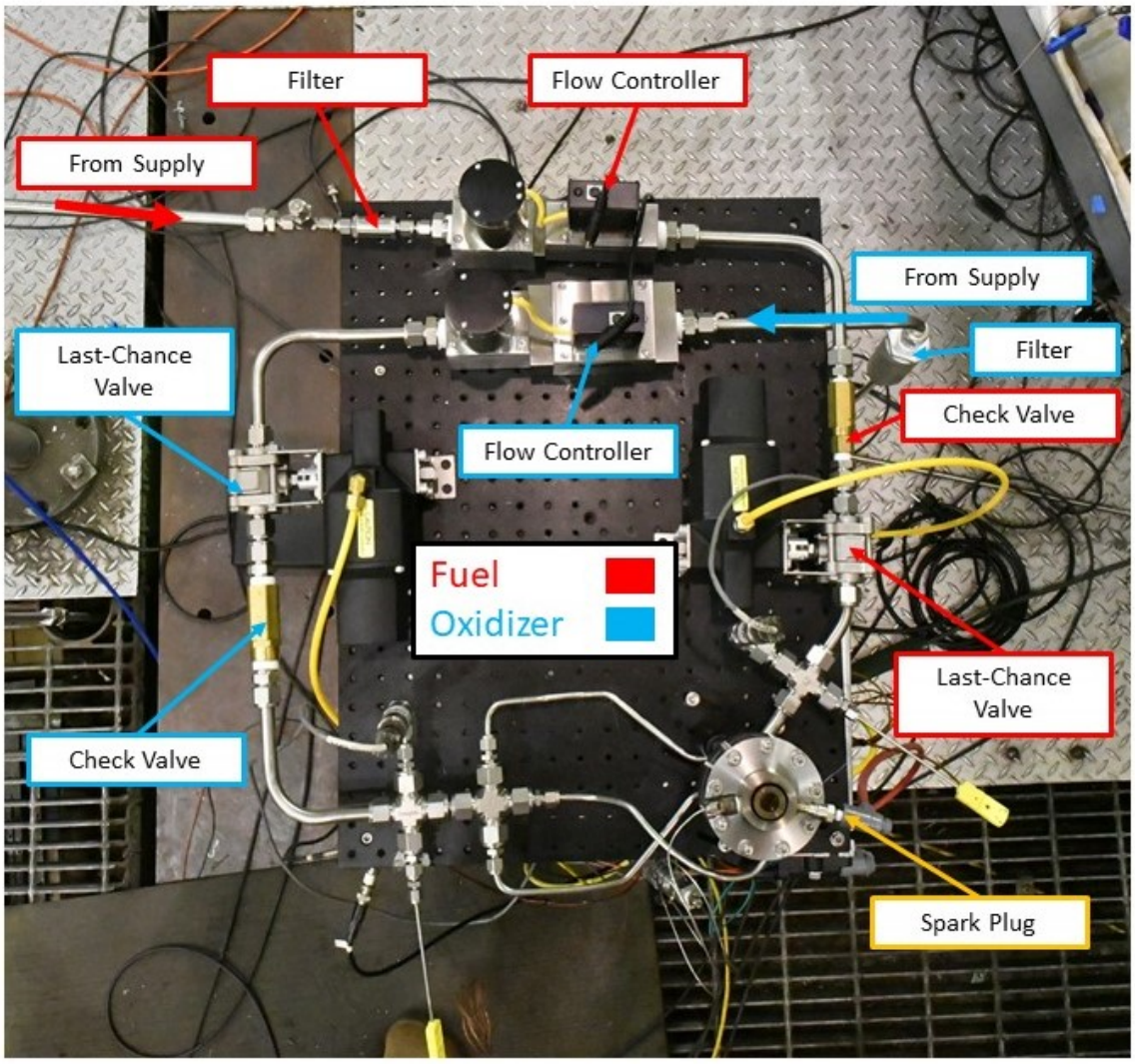

Figure 32. RDE control system layout

controllers. Although the oxidizer flow rates for this research were orders of magnitude lower than an RDE of average size (150 mm diameter), the 0.011-0.036 m^3/s flow rate requirement was still considered high for most regulators. A regulator's flow capacity can measured by its flow coefficient, C_v, where a higher C_v value equates to more flow that can be passed through the regulator. Volumetric flow rate, Q, as a function of C_v is shown in Eq. 15 [26], where P_1 is the upstream pressure in psia, SG is the specific gravity, and T is the gas temperature in Rankine. The regulator

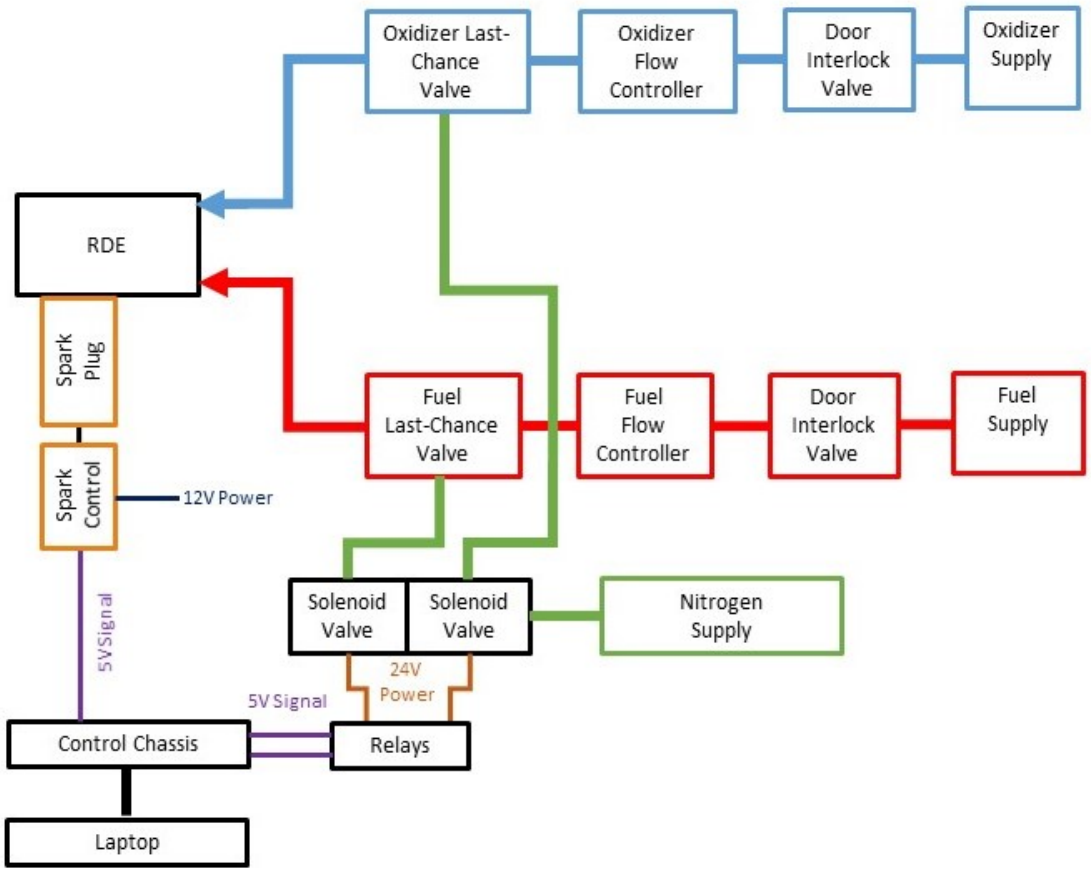

Figure 33. RDE control system schematic

is typically the lowest C_v component in the fluid delivery system. For example, a typical 1/2" ball valve may have a $C_v = 12$ whereas a regulator may only have a $C_v = 0.1$. Therefore, a high C_v regulator was desired to deliver the oxidizer. To overcome flow rate concerns, two regulators with C_v values of 0.06 and 0.17 were used initially with two supply bottles which allowed for parallel flow paths through the regulators as shown in Figure 34a. However, this combination only allowed for a flow rate of 0.02 m^3/s, when 0.011-0.036 m^3/s was needed for testing. When this attempt failed, a specialty "dome-loaded" regulator was acquired which had a $C_v = 2.0$; high enough so that the system no longer needed to have parallel paths as shown in Figure 34b. To find a flow rate for this configuration, a combined C_v for both the

regulator and "K" bottle in a series needed to be accounted for. This was calculated using Eq. 14, which resulted in a combined C_v value of 1.14. Using this value, the maximum flow rate that could be delivered by the system was found to be 0.2 m^3/s, as calculated by Eq. 15 with P_1 = 800 psi, T = 540° R, and $SG = 1.53$. This flow rate was over five times the maximum anticipated oxidizer flow rate of 0.036 m^3/s. After being regulated down to 2.2 MPa, the oxidizer could be fed directly to the flow rate controller.

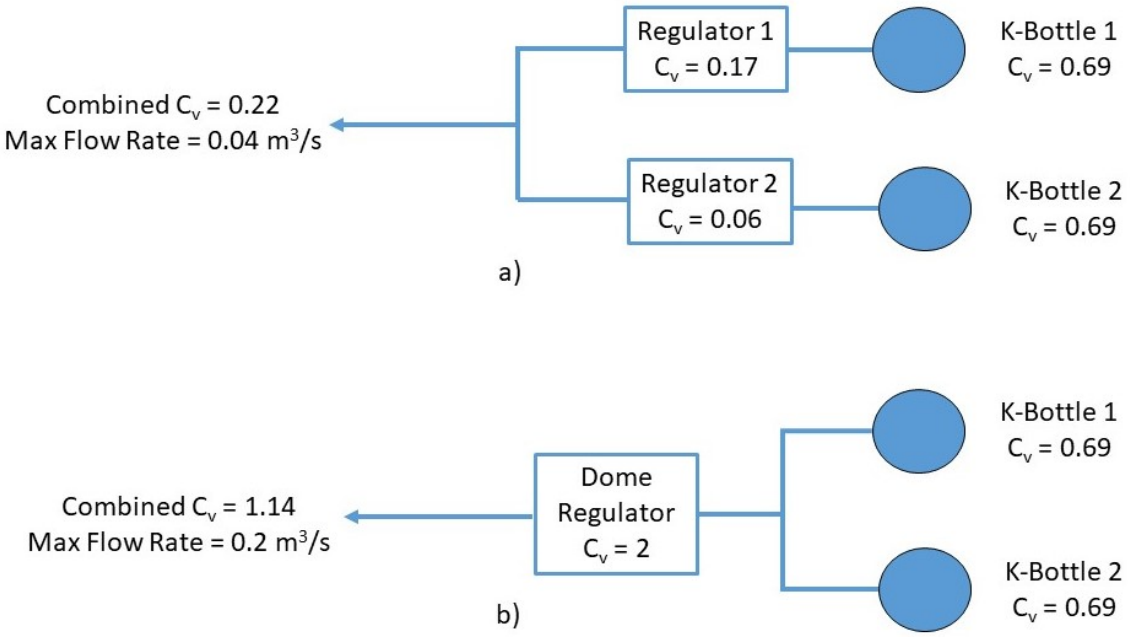

Figure 34. Diagram of a) initial regulator configuration and b) final configuration

$$\frac{1}{C_v^2} = \frac{1}{C_{v1}^2} + \frac{1}{C_{v2}^2} + \frac{1}{C_{vn}^2} + ... \tag{14}$$

$$Q = \frac{6.418 * 10^{-3} C_v P_1}{\sqrt{SG * T}} \tag{15}$$

For the fuel supply, the required volumetric flow rate of ethylene was an order of magnitude lower than nitrous-oxide and a specialty regulator was not needed. The

regulator and supply bottle valve had C_v values of 0.06 and 0.69 respectively, which resulted in a combined C_v of 0.06 using Eq. 14. The maximum flow rate the fuel system could achieve was found to be 0.030 m^3/s using Eq. 15, where $P_1 = 800$ psi, T = 540° R, and $SG = 0.992$. The 0.030 m^3/s flow rate was far above the anticipated testing range of 0.001-0.0082 m^3/s. After being regulated down to 2.2 MPa, the fuel could be fed directly the flow controller downstream. Between the flow controllers and the supply system for both the fuel and oxidizer, there were valves designed to shut off the flow of ethylene and nitrous-oxide when the bay doors were opened. This served as a safety mechanism so that any testing would be terminated in the event that the bay door was inadvertently opened.

Downstream of the supply components were flow controllers for the fuel and oxidizer as shown in Figure 32. The flow controllers selected were Alicat® MCRQ Flow Controllers due to their extensive use and familiarity at AFRL's DERF. The flow controllers were needed to ensure that an appropriate amount of reactants were being delivered to the engine. In addition to simply delivering the reactants to the engine, the flow controllers could be adjusted so that changes to the equivalence ratio could be made. The equivalence ratio, ϕ, could be calculated using Eq. 16, where $\dot{m}_f$ is the mass flow rate of the fuel, $\dot{m}_{ox}$ is the mass flow rate of the oxidizer, and *stoic* is the stoichiometric ratio of the fuel and oxidizer.

$$\phi = \frac{\left(\frac{\dot{m}_f}{\dot{m}_{ox}}\right)}{\left(\frac{\dot{m}_f}{\dot{m}_{ox}}\right)_{stoic}} \tag{16}$$

The desired test regime covered total mass flow rates between 0.025-0.075 kg/s and equivalence ratios between 0.5-1.5. The fuel controller supplied a mass flow rate of up to 0.011 kg/s for ethylene at standard temperature and pressure. With anticipated rates between 0.0013-0.010 kg/s, this offered enough range to meet the test objectives.

The oxidizer controller operated up to 0.082 kg/s allowing for testing between the anticipated 0.022-0.071 kg/s needed. The flow controllers could tolerate pressures up to 2.2 MPa and provide a measurement accuracy of ± 167 cm^3/s (±0.21 g/s at standard temperature and pressure) for the fuel controller and ±833 cm^3/s (±1.6 g/s at standard temperature and pressure) for the oxidizer. The flow controllers are discussed further in Section 3.3.

The flow controllers can be set remotely from the control room using a stand-alone laptop and Alicat Flow Vision® control software. In addition to operating the flow controllers, the software acts as a secondary data acquisition source since it was able to record flow rate, temperature, and pressure data from the controller.

Downstream of the flow controllers and immediately upstream of the engine were the last-chance isolation valves as shown in Figure 32. These valves were placed as close to the engine as possible to serve as the last-chance to turn-on or shut-off fuel and oxidizer to the engine. They were also the primary on/off mechanism for initiating fuel and oxidizer flow to the engine. The valves used were Swagelok® pneumatically actuated valves using 0.69 MPa shop nitrogen supply. The valves are normally closed but were opened when pressurized nitrogen was supplied to the valve.

Although last-chance valve actuation was done pneumatically, the remote operation of the valve was done digitally as shown in Figure 33. To command the valves open, a 5V signal was sent to a relay that activated a 24V circuit. When the 24V circuit was activated, a solenoid opened the pressurized nitrogen supply that actuated the last-chance valve open. The opened last-chance valve allowed fuel and oxidizer to flow into the engine. When the 5V control signal was turned off, the 24V circuit was de-activated which closed the solenoid and last-chance valve, cutting the flow of fuel and oxidizer to the engine.

Beyond controlling fuel and oxidizer to the engine, a mechanism for initiating a

detonation was needed. This was accomplished by using an automotive spark and ignition coil as shown in Figure 35. Initially the spark plug was placed at the exit plane of the RDE, but due to ignition issues, it was later re-positioned so that the electrode was inside the detonation channel (discussed in Section 4.1). The spark was initiated by sending a 5 ms, 5V trigger to an ignition coil. Once triggered, the ignition coil converted 12V power supplied by the facility to a 40 kV ignition pulse for the spark plug. The energy produced by the spark plug then ignited the reactants.

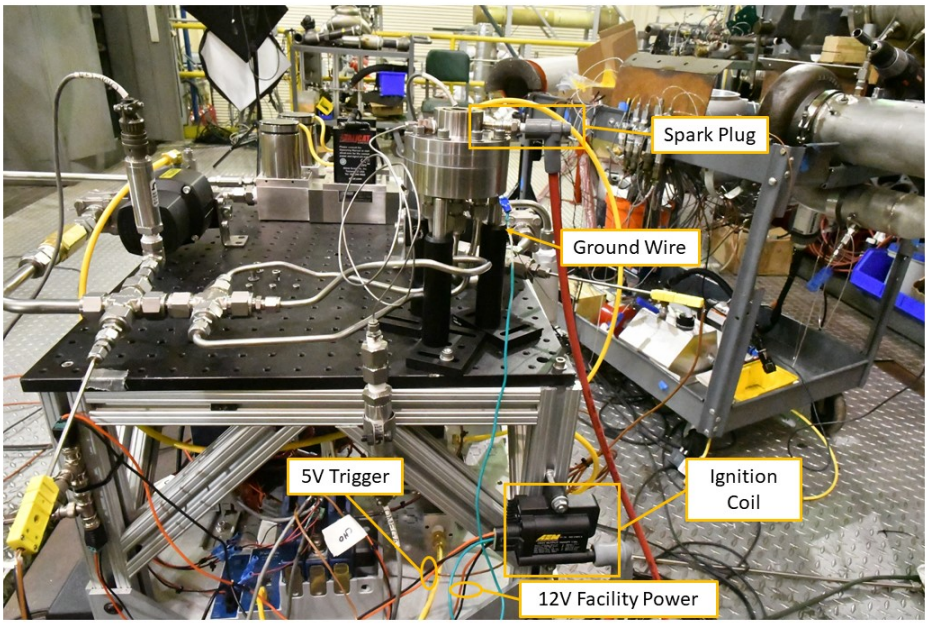

Figure 35. Layout of RDE ignition system

Opening of fuel and oxidizer valves, spark/detonation initiation, and valve cut-off needed to be carefully timed to achieve a successful test sequence. Figure 36 shows the timing sequence of one test run. Upon test initiation, there was a 1.0 s delay to serve as a momentary chance to stop an accidental activation of the test. At 1.0 s the oxidizer last-chance valve was opened. At 1.2 s, the fuel last-chance valve was opened. Fuel and oxidizer was then allowed to flow through the engine and soak the detonation channel with reactants while also allowing the mass flow rate controllers to

stabilize. At 5.5 s, the spark was activated for 5 ms to initiate the detonation. Finally, at 6.0 s the fuel and oxidizer valves were closed and the test case was terminated. The 0.5 s between spark initiation and the end of the test could be interpreted as a small amount of time, but with a 20 kHz detonation frequency, this allowed for 10000 detonation wave revolutions.

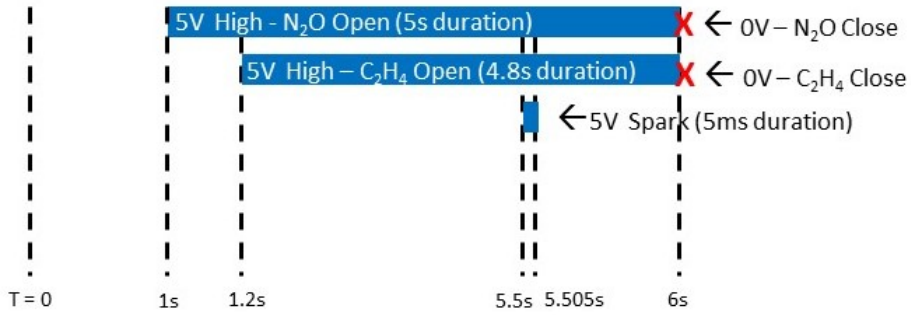

Figure 36. Timing of valves and spark during test sequence

The timing sequence was controlled using LabView® software and National Instruments® controller and data acquisition hardware. LabView® software was the user interface to control and monitor the test sequence as shown in Figure 37. The timing sequence of each component can be adjusted, where the time was in milliseconds. To begin data acquisition, the "RUN" icon was selected, then "Start Valve Sequence" was pressed to initiate the test sequence outlined in Figure 36. As shown in Figure 38, a laptop with LabView® software was connected to a National Instruments® NI-cDAQ9185 chassis via ethernet cable. The chassis hosted three data acquisition and control boards. Board one was a NI-9214 used to acquire temperature data and board two was a NI-9215 used to collect pressure readings. Board three was a NI-9923 which utilized three channels with a 5V signal to operate the fuel and oxidizer valves and trigger the spark during the control sequence.

An example test sequence can be seen in Figure 39. At approximately 1.2 s the N_2O and C_2H_4 valves are opened. The flow rates are allowed to stabilize as indicated

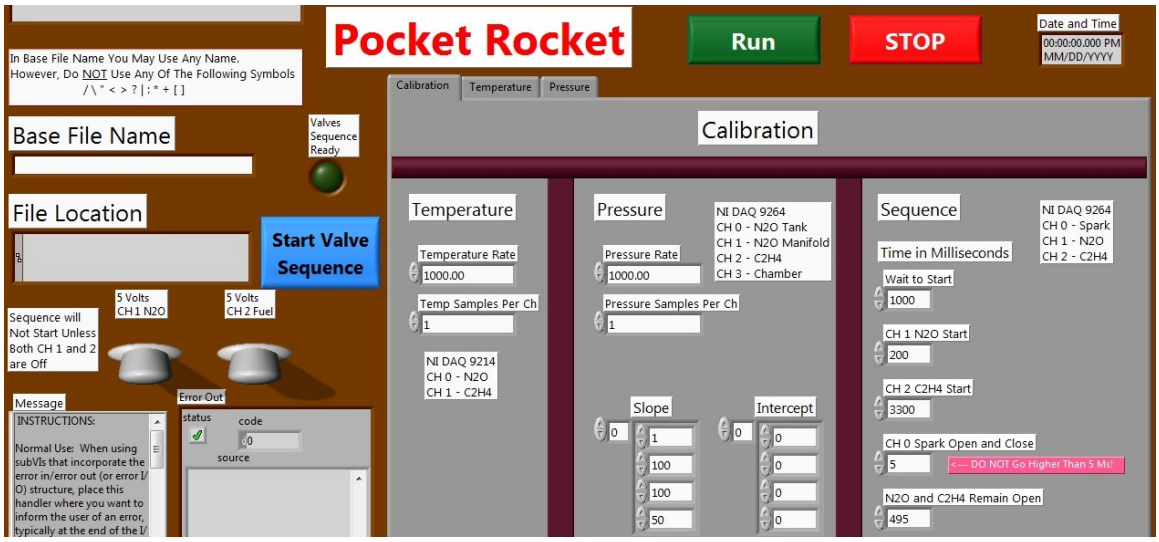

Figure 37. User interface for RDE control and data acquisition system

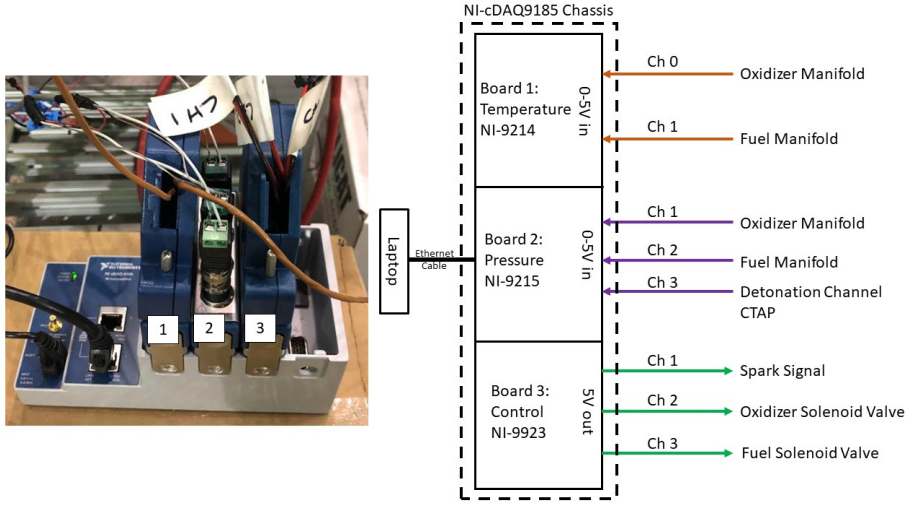

Figure 38. Data acquisition system control board and channel configuration

by the relatively constant pressures in both the fuel and oxidizer plenum pressures. At approximately 5.7 s the initiation of a detonation can be observed with the sharp rise in chamber pressure. At 6.5 s the N_2O, C_2H_4, and chamber pressure sharply fall indicating that the N_2O and C_2H_4 valves have been closed. There was an approximate 0.2-0.5 s delay between the commanded times and the actual times of the events in the control sequence. This did not pose a concern during the testing process as long

as the plenum pressures were able to stabilize prior to the spark/ignition.

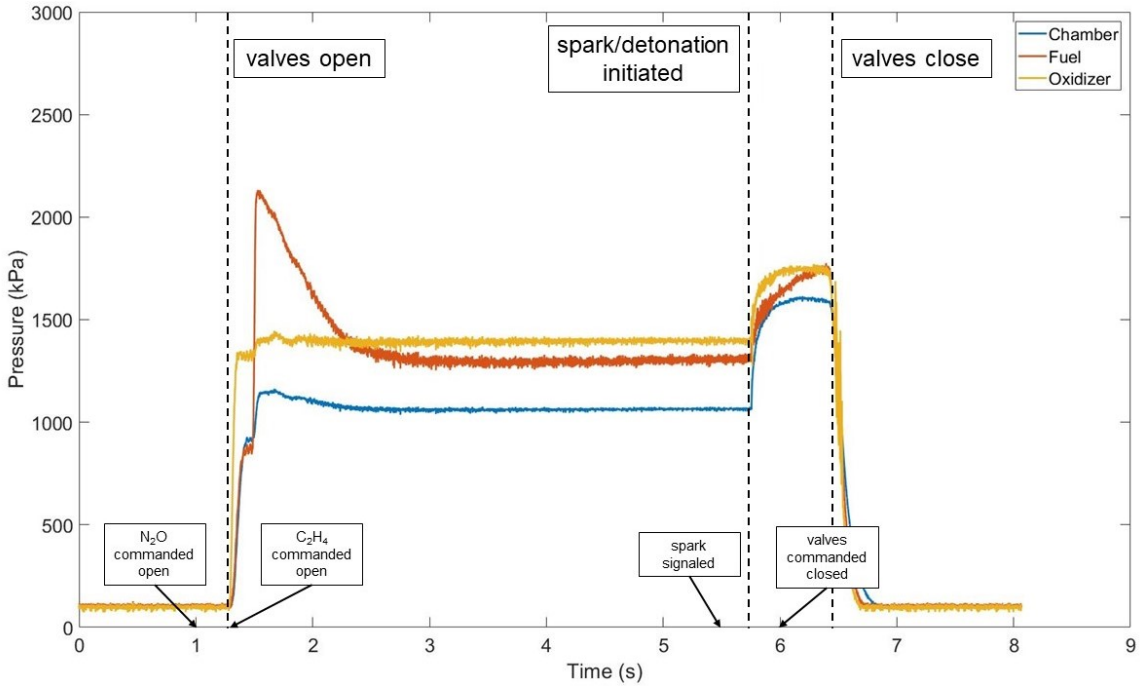

Figure 39. Example of pressure data captured during a test sequence

3.3 Instrumentation

Figure 40 shows a general layout of the instrumentation along the fuel and oxidizer paths to measure plenum pressures, plenum temperatures, detonation channel pressures, and monitor flow rates. Flow controllers for both the fuel and oxidizer were used to monitor and control the flow rates of reactants into the engine. Plenum pressure and temperature measurements in combination with detonation channel pressure instrumentation were used to understand the environment inside of the detonation channel as well as provide key information about the injection system's performance. Figure 40 also shows the location of the high speed camera and microphone used to capture the detonation frequency and engine acoustics.

Alicat® MCRQ flow controllers were used to monitor flow rates for both the fuel

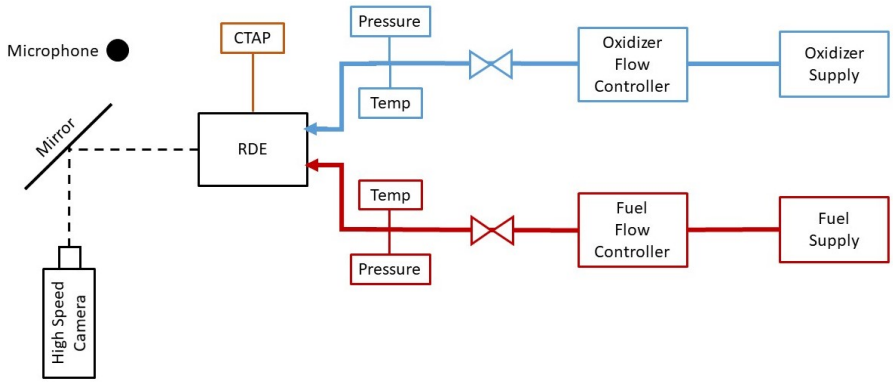

Figure 40. Schematic of RDE Instrumentation

and oxidizer. Their specifications can be seen in Table 1 below and were capable of measuring the required fuel flow rates of 1000-8180 cm^3/s and oxidizer flow rates of 10900-36000 cm^3/s needed for testing. The flow controllers also had temperature and pressure data available, but this was only used as a secondary measurement to the temperature and pressure instrumentation further downstream.

Table 1. Specifications for Alicat® MCRQ Flow Controllers

Fuel	
Operating Range	167-8330 cm^3/s
Maximum Pressure	2.2 MPa
Accuracy	$\pm$ 167 cm^3/s (2% of Max Flow Rate)
Oxidizer	
Operating Range	833-41700 cm^3/s
Maximum Pressure	2.2 MPa
Accuracy	$\pm$833 cm^3/s (2% of Max Flow Rate)

Temperature and pressure were measured just upstream of the connection plate on both the fuel and oxidizer supply lines which served as a means to capture plenum data as shown in Figures 41 and 42. The thermocouples could not be inserted directly into their respective plenums due to the limited space on the connection plate as shown in Figure 28. Temperature was measured using "K" type Omega® thermocouples in combination with National Instruments® NI-9214 Temperature Input

Module. The input module interpreted the voltage signal from the thermocouples to an accuracy of ±2.12K at temperatures between 233-343K, which covered the anticipated temperature range of 250-300K.

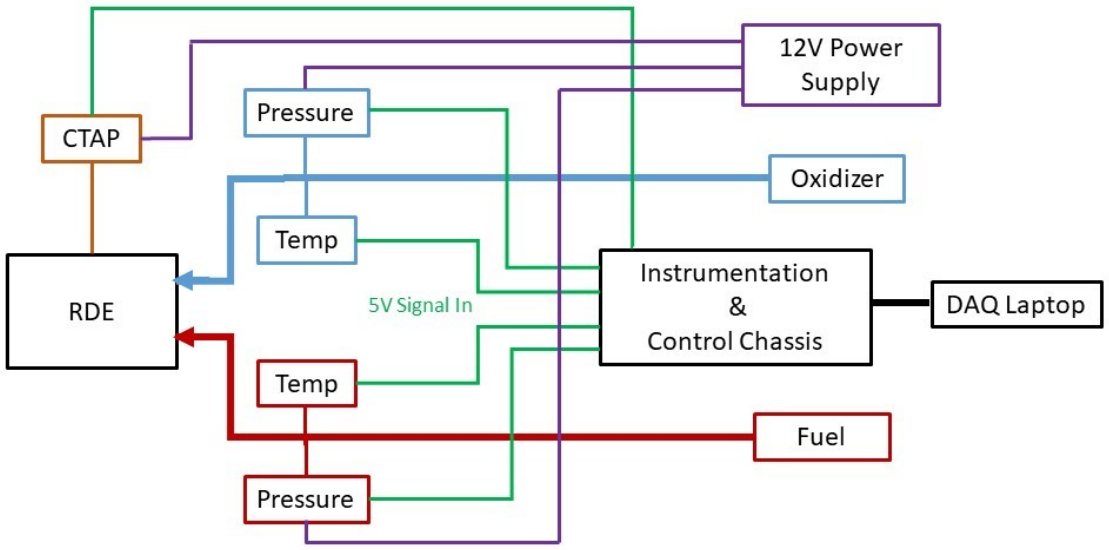

Figure 41. Schematic of temperature and pressure instrumentation

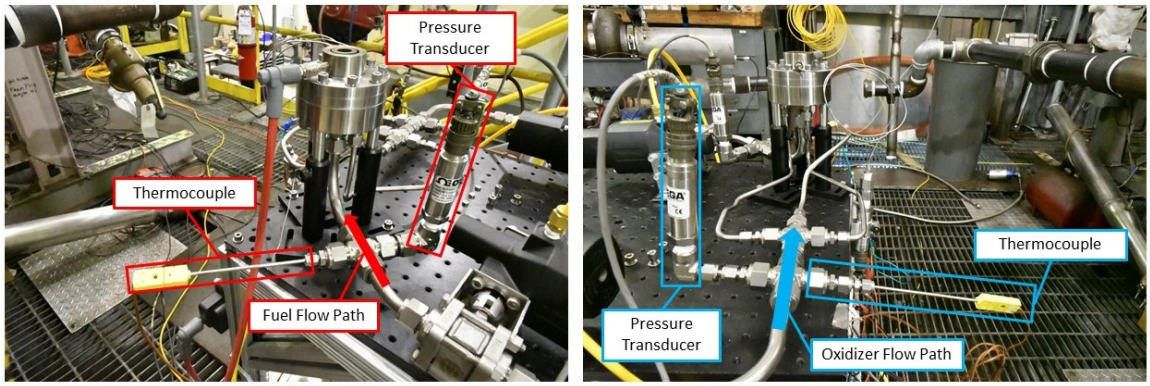

Figure 42. Layout of temperature and pressure instrumentation for a) fuel and b) oxidizer

Pressure transducers to capture plenum data were also placed just upstream of the connection plate due to space restrictions. The transducers used were Omega ®

PX429-500A5V transducers rated for 0-3.45 MPa and were accurate between ±0.08% of the reading. The transducers were powered by a 12V power source or "excitation" voltage as shown in Figure 41. The transducers returned a 0-5V output signal to the National Instruments® NI-9215 module which interpreted the signal and converted it into a pressure reading. The module interpreted the transducer voltage with an accuracy of ±0.2% of the reading at temperatures between 233-343K. Pressure was calculated by linearly scaling the voltage across the transducer's pressure range. As seen in Figure 37, the slope was set to 100 so that for every 1V of output, the pressure reading increases by 0.69 MPa. In this configuration, the probes captured static pressures of the fuel and oxidizer directly upstream of their respective plenums.

A Capillary Tube Averaged Pressure (CTAP) device was used to capture the average static pressure inside of the detonation channel as shown in Figure 43. A 1.6 mm diameter, 1 m long tube was connected to the outer body of the RDE 10 mm downstream of the oxidizer manifold. At the opposite end of the tube was an Omega® PX429-250A5V transducer. The transducer was connected to the NI-9215 module and was powered in the same manner as the fuel and oxidizer plenum transducers discussed previously. The transducer was rated to 0-1.7 MPa with an accuracy of ± 0.08% of the reading.

Using a the fuel plenum pressure, P_f, oxidizer plenum pressure, P_{ox}, and the channel pressure, P_c, an relationship between the detonation channel pressure and the injection pressures could be developed. Additionally, momentum flux ratios could be quantified to determine their influence on the operating parameters of the RDE. Figure 44 is a sample test run at $\phi = 1.2$, $\dot{m} = 0.075$ kg/s. The pressure ratios remain stable prior to ignition with $\frac{P_{ox}}{P_f} = 1.1$, $\frac{P_f}{P_c} = 1.2$, and $\frac{P_{ox}}{P_c} = 1.3$. Following detonation at 5.9 s, $\frac{P_{ox}}{P_f}$ increased in fluctuation, but was still ≈ 1.1, $\frac{P_f}{P_c}$ decreased to 1.0, and $\frac{P_{ox}}{P_c}$ = 1.1. Just prior to the valves closing, $\frac{P_{ox}}{P_f}$ decreased to 1.0, $\frac{P_f}{P_c}$ increased to 1.1, and

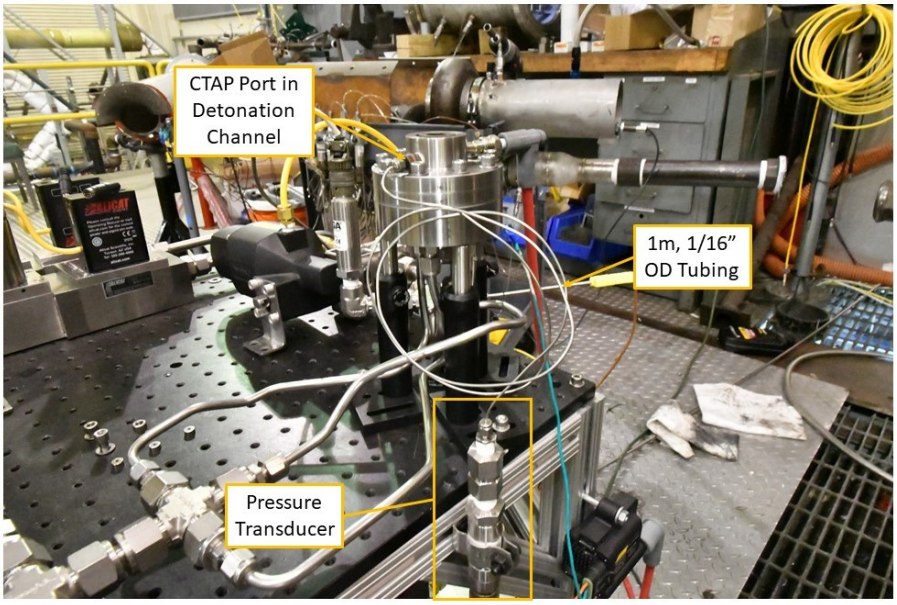

Figure 43. View of CTAP instrumentation set-up

$\frac{P_{ox}}{P_c}$ remained at 1.1. Using this data, conditions before and during the detonation can be analyzed to understand how injection pressures affected engine operability.

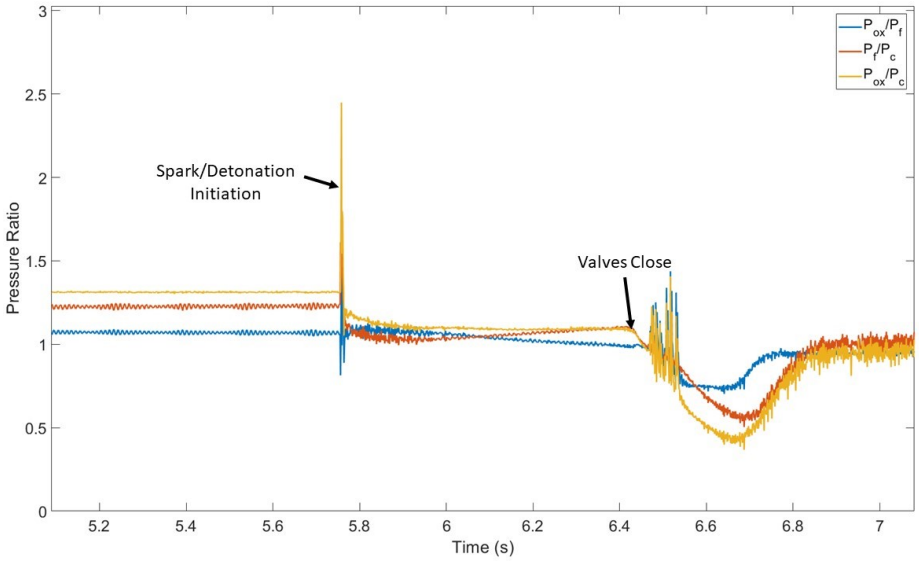

Figure 44. Sample of pressure ratio data from a test case at ϕ= 1.2, $\dot{m}$ = 0.075 kg/s

To determine the detonation frequency, a Phantom® v711 high-speed camera

was used to capture footage of the rotating detonation wave as shown in Figures 46 and 47. To protect the camera from the hot RDE exhaust, a mirror was placed above the RDE so that the camera could be located to the side of the test stand. Camera recording was triggered by the same 5V signal that triggered the spark used to initiate the detonation. For the current research, the camera was set to 210,000 frames per second at a resolution of 128 x 128 pixels which offered an ideal balance of frame rate and resolution. At this frame rate, the position of the detonation wave could be over-sampled approximately ten times per revolution at a 20 kHz detonation frequency. The detonation wave was expected to produce the brightest light through the duration of the test run. Therefore, the exposure duration was set so that other sources of light such as deflagration or bay lighting would be filtered out. An exposure setting between 1-1.7 μs produced favorable results to filter out light not associated with the detonation while still allowing the detonation wave to be visible. In all cases, the camera settings were subjective to the user and could be adjusted based on personal visual preferences. In terms of accuracy, the camera was able to capture frames equally spaced in time, $\pm$ 20 ns.

Initially, techniques similar to those used by Boller et al. [27] to determine the detonation's location and velocity was attempted by determining the peak light intensity of each frame captured by the camera. The individual frames from each video were imported into MATLAB, and the location of the top 1% of the brightest pixels was found. Then, the center point of this area was used to determine the detonation's location. This process was repeated to calculate the angular velocity, ω, between each frame using Eq. 17, where $d\theta$ is the angular change between frames and dt amount of time between frames. The average of these velocities were then taken to determine an overall velocity of the test. With a known angular velocity, the detonation frequency could be found using Eq. 18, where r_o is the outer radius of the detonation channel.

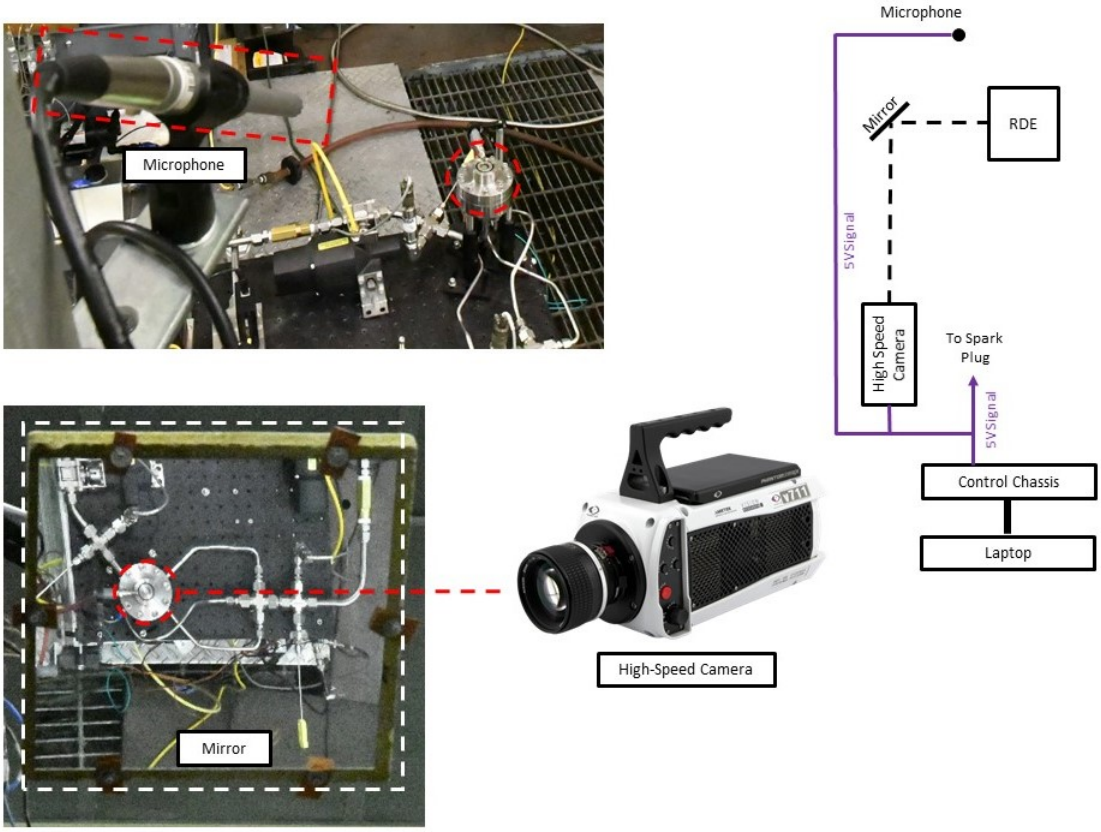

Figure 45. Layout of high-speed camera and microphone

$$\omega = \frac{d\theta}{dt} \tag{17}$$

$$D = \omega r_o \tag{18}$$

As seen in Figure 47, the detonation wave was not encapsulated by a single point, which made defining the detonation wave location difficult. The MATLAB program attempted to define the wave's location by finding the center point of the brightest pixels in each frame, but this may not be the actual location of the wave. Later testing revealed that the detonation wave was generally unstable and the point of brightest light in the image was not necessarily the location of the detonation wave.

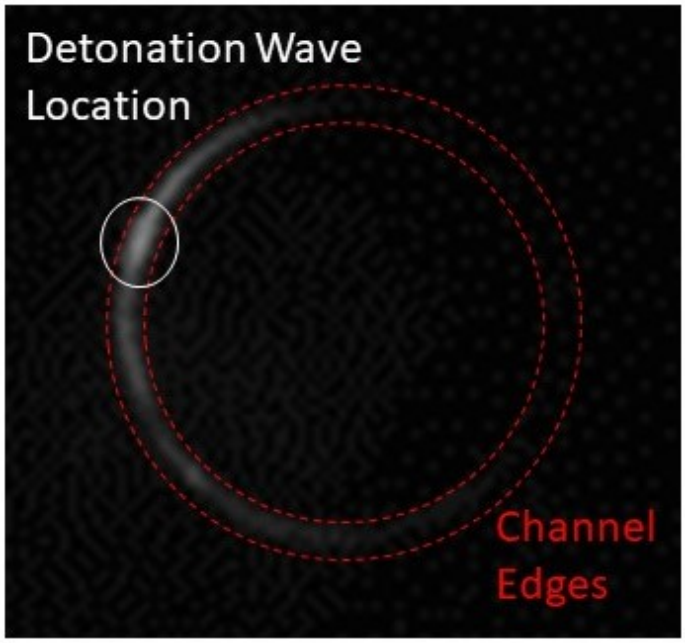

Figure 46. Sample image from high-speed camera during test run

Additionally, there were intermittent periods where the detonation wave dissipated. Using an automated process could have introduced erroneous velocity data (discussed in Section 4.5). Therefore, the detonation wave speed was manually calculated by counting the number of frames required for the wave to make one full revolution around the detonation channel as shown in Eq. 19. From this data the detonation frequency could also be calculated using Eq. 20.

$$D = \frac{d_c \pi}{n_{frames} \Delta t} \tag{19}$$

$$f = \frac{D}{d_c \pi} \tag{20}$$

The high-speed camera data was supplemented by a Behringer® ECM 8000 condenser measurement microphone as shown in Figure 48a. The microphone signal was processed by a Behringer® UM2 interface where microphone gain settings and the sig-

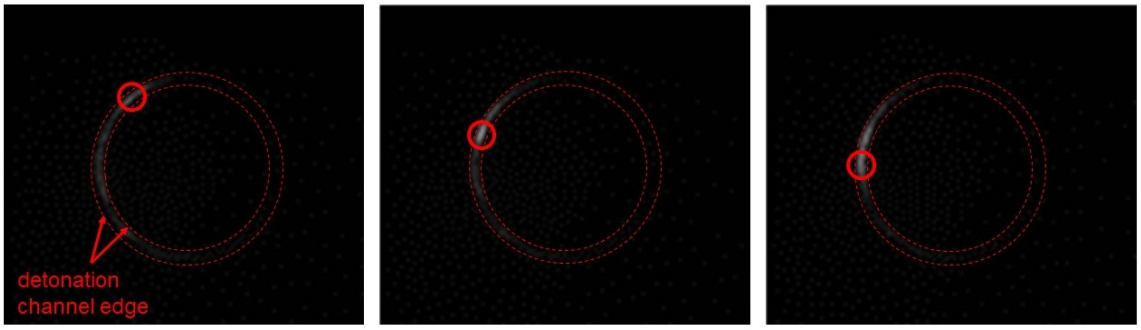

Figure 47. Sequential images showing the angular movement of a detonation wave separated by 4.8 μs between frames

nal output level could be adjusted as shown in Figure 48b. The gain setting adjusted the input voltage to the microphone and the output setting determined the level of signal amplification that was output from the interface device. The interface device produced a voltage that was sent to a high-speed data acquisition system (DAQ) in the control room.

The voltage readings were sampled at 100 kHz and interpreted by the DAQ software to be logged as data as shown in Figure 49 during a test run at $\dot{m} = 0.075$ kg/s, $\phi = 1.0$. Steady amplitude peaks/valleys can be seen at ± 0.85 V for 0.82 s, which was the result of sound produced from the detonation wave. After 0.82 s, the amplitude of signal begins to taper as the test sequence ends and the detonation wave dissipates. This acoustic data was then read into MATLAB® and using a FFT, the dominant frequencies could be observed. The peak magnitude was assumed to be the detonation frequency. This result was reinforced by high-speed imagery data that revealed a frequency range that agreed with the acoustic data. In this example, the detonation frequency was found to be 13.3 kHz.

Testing later revealed that tuning the microphone to produce usable data was a significant challenge. In most cases, the microphone either did not pick up any acoustic data or the sound levels were too intense and the microphone became satu-

Figure 48. Images of the a) Behringer® ECM 8000 condenser-measurement microphone and b) UM2 interface device

rated. Microphone readings immediately after the data capture shown in Figure 49 did not produce usable data with the same microphone settings and engine operating conditions. The microphone likely had a narrow operating band where it was able to capture acoustic readings and slight variations in decibel levels for each test case may have pushed the microphone out of this band. Few test runs produced acoustic data that could be interpreted as operating frequency from the engine. Therefore, the acoustic data was generally not used (discussed in Section 4.5).

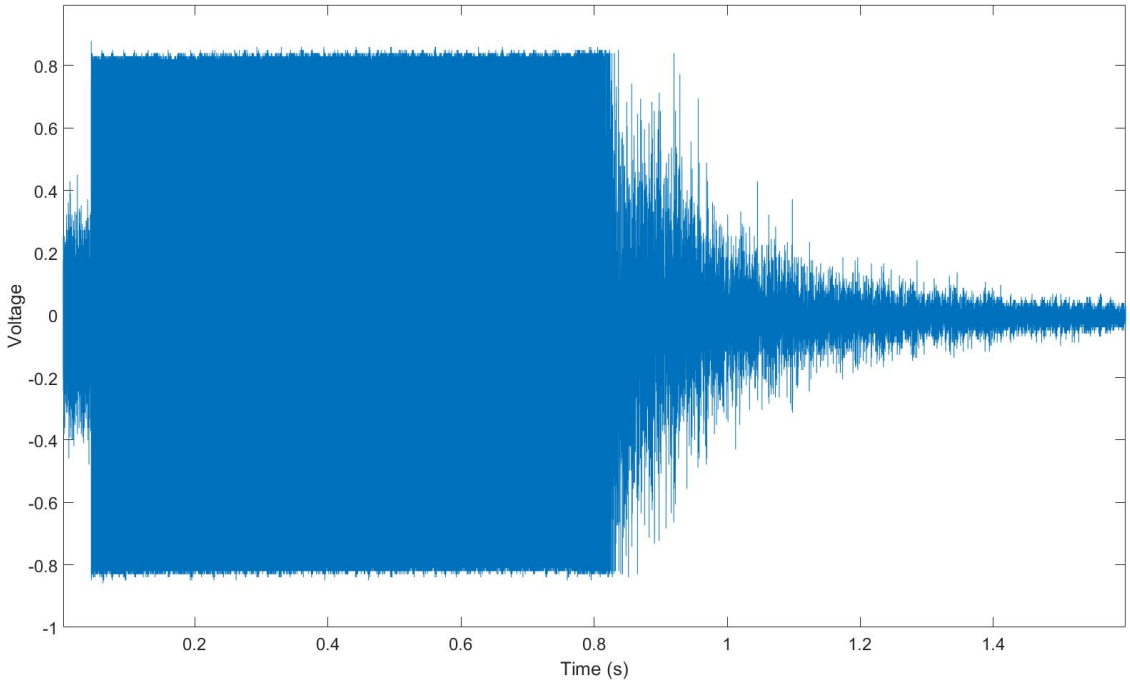

Figure 49. Sample of acoustic data captured during a test run at $\dot{m} = 0.075$ kg/s, $\phi = 1.0$ from the Behringer® ECM 8000 microphone

3.4 Uncertainty Analysis

An uncertainty analysis was conducted for pressure ratio, momentum ratio, equivalence ratio, and detonation wave speed/frequency calculations to account for the error associated with the measurements used to find these parameters. The uncertainty analysis was completed using methods from Moffat [28]. The general equation for total error, δ_α, is shown in Eq. 21, where α is the value being calculated, β is the measured value, δ_β is the systematic error of the instrument, and n is the number of measured values associated with the calculation, α. A summary of uncertainty error for the calculations discussed in this section are presented in Table 3.

$$\delta_\alpha = \sqrt{\sum_{i=1}^{n} \frac{d\alpha}{d\beta}^2 \delta_\beta^2} \tag{21}$$

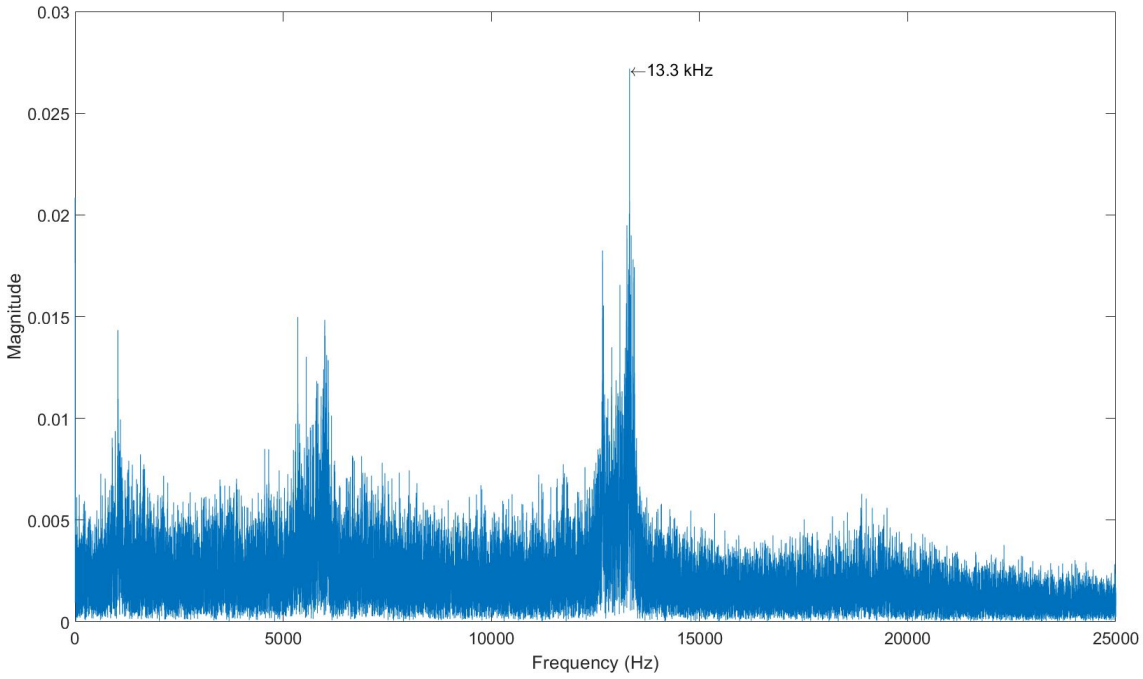

Figure 50. Sample FFT of acoustic data to determine detonation frequency

To determine the uncertainty for the ratio of fuel pressure to channel pressure, $R_{f,c}$, the partial derivative of Eq. 22 was taken for each variable as shown in Eqs. 23 and 24.

$$R_{f,c} = \frac{P_f}{P_c} \tag{22}$$

$$\frac{dR_{f,c}}{dP_f} = \frac{1}{P_c} \tag{23}$$

$$\frac{dR_{f,c}}{dP_c} = \frac{P_f}{P_c^2} \tag{24}$$

With a known accuracy of the pressure transducer, δ_P, the error associated with the ratio of fuel pressure to channel pressure, $\delta_{Rf,c}$, was calculated using Eq. 25.

$$\delta_{Rf,c} = \sqrt{\frac{dR_{f,c}}{dP_f}^2 \delta_{P_f}^2 + \frac{dR_{f,c}}{dP_c}^2 \delta_{P_c}^2} \tag{25}$$

The same process was followed to calculate error associated with the ratio of oxidizer pressure to channel pressure, $R_{ox,c}$, and the ratio of oxidizer pressure to fuel pressure, $R_{ox,f}$. Minimum and maximum error values for $R_{f,c}$, $R_{ox,c}$ and $R_{ox,f}$ are shown in Table 3.

To calculate the error associated with momentum flux ratio, the partial derivative of $J = \gamma_f P_f M^2 / \gamma_{ox} P_{ox} M^2$ was taken as shown in Eqs. 26 and 27, where M was assumed to be 1.0 with choked flow through the injectors.

$$\frac{dJ}{dP_f} = \frac{\gamma_f}{\gamma_{ox} P_{ox}} \tag{26}$$

$$\frac{dJ}{dP_{ox}} = \frac{-\gamma_f P_f}{\gamma_{ox} P_{ox}^2} \tag{27}$$

The error associated with momentum flux ratio, δ_J, was then calculated using Eq. 28 using the accuracy of the pressure transducers.

$$\delta_J = \sqrt{\frac{dJ}{dP_f}^2 \delta_{P_f}^2 + \frac{dJ}{dP_{ox}}^2 \delta_{P_{ox}}^2} \tag{28}$$

The equivalence ratio for each test case was a function of how accurately the mass flow rate controllers could control the flow. In addition to the inherent variability of the mass flow rate controllers themselves, there were inaccuracies associated with what equivalence ratio was reported during each test run. The mass flow rate controllers were not operated from the same computer as the main DAQ/sequence controller. Therefore, the timing information from the mass flow controllers and the DAQ were not the same. Because of this, it was impossible to synchronize the mass flow rate data with the sequence of events from a test run. Instead, the individual responsible for

operating the mass flow controllers would observe the flow rates just prior to ignition and report whether or not the flow rate was within 5% of the desired value. This additional uncertainty needed to be accounted for in the total measurement accuracy. The combined accuracy for the mass flow rate controllers was found using Eq. 29, where δ_{ctr} is the accuracy of the mass flow rate controller, δ_{obs} is the accuracy of the observed value, and $\delta_{\dot{m}}$ is the combined accuracy.

$$\delta_{\dot{m}} = \sqrt{\delta_{ctr}^2 + \delta_{obs}^2} \tag{29}$$

With the combined accuracy, an uncertainty for equivalence ratio was calculated using the same method as discussed previously using Eq. 16 from Section 3.2 and Eqs. 30-32.

$$\frac{d\phi}{d\dot{m}_f} = \frac{1}{\dot{m}_{ox}} \left(\frac{\dot{m}_{ox}}{\dot{m}_f} \right)_{stoic} \tag{30}$$

$$\frac{d\phi}{d\dot{m}_{ox}} = \frac{-\dot{m}_f}{\dot{m}_{ox}^2} \left(\frac{\dot{m}_{ox}}{\dot{m}_f} \right)_{stoic} \tag{31}$$

$$\delta_\phi = \sqrt{\left(\frac{d\phi}{d\dot{m}_f} \right)^2 \delta_{\dot{m}_f}^2 + \left(\frac{d\phi}{d\dot{m}_{ox}} \right)^2 \delta_{\dot{m}_{ox}}^2} \tag{32}$$

The equivalence ratio error had a minimum value of ± 0.05 and a maximum value of ± 0.2. The operating condition that corresponded with maximum error was at $\dot{m}$ = 0.025 kg/s, $\phi = 1.5$. Error associated with δ_{obs} was negligible when compared to δ_{ctr}. The δ_{obs} only affected measurement accuracy by $\phi \pm 0.01$.

Determining the detonation wave speed and frequency also included some error from both the camera and the observer. The error associated with wave speed and frequency as a result of the camera's timing accuracy was found by first taking the partial derivatives of Eqs. 19 and 20 from Section 3.3. Error could then be calculated

using Eqs. 33 and 34.

$$\delta_D = \sqrt{\left(\frac{-\pi d_c}{n_{frames}\Delta t}\right)^2 \delta^2_{\Delta t,cam}} \tag{33}$$

$$\delta_f = \sqrt{\left(\frac{1}{d_c \pi}\right)^2 \delta^2_D} \tag{34}$$

Because the location of the wave was manually determined, some subjectivity was inherently introduced into the wave speed and frequency calculations that was not quantifiable. Additionally, the exact amount of time required for the wave complete one full rotation could not be precisely determined since the wave front may change angular position 15-30° between frames as shown in Figure 51. Therefore, instead of stating an exact wave speed and frequency, a possible range was given based on the frame count immediately prior to the wave completing one revolution and just after it passed the origin as shown in Table 3. To observe one full revolution of the detonation wave, 15-18 frames were needed. Minimum and maximum error values for detonation wave speed and frequency as a result of the camera's timing accuracy are shown in Table 2.

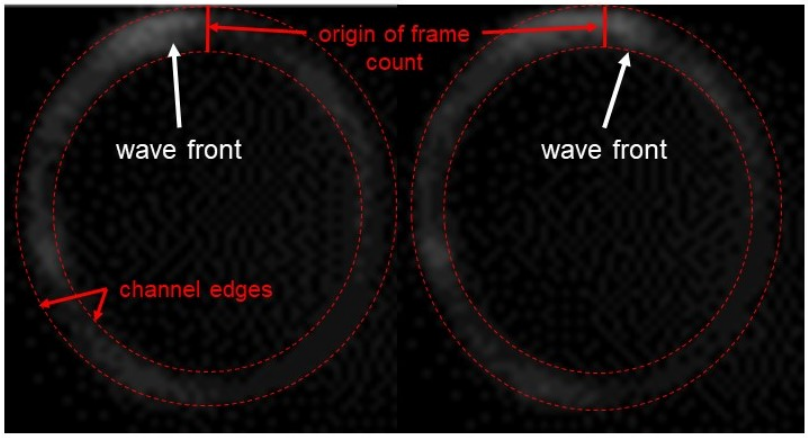

Figure 51. Images of detonation wave prior to completing one revolution (left) and immediately after (right)

Table 2. Summary of error for calculated values

Parameter	**Minimum Error (±)**	**Maximum Error (±)**
P_f/P_c	0.0011	0.003
P_o/P_c	0.0014	0.0034
P_o/P_f	0.002	0.0010
J	0.00062	0.0013
ϕ	0.05	0.2
D	$2.05{\cdot}10^{-5}$ m/s	$2.46{\cdot}10^{-5}$ m/s
f	$2.33{\cdot}10^{-4}$ Hz	$2.80{\cdot}10^{-4}$ Hz

IV. Results and Discussion

The engine discussed in this research was built to operate at a detonation frequency of 20 kHz while also reducing mass flow rates. To accomplish this, the engine was designed with a 28 mm detonation channel diameter, assuming that the detonation wave speed was approximately 1760 m/s (80% of CJ velocity) using ethylene and nitrous-oxide as the fuel and oxidizer. Section 4.1 discusses the initial testing attempts and the challenges that were encountered with the original engine design. Section 4.2 investigates the the operating characteristics after incorporating a nozzled centerbody. This analysis is followed by an examination of detonation behavior in Section 4.3. Section 4.4 analyzes the operation of the engine in terms of injection performance. Finally, a detonation frequency analysis is presented in Section 4.5.

4.1 Initial Results with Original Engine Configuration

The initial design of the RDE shown in Figure 52 did not initially produce a detonation wave. The engine was tested at mass flow rates between 0.025-0.075 kg/s at equivalence ratios between 0.5-1.5. For each test case, a high speed camera captured images of the aft end of the detonation channel. The images were investigated for evidence of a detonation wave, where the expected condition for a detonation was a point of bright light rotating around the detonation channel. The high speed imagery was also supplemented by acoustic data that was captured by a microphone, where the expected frequency of would be approximately 20 kHz.

All cases tested in the configuration shown in Figure 52 failed to yield evidence of a successful detonation. The primary reason for unsuccessful denotation was thought to be the inability of the flame to reach the detonation channel after being ignited at the exit plane of the engine. Figure 53 shows high-speed imagery of test cases at: a)

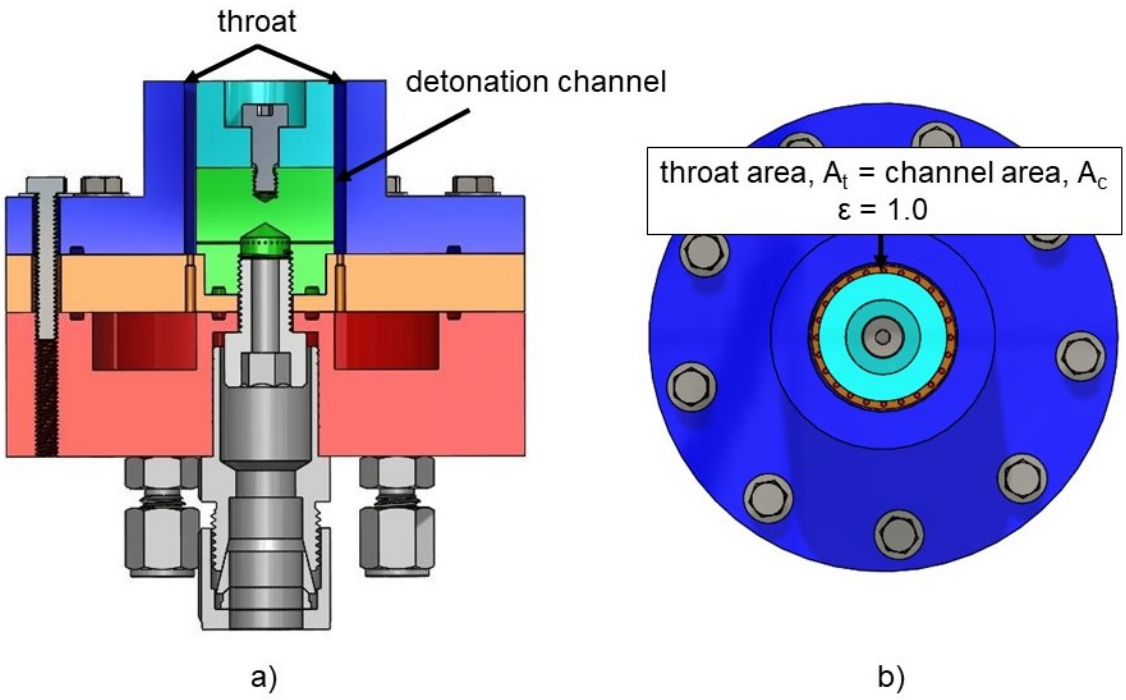

Figure 52. Original configuration of the RDE showing a) side cross-section and b) aft end looking into the detonation channel

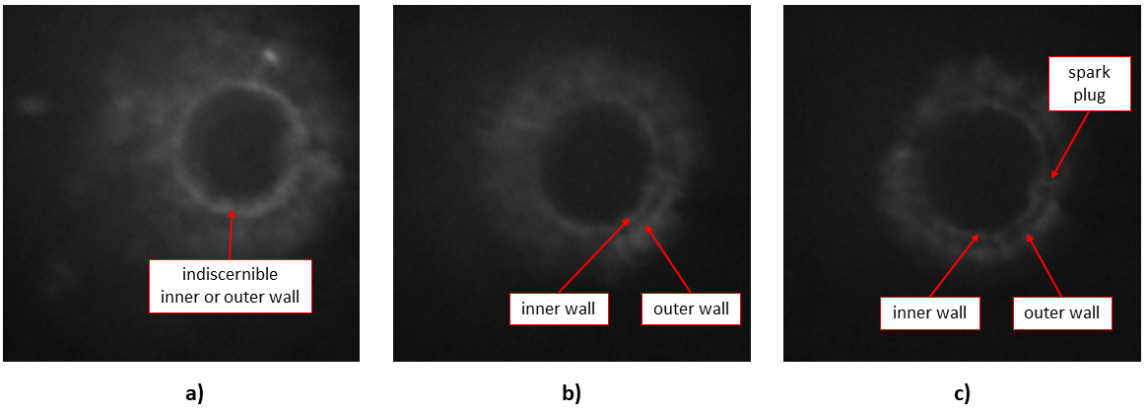

Figure 53. High-speed imagery of deflagration at a) $\dot{m}$=0.05 kg/s, ϕ=1.0 b) $\dot{m}$=0.025 kg/s, ϕ=1.0, and c) $\dot{m}$=0.0125 kg/s, ϕ=1.2.

$\dot{m}$=0.05 kg/s, ϕ=1.0, b) $\dot{m}$=0.025 kg/s, ϕ=1.0, and c) $\dot{m}$=0.0125 kg/s, ϕ=1.2. At a mass flow rate of 0.05 kg/s the flame could be seen on either the inner or outer rim of the detonation channel (indiscernible). The combustion event shown appeared to be

deflagration only due to the generally uniform intensity of light at the exit plane of the engine. When mass flow rate was reduced to 0.025 kg/s, flames on portions of both the inner and outer edges of the detonation channel became visible. Deflagration was seen around the full circumference of the inner channel edge and on the bottom-right quadrant of the outer edge. Reducing the mass flow rate even further to 0.0125 kg/s (beyond the planned test range), flames on the inner and outer wall edges became more distinguishable and could be seen around the full circumference of both wall edges. The inner and outer wall edges appear to be serving as a flame holding region for the reaction, but even the edges appeared to be on the cusp of the flame's blowout velocity at the higher mass flow rates of 0.025 and 0.05 kg/s since the flame could not be clearly seen around the full circumference of both edges. Flame holding on the inner and outer edges of the channel could indicate that the velocity of the gas in the center of the channel was too high relative to flame speed of the reactants.

Further reduction of mass flow rates below 0.0125 kg/s may have decreased the exit velocity to be within the range of the reactant flame speeds. However, reducing the mass flow rate would be counterproductive to achieving the fill height necessary for detonation. Attempts to ignite the reactants at mass flow rates between 0.06-0.075 kg/s proved to be unsuccessful. The gas exit velocity further overpowered the flame speed of the reactants to a point where they could not be ignited at all. The gas exit velocity from the channel was found to be between 84-148 m/s for the range of mass flow rates tested, where the flow was assumed to be unchoked exiting the engine in the absence of a nozzle or flow constriction.

Research by Wang et al. found maximum laminar flame speeds, S_l, for ethylene and nitrous-oxide mixtures to be approximately 1.10 m/s at an equivalence ratio between 1.2-1.4 [29]. With a known laminar flame speed, the maximum turbulent flame speed, S_t, was calculated using Eq. 35, which resulted in a value of 23.8 m/s

(assuming velocity fluctuation, $v_{rms}^{'}$, was 10% of the exit gas velocity) [2].

$$S_t = 3.5 S_l (\frac{v_{rms}^{'}}{S_l})^{0.7} \tag{35}$$

With this disparity between the flame speed and exit velocity, the flame was unable to enter the channel and could only anchor in recirculation zones at the inner and outer edges of the channel wall.

In order to overcome detonation initiation issues, two possible solutions were considered: the addition of a back plate at the exit plane of the engine and installing the spark plug inside the detonation channel. The back plate would serve to increase the channel pressure which could slow the flow velocity inside of the channel. Using Eq. 36, Mach number would be reduced if the ratio of static pressure, P_s, over the total pressure, P_t, was increased.

$$\frac{P_s}{P_t} = (1 + \frac{\gamma - 1}{2} M^2)^{\frac{-\gamma}{\gamma - 1}} \tag{36}$$

Therefore, by increasing the static pressure in the channel, the Mach number and resulting axial velocity inside the detonation channel would be reduced. As an added benefit, the increased pressure could result in decreased cell size as shown by Babbie et al. [15]. Additionally, decreased cell size could improve detonation stability as researched by Kudo et al. by increasing r_i/λ [8] (discussed in Section 2.5).

In the configuration shown in Figure 52, there was no flow constriction or nozzle at the aft end of the detonation channel. Therefore, the exit area ratio, ϵ, was equal to 1.0 as calculated by Eq. 37, where A_t is the area of the throat (i.e. area at the exit plate) and A_c is the area of the channel ($A_c = A_t = 163$ mm^2).

$$\epsilon = \frac{A_t}{A_c} \tag{37}$$

To increase static pressure and reduce the Mach number in the channel, the addition of a back plate was implemented by fastening a 27.5 mm washer to the centerbody of the engine which reduced the exit area from 163 mm^2 to 21.8 mm^2 as shown in Figures 54a and 54b. As shown in Figure 54c, this resulted in an area ratio, ϵ, of 0.133. With a smaller exit area, the flow was assumed to be choked at the exit plane/throat for the range of mass flow rates tested.

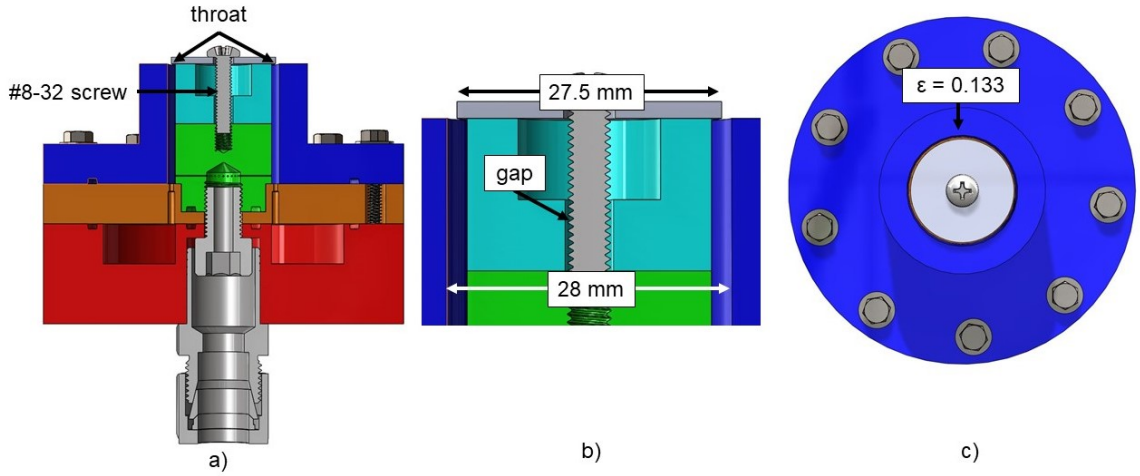

Figure 54. Configuration with washer/back plate a) cross-section view b) exploded view of washer, screw and centerbody and c) aft view of detonation channel/washer

Using this area ratio, the Mach number in the channel could be calculated using the transcendental equation, Eq. 38, and iteratively solving for M.

$$\frac{1}{\epsilon} = \frac{\gamma+1}{2}^{-\frac{\gamma+1}{2(\gamma-1)}} \frac{(1+\frac{\gamma-1}{2}M^2)^{\frac{\gamma+1}{2(\gamma-1)}}}{M} \tag{38}$$

The Mach number in the channel was calculated to be 0.078, which reduced the velocity of the flow in channel from the previous 84-148 m/s to approximately 20.7 m/s, which was now within the range of ethylene and nitrous-oxide's turbulent flame speed.

With a reduced Mach number in the channel, CTAP data indicated that static pressure also increased as expected. The static pressure ranged between 103-176 kPa

at mass flow rates between 0.025-0.075 kg/s at an equivalence ratio of 1.0 prior to adding a back plate. After adding the back plate, the channel pressure was increased to 176-345 kPa under the same conditions.

Although increased pressure created by the back plate slowed the flow velocity inside the detonation channel, the velocity at the exit plane would increase due to the reduced cross sectional area. The exit velocity was calculated to be 269 m/s using Eq. 12, assuming that $M = 1.0$ at the throat. As shown in Figure 55, the spark plug was positioned at the exit plane/throat of the channel where the flow velocity was at a maximum. With this configuration it became more difficult to ignite the reactants.

To overcome this, the electrode tip of the spark plug was re-positioned inside the detonation channel to take advantage of the lower velocity inside of the channel using the washer/back plate to reduce the exit area as shown in Figures 55b and 55c. Placing the spark plug in the channel was not initially implemented due to concerns of the spark plug creating flow disturbances in the relatively small geometries of the RDE's detonation channel. As shown in Figure 55c, the spark plug required an 8 mm diameter hole, which was relatively large in comparison to the 30 mm long and 2 mm gap of the detonation channel. However, this configuration was reconsidered after failed attempts to initiate a detonation with the spark plug at the exit plane of the engine.

Using the washer/back plate and repositioned spark plug, test cases were run at equivalence ratios of 0.8-1.2, and mass flow rates between 0.04-0.08 kg/s. More test points were not pursued due to the challenges encountered using this configuration (discussed later in this section). Of the 14 operating conditions attempted, 4 points resulted in successful detonation as shown in Figure 56. At an equivalence ratio of 1.0, detonation was achieved at mass flow rates of 0.065, 0.07, and 0.08 kg/s. Additionally, a detonation was achieved at an equivalence ratio of 0.9 and mass flow

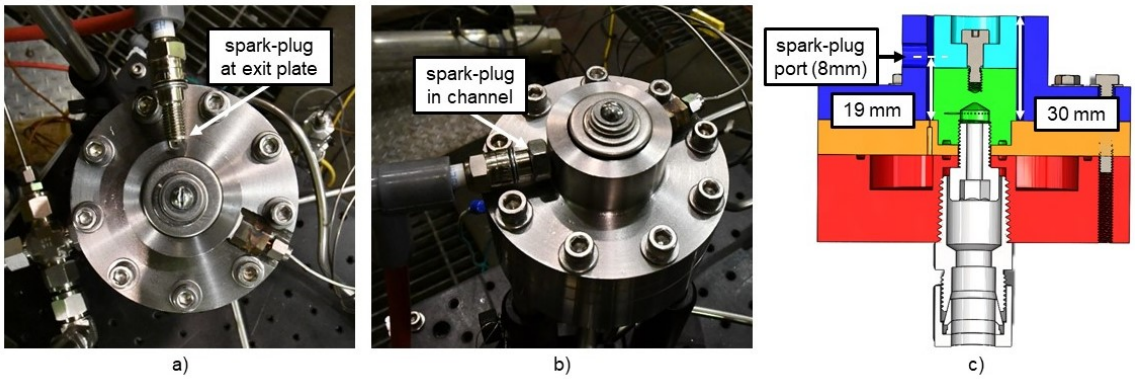

Figure 55. Position of the spark plug a) at the exit plane b) in the detonation channel and c) cross-section view of axial location

rate of 0.08 kg/s. These results were not unexpected as the detonation cell size should be minimized at an equivalence ratio around 1.0. Additionally, the increased channel pressure, as a result of increased mass flow rate, should also reduce cell size. Reduction of cell size aids in detonation stability as researched by Kudo et al. [8]. Alternatively, detonation was expected at a mass flow rate of 0.075 kg/s and equivalence ratio of 1.0, but this was not observed. In this instance, the washer may have shifted from a previous test, which reduced the channel pressure and detonability.

As shown in Figure 57, the detonations that were achieved using the back plate configuration appeared distinctly different on the high speed imagery when compared to the test cases that resulted in deflagration using the original configuration. The previous deflagration imagery, as shown in Figure 57a, displayed a generally uniform ring of bright light around the detonation channel edge that exhibited no sign of rotation. The test cases that indicated detonation revealed a more singular point of bright light that moved circumferentially around the channel as expected, as shown in Figure 57b.

Although detonation was achieved, the detonation wave exhibited unstable behavior as it travelled around the detonation channel. In all four cases, the detonation

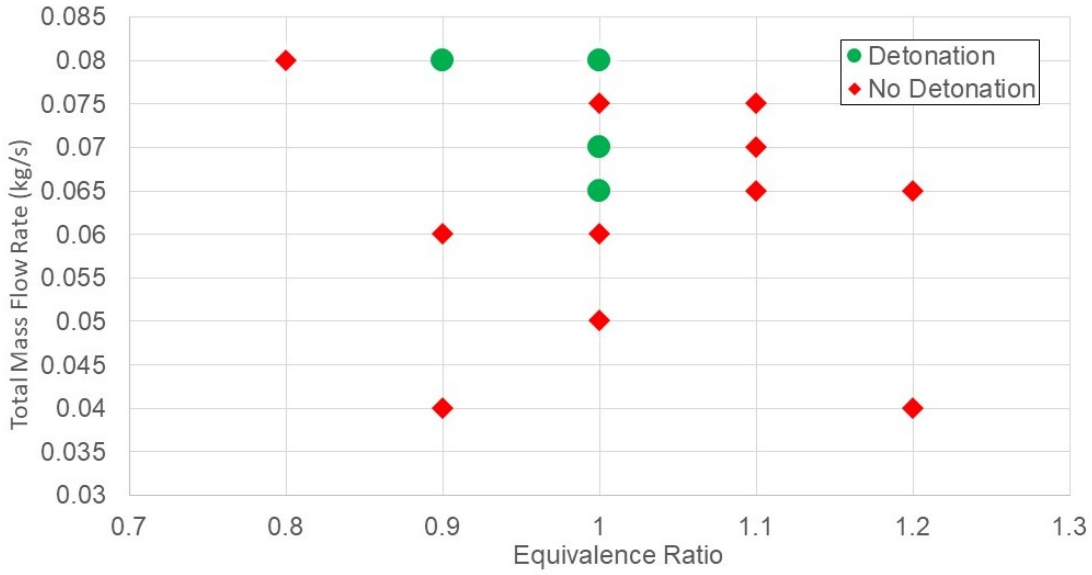

Figure 56. Operating map for testing using a washer as a backplate

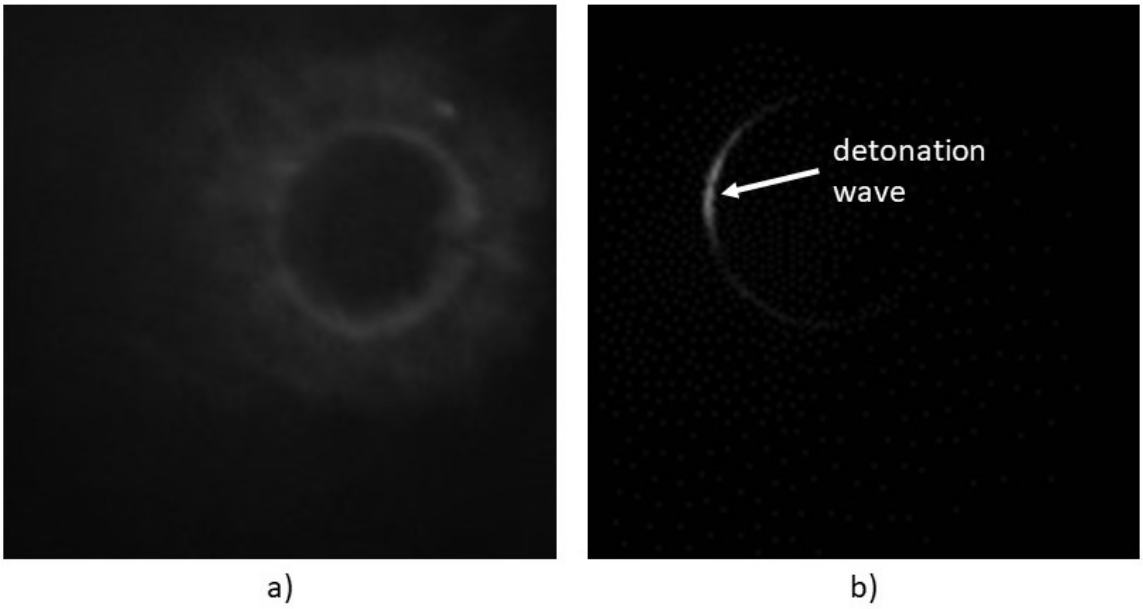

Figure 57. Comparison of a) deflagration at $\dot{m} = 0.05$ kg/s, $\phi = 1.0$ with original configuration vs. b) detonation at $\dot{m} = 0.075$ kg/s, $\phi = 1.0$ using back plate configuration

wave could be seen changing direction or displayed evidence of a possible second wave/clapping mode forming. Both behaviors could be seen during a single test run.

As shown in Figure 58, the detonation wave traveled in a counterclockwise (CCW) direction around the channel in Frames 1-4. In Frames 5-8, the view of the wave became partially blocked by the washer from approximately the 11 o'clock to 4 o'clock position around the annulus, but then became visible again in Frames 9-12 and was observed travelling in a clockwise (CW) manner.

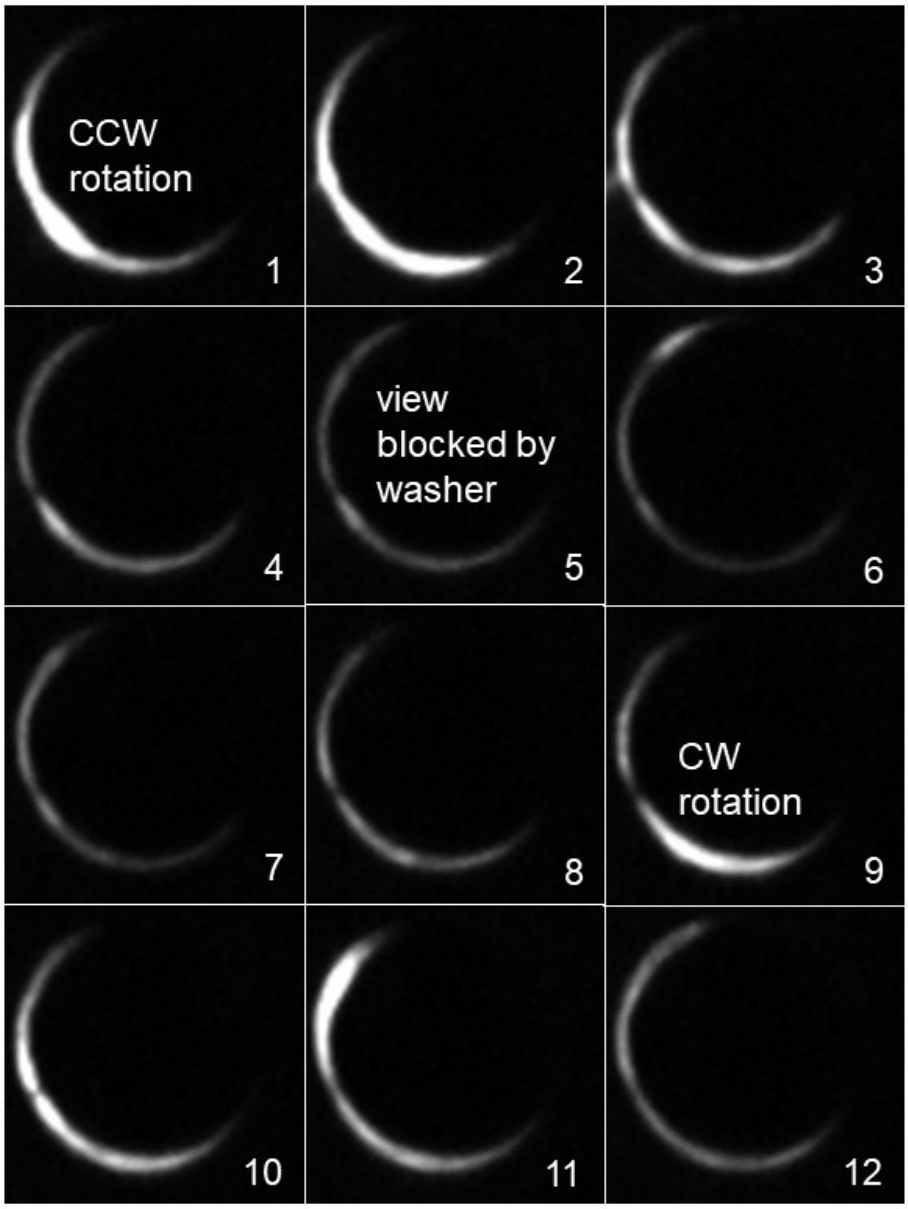

Figure 58. Detonation wave rotation changes from counter clockwise (CCW) to clockwise rotation (CW)

Alternatively, a clapping mode can be seen in Figure 59, where two waves were travelling in opposite directions in Frames 1-5 and then collided in Frame 6 at approximately the 7-8 o'clock position. The waves then appeared to reflect off of each other and change direction in Frames 9-12. Figures 60a and 60b compare the location of the wave collision point to the position of the spark plug and CTAP ports in the detonation channel. Figure 60a is a screen capture from the high speed camera prior to adjusting the exposure settings/darkening the image for testing. Using this image, the exact location of the ports were known when analyzing the detonation wave behavior. Viewing the images side-by-side, the wave appeared to collide with the edge of the spark plug.

In any case, there are several possibilities that could have influenced the detonation wave's behavior. The behavior could have been a result of inconsistent geometry in the detonation channel due to a misaligned centerbody (discussed below). Additionally, the wave could be colliding and reflecting off of the spark plug or CTAP port. Poor injector performance or mixing could have also been responsible for the detonation wave's instability. Furthermore, the engine's small channel radius in relationship to cell size may have been on the cusp of stability as demonstrated by Kudo et al. in their work with curved rectangular detonation tubes [8]. However, it was difficult to fully observe the behavior of the detonation wave using the high speed imagery because the washer became misaligned and blocked the camera's view in all test cases.

Using the washer/back-plate configuration did serve to overcome the initial detonation initiation issues, but this configuration proved to be problematic as testing continued. The use of a washer as a means to reduce the Mach number and increase the static pressure in the channel was only intended to be a quick solution and was not part of the initial engine design. As shown in Figures 54a and 61a, the washer was attached to the centerbody and fuel manifold using a simple #8-32 screw. As

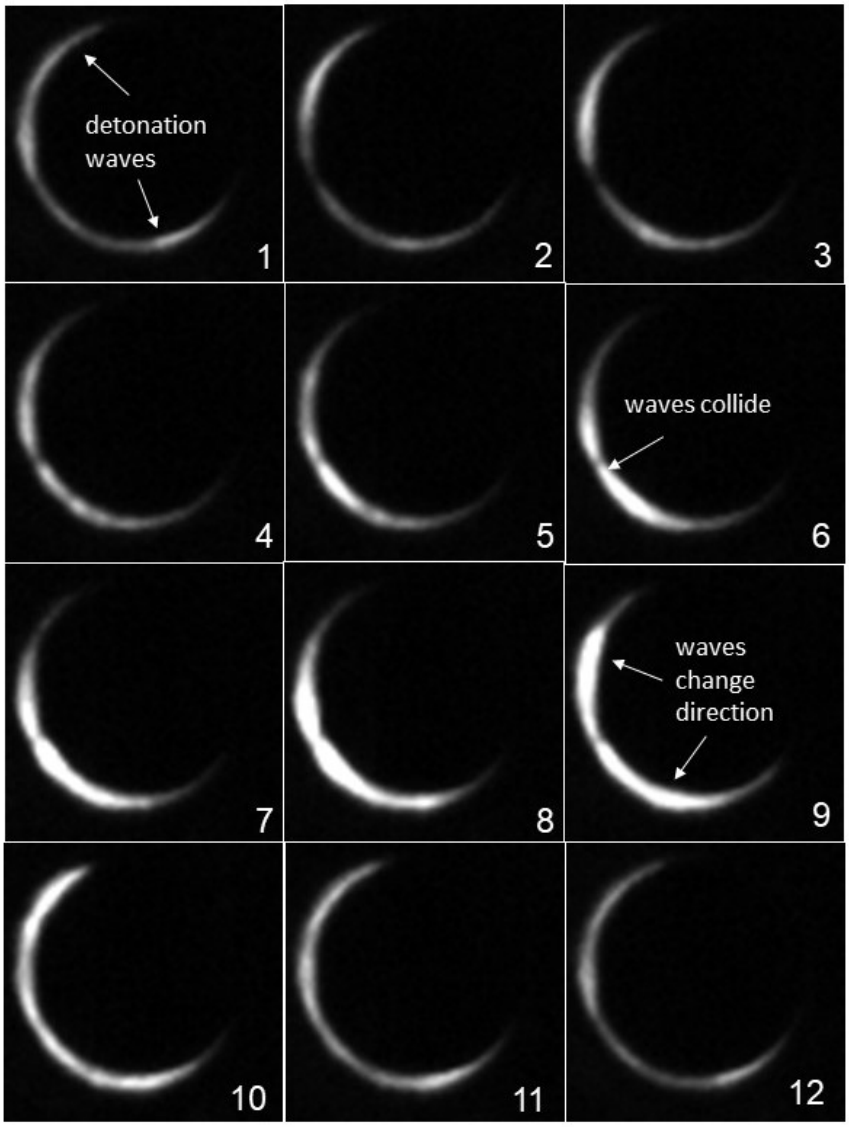

Figure 59. Detonation wave exhibiting clapping behavior

shown in Figure 54b and 61b, there was a small gap between the outer diameter of the screw and the inner diameter of the centerbody that made it difficult to ensure that the centerbody was properly aligned upon installation. When positioning the washers or tightening the screw, the centerbody could also be accidentally tapped out of alignment, and because the washer was larger in diameter than the centerbody, it was impossible to look into the detonation channel and confirm that the centerbody

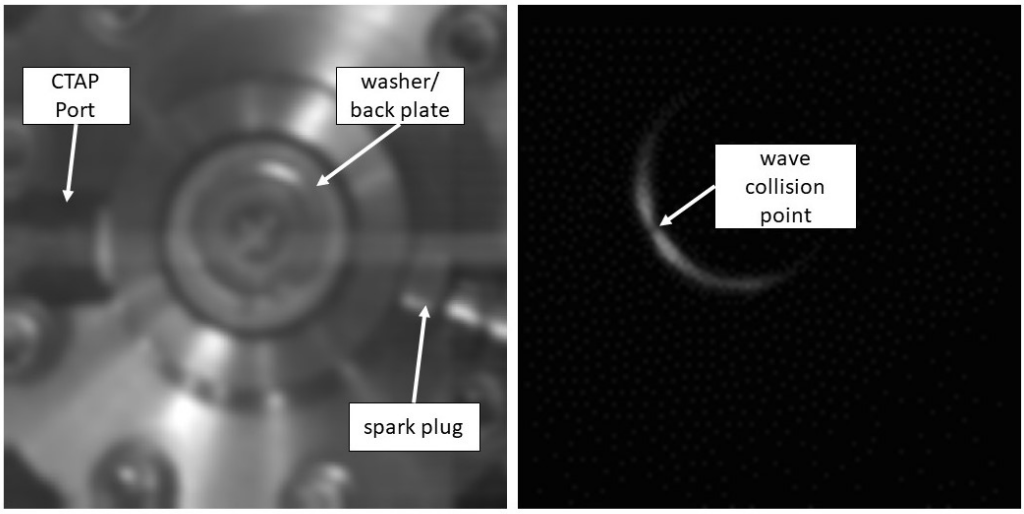

Figure 60. Image of a) spark plug and CTAP position from high-speed camera in comparison to b) collision location

was aligned after the centerbody/washer/screw assembly was installed.

The small gap also allowed for variability in how "aligned" the centerbody was from test to test in the event it needed to be removed and replaced between test runs. The #8-32 screw also had a tendency to loosen and allow the centerbody and/or washer to shift during the test sequence. When the screw needed to be re-tightened there was no way to guarantee that centerbody and washer were in the same place as previous tests. Additionally, there was no physical mechanism to ensure that the washers were centered over the detonation channel. Visual inspection was the only method to align the washers over the detonation channel.

The misaligned washer created issues when attempting to analyze the high speed imagery for detonation wave behavior. As shown in Figure 62, the detonation wave was traveling counterclockwise around the detonation channel in Frames 1-7, and then in Frame 8 the detonation wave began to disappear due to the washer blocking the camera's view. This obstruction made it more difficult to diagnose what was causing the detonation wave's instability.

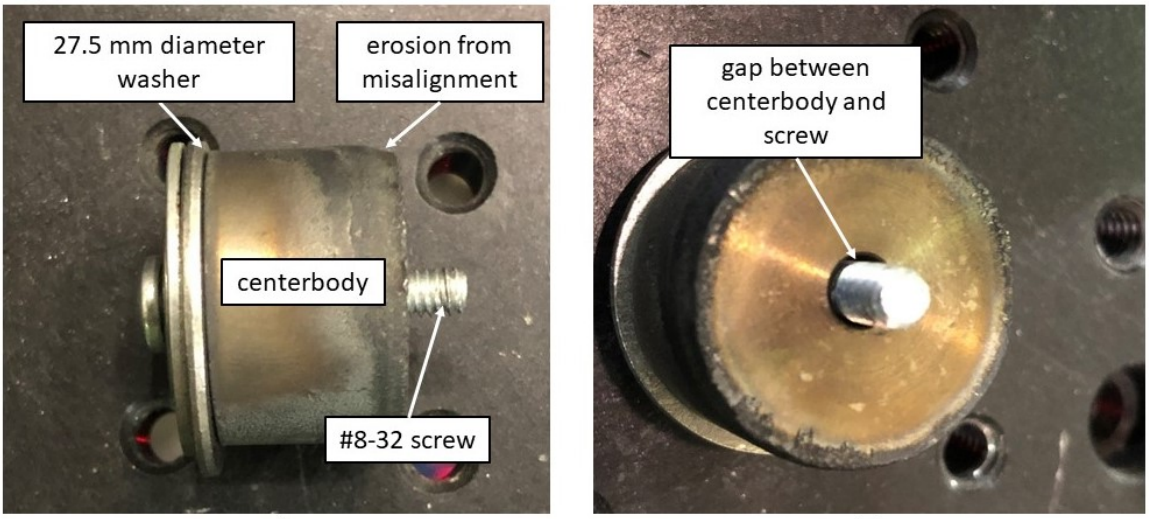

Figure 61. Configuration of the centerbody using a washer as a back plate a) side view b) mating surface to fuel manifold

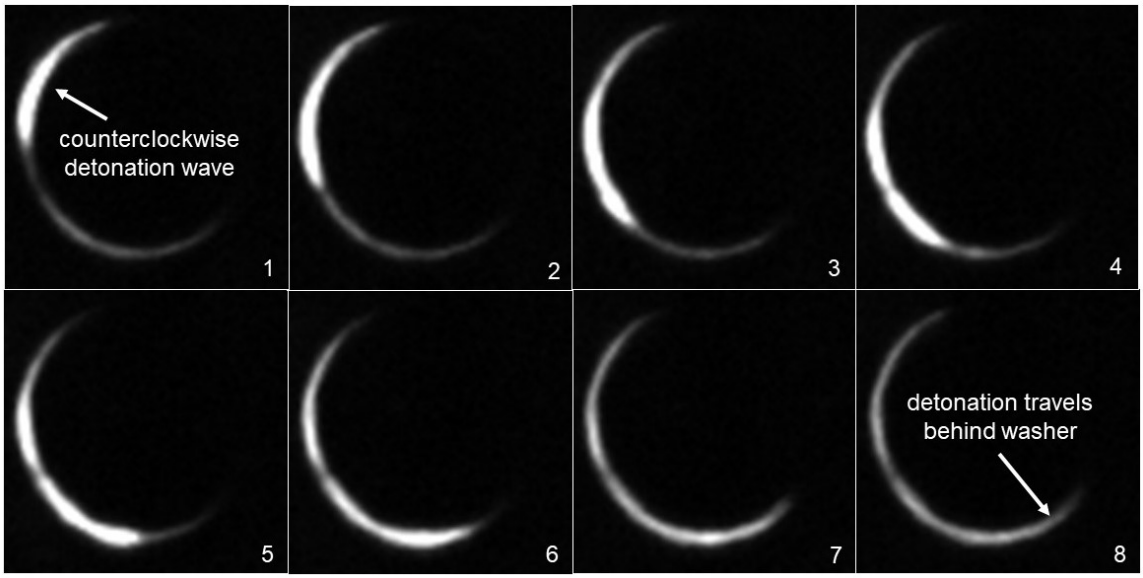

Figure 62. Frame by frame images of detonation wave motion with washer as a back-plate

The shifting and off-centered washer also created inconsistencies among test cases. If the washer was not in the same position for each test run, it could not be guaranteed that the exit area would remain the same for each test. Additionally, if the washer

shifted during the test, the exit area could change throughout the test run. The screw had a tendency to loosen during the test run and allow the washer to shift. In either case, a change in the exit area could change the static pressure in the channel which could effect the behavior of the detonation wave or alter the conditions in the channel to a point where a detonation may not even occur. Testing was also attempted without a washer, but did not produce a detonation under any conditions that were attempted.

The inability to ensure that the centerbody was aligned caused additional problems for testing consistency. The misaligned centerbody could cause the detonation channel gap to vary as the detonation wave travelled circumferentially around the annulus. The varying geometry could reduce the detonation stability or the possibility that a detonation could occur if the channel gap was too small in a particular circumferential location around the centerbody. In addition to inconsistency, the misaligned centerbody was also causing erosion issues as shown in Figure 61a.

4.2 Engine Operation with the Addition of a Nozzled Centerbody

Because of the issues encountered with the washer/back plate configuration, a new method of increasing the static pressure in the channel was needed. A common approach to increasing channel pressure at the DERF was to use an aerospike nozzle as shown in Figure 63 [30]. Aerospike nozzles perform the same function as bell-shaped nozzles that are common on traditional rocket engines, but the aerospike nozzle was easier to implement with RDE detonation channel geometry. Typically, diameter, length, and shape of the nozzle's curve are carefully analyzed to optimize thrust [20]. However, the aerospike nozzles that were designed for the current research were not intended to create thrust. Therefore, the diameter of the aerospike was the only parameter that was critical during the design process. The diameter of the

nozzle determines the geometry of the throat and ultimately the area ratio which is defined as the area of the throat divided by the area of the detonation channel. This dimension would also affect the detonation channel's static pressure for a given mass flow rate. As shown in Figure 64, nozzles with diameters of 26.5 mm and 27.5 mm were used during testing which yielded area ratios of 0.40 and 0.14 respectively.

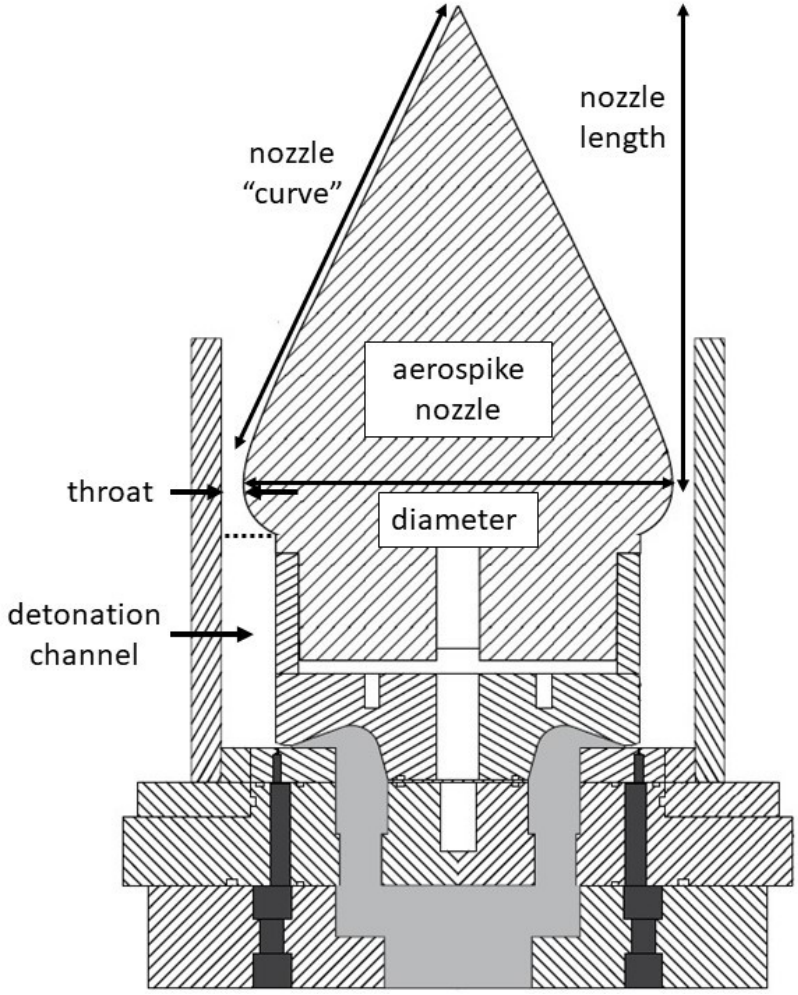

Figure 63. Diagram of aerospike nozzle used in the DERF [30]

The nozzles were designed to replace the centerbody that was previously mated to the fuel manifold as shown in Figure 64. The nozzles were attached to the fuel manifold via a 12.5 mm long, #8-32 threaded rod, which ensured that the nozzle was

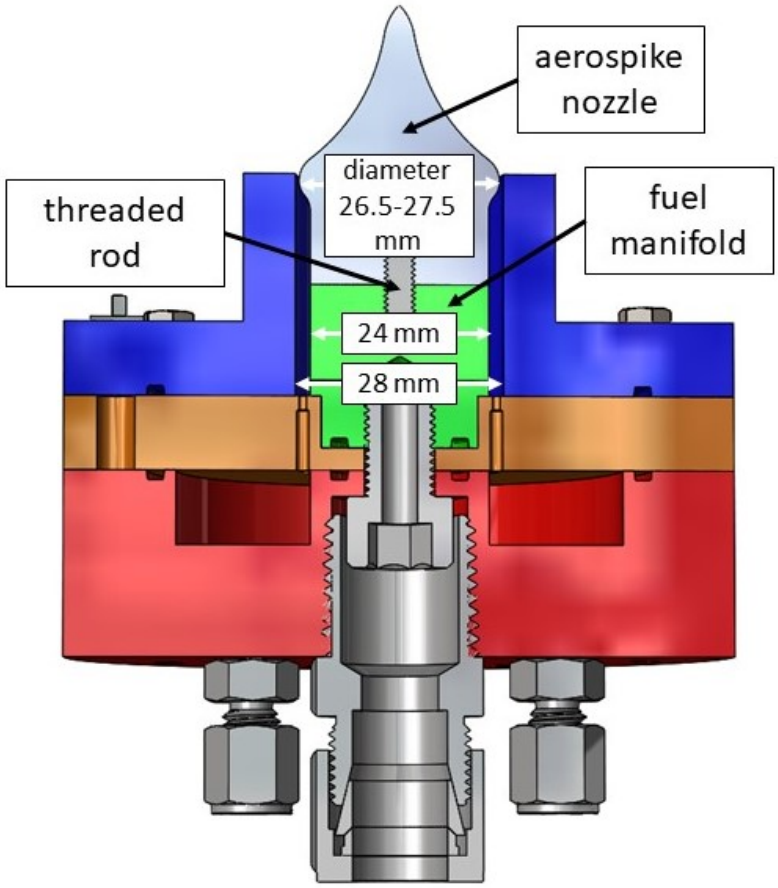

Figure 64. Diagram of aerospike nozzle installed in the Small Scale RDE

properly aligned. This configuration eliminated the small gap between the through-bolted screw and centerbody that previously caused alignment issues. Additionally, this implementation method did not require any modifications to existing hardware.

The two nozzles were tested over equivalence ratios of 0.5-1.5 and mass flow rates of 0.025-0.075 kg/s to build an operating map for the engine. Testing occurred at equivalence ratios of 0.5, 0.8, 1.0, 1.2, 1.3, and 1.5. At each equivalence ratio, mass flow rates of 0.025, 0.035, 0.04, 0.05, 0.06, and 0.075 kg/s were tested. These points offered enough fidelity to characterize the operating regime of the engine, while also reducing the amount of test runs required. More test conditions could have been attempted, but the nitrous-oxide and spark plugs consumed during testing were rel-

atively expensive.

Using the two different size nozzles allowed for analysis on the effects of channel pressure on detonability. The expected result was that the larger diameter nozzle would increase flow constriction and channel pressure which would offer an expanded range of mass flow rates and equivalence ratios that the engine would be able to achieve a detonation. Testing revealed that the larger diameter nozzle produced a detonation at a lower mass flow rate in comparison to the smaller nozzle, but detonation occurred in a narrower band of equivalence ratios when compared to the smaller nozzle.

As shown in Figure 65, the channel pressure increased as a function of mass flow rate for both the $\epsilon = 0.14$ and 0.40 nozzles from data captured immediately before the ignition sequence (average of 100 data points/0.1 s of data prior to ignition). The trend line for the $\epsilon = 0.14$ nozzle was steeper than the $\epsilon = 0.40$ nozzle indicating that the larger diameter, $\epsilon = 0.14$ nozzle, created more channel pressure for a given mass flow rate when compared to the $\epsilon = 0.40$ nozzle. Above the $\epsilon = 0.14$ trend line, five data points are seen at pressures approximately 100-300 kPa above their expected value. This particular set of points was from back-to-back test runs that achieved detonations and were only 1-2 minutes apart. This likely caused the detonation channel to become hotter than usual which resulted in higher than expected channel pressures. The exact disparity of the elevated channel temperature versus the typical channel temperature can not be quantified since there was not a thermocouple installed in the detonation channel.

Similarly there was a data point at a mass flow rate of 0.065 kg/s and a channel pressure of 400 kPa that was approximately 250 kPa lower than the $\epsilon = 0.14$ trend line. This was due to a previous test attempt that that failed to yield a detonation at the same operating condition. The expanding gas from the injection manifolds cooled

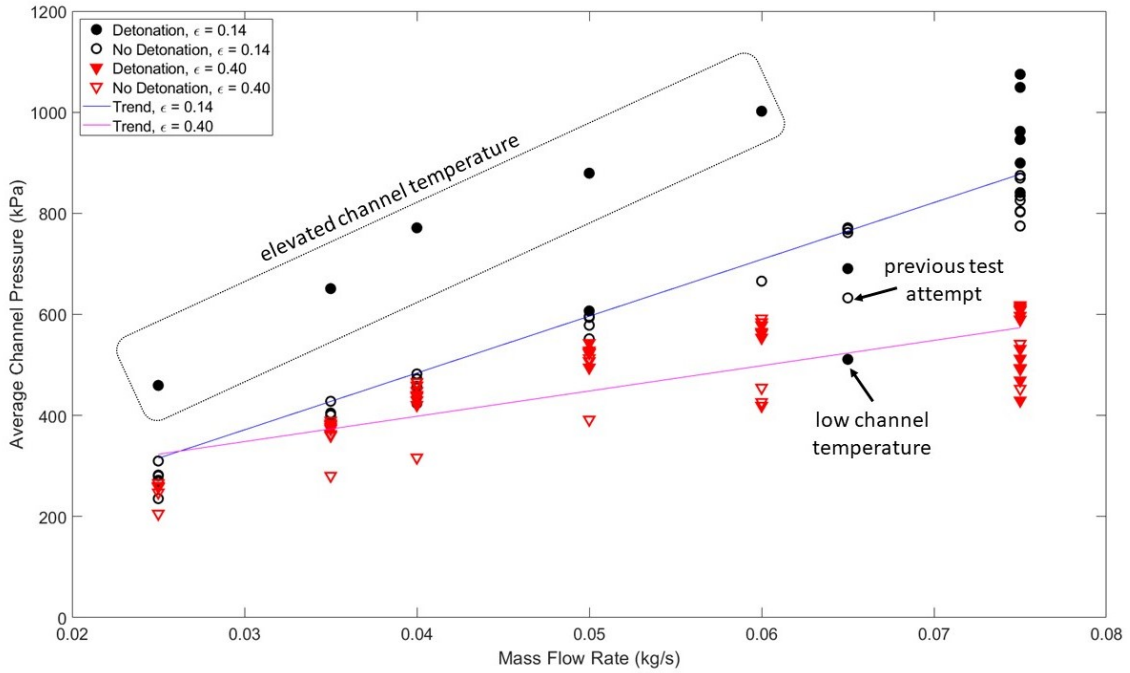

Figure 65. Channel pressure vs. total mass flow rate for $\epsilon = 0.14$ and $\epsilon = 0.4$ nozzles

the detonation channel, and this particular instance likely had a more pronounced effect since it was near the higher end of the mass flow rate test range. Because the channel gap was narrow, there was a large amount of channel surface area relative the volume of the channel which would have allowed for a significant amount of heat transfer between the channel walls and the flow.

Figure 66 shows the operating map where detonation was achieved using the $\epsilon = 0.14$ nozzle. Each point was attempted at least twice before making a determination on whether or not the test point detonated. If the first attempt resulted in detonation, the test point was considered to have detonated and no further attempts were made in an effort to conserve the oxidizer and spark plugs and to also reduce wear on the engine. Additionally, if the first attempt failed to detonate, but the second attempt yielded a detonation, the test point was considered to have detonated. Of the 36 operating conditions attempted, detonation was achieved at 13 points. Detonation

occurred at equivalence ratios between 1.0-1.3. An equivalence ratio of 1.2 produced the greatest range of mass flow rates where detonation occurred, which spanned between 0.025-0.075 kg/s.

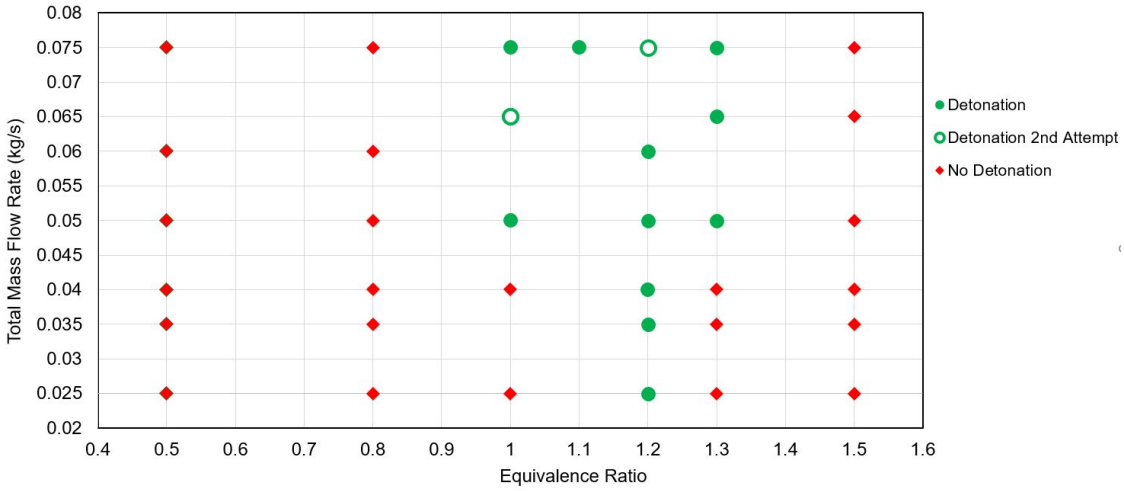

Figure 66. Operating map using a $\epsilon = 0.14$ nozzle

Figure 67 investigates all 52 test runs attempted with the $\epsilon = 0.14$ nozzle in terms of average channel pressure just prior to the ignition (average of 100 data points/0.1 s of data) sequence versus equivalence ratio, to include duplicate attempts at the same ϕ and $\dot{m}$. Similar to Figure 66, an equivalence ratio of 1.2 yielded the largest range of pressures where a detonation occurred, with 460 kPa being the minimum pressure. If the equivalence ratio was increased or decreased from 1.2, it required pressure greater than 460 kPa to produce a detonation. To characterize the lower pressure limit versus equivalence ratio, the curve fit shown in Eq. 39 can be applied, where $P_{c,min}$ is the minimum channel pressure required to produce a detonation as a function of ϕ.

$$p_{c,min,0.14} = 6203\phi^2 - 13960\phi + 8266 \tag{39}$$

There are three points shown in Figure 67, where detonation was expected, but not achieved. Point 2 was the first of two test attempts at a mass flow rate of 0.065 kg/s,

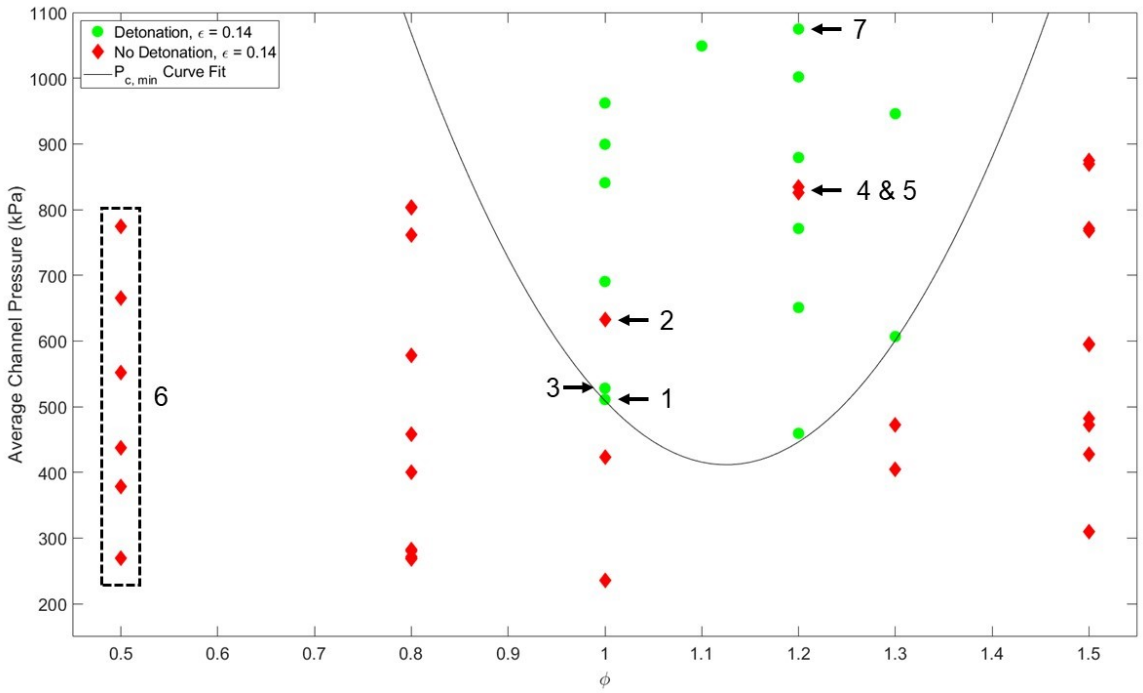

Figure 67. Channel pressure influence on detonability using a $\epsilon = 0.14$ nozzle

$\phi = 1.0$, but there was no apparent reason why detonation was not achieved. The previous test run at Point 1 ($\dot{m} = 0.05$ kg/s, $\phi = 1.0$) produced a detonation, which would have heated the channel walls and created favorable conditions for detonation to occur. The second test attempt at $\dot{m} = 0.065$ kg/s, $\phi = 1.0$ (Point 3) produced a detonation, which was also perplexing since this attempt would have had a less conducive environment for detonation with cooled channel walls from non-detonation at Point 1.

Points 4 and 5 were at an operating condition of 0.075 kg/s, $\phi = 1.2$. Here, detonability may have been affected by cool channel wall temperatures. The test points enclosed in Box 6 were all attempted just prior to Points 4 and 5. Because they did not achieve detonation, the channel walls would have been particularly cold from the expanding injection flow. An additional attempt at Point 7 was made under the same operating conditions as Points 4 and 5, but this attempt was completed after

a significant amount of time had passed and the channel walls were no longer cooled. The effect of channel wall cooling was evident in the difference of approximately 250 kPa between channel pressures at the same operating conditions.

Figure 68 shows the operating map for the $\epsilon = 0.40$ nozzle, where 56 tests were attempted at 35 different operating conditions. Of the 35 operating conditions tested, 16 of them produced a detonation. Detonation was achieved at equivalence ratios of 0.8, 1.0, 1.2, 1.3, and 1.5 and at a mass flow rates between 0.04-0.75 kg/s. The operating map for the $\epsilon = 0.40$ nozzle has the same general trend as the $\epsilon = 0.14$ operating map where the lowest mass flow rate where detonation occurred was at an equivalence ratio of 1.2-1.3. However, the lowest mass flow rate where detonation was achieved was 0.015 kg/s higher for the $\epsilon = 0.40$ nozzle when compared to the $\epsilon = 0.14$ nozzle. This was the expected result, as the $\epsilon = 0.40$ would need higher mass flow rates to achieve the equivalent channel pressure as the $\epsilon = 0.14$ nozzle. The $\epsilon = 0.40$ nozzle was also able to achieve detonation over a greater span of equivalence ratios when compared to the $\epsilon = 0.14$ nozzle, where the range of ϕ was increased by ± 0.2.

Three operating conditions required a second run attempt to produce a detonation. All three of these cases were at the highest mass flow rate that was tested. An additional attempt was likely needed due to cooled channel walls. Testing progressed through each equivalence ratio, where all mass flow rates were attempted before moving to the next equivalence ratio value. For each equivalence ratio, 0.075 kg/s was tested first, then progressively reduced until reaching the bottom of the test range at 0.025 kg/s. Testing at the lower range of mass flow rates often did not produce a detonation, which resulted in cool channel walls prior to initiating the next set of testing at another equivalence ratio.

As shown in Figure 68, detonation occurred at $\phi = 1.5$, $\dot{m} = 0.05$ kg/s, which was not an anticipated result. The operating point was attempted three additional times

without a detonation. For the one instance where there was a detonation, accuracy of the mass flow controller could be to blame. At this particular point, the equivalence ratio error could be as high as ±0.13, which could have moved this test case into a more detonable regime with a lower equivalence ratio.

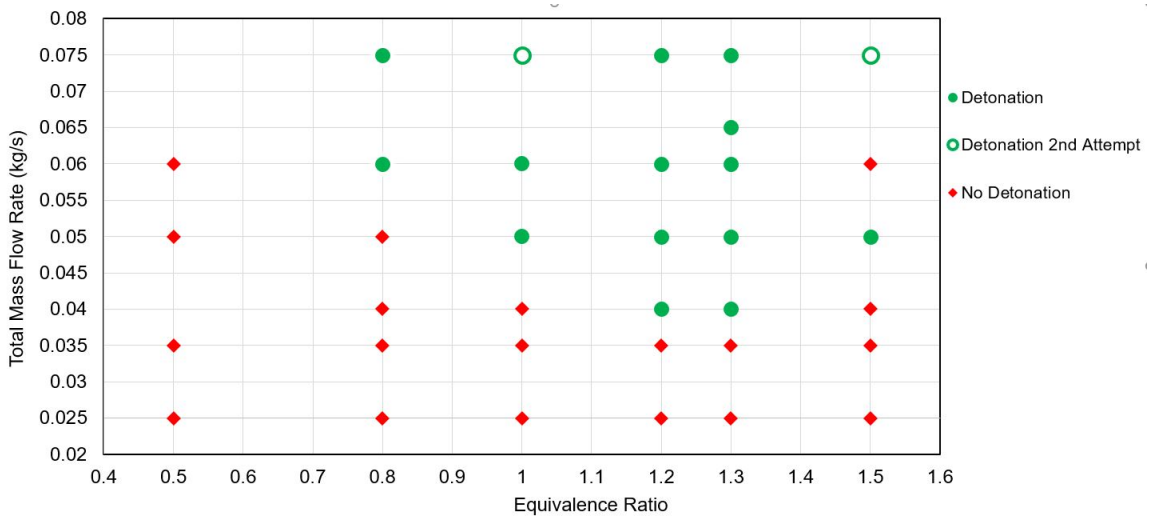

Figure 68. Operating map using a $\epsilon = 0.40$ nozzle

The 56 test runs were also analyzed to determine a correlation between the average channel pressure just prior to ignition, equivalence ratio, and detonability for the $\epsilon = 0.40$ nozzle as shown in Figure 69. The lowest channel pressure where detonation was achieved was at 421 kPa, at $\phi = 1.2$, which was nearly identical to the minimum pressure conditions of the $\epsilon = 0.14$ nozzle at 460 kPa, $\phi = 1.2$. As equivalence ratio was increased or decreased from 1.2, more pressure was required to achieve detonation, which also followed the trend of the $\epsilon = 0.14$ nozzle. As determined by the trend line shown, the minimum required channel pressure for the $\epsilon = 0.40$ nozzle, can be calculated from Eq. 40.

$$p_{c,min,0.4} = 1362\phi^2 - 3054\phi + 2126 \tag{40}$$

There are three instances where detonation was expected but did not occur as

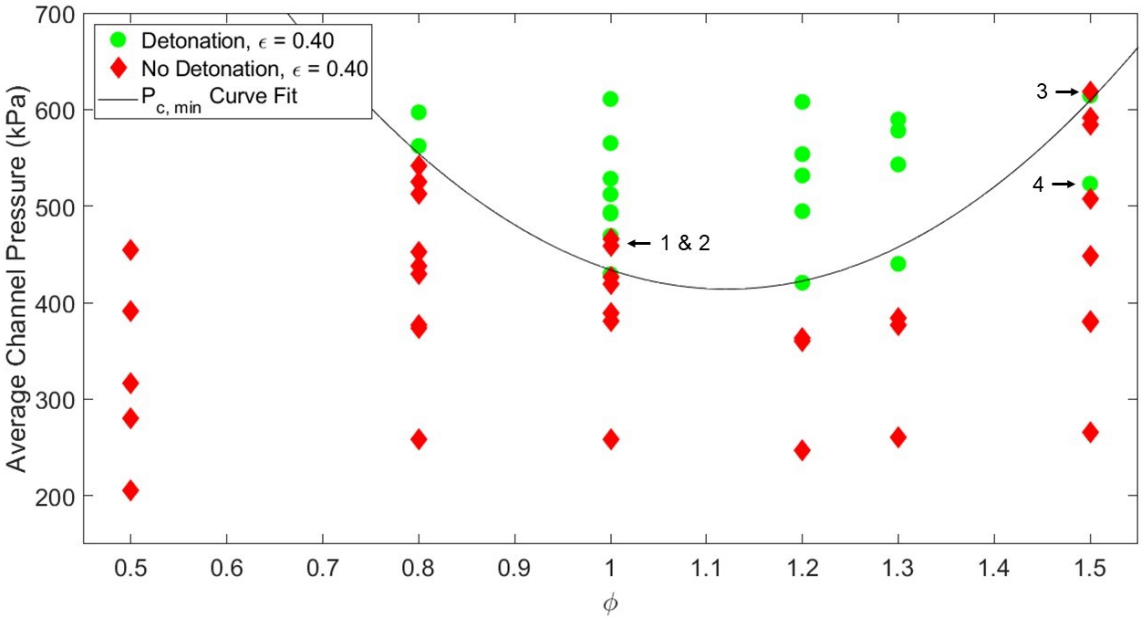

Figure 69. Channel pressure influence on detonability using a $\epsilon = 0.40$ nozzle

indicated on Figure 69. At Points 1 and 2, there was no obvious reason why detonation did not occur. The previous test attempt achieved a detonation, which would have heated the channel and created favorable conditions for detonation. Points 1 and 2 were only 20-30 kPa above the P_{cmin} curve and may have simply been on the cusp of where detonation was possible. For Point 3, this was the first test attempt at $\dot{m} = 0.075$ kg/s, $\phi = 1.5$. The second test attempt at this operating condition yielded a detonation as indicated by the green data point immediately below Point 3. Point 4 was the test case at $\phi = 1.5$, $\dot{m} = 0.05$ kg/s discussed previously, where flow controller accuracy may have affected detonability.

The combined pressure versus equivalence ratio data from both the $\epsilon = 0.14$ and $\epsilon = 0.40$ nozzles is shown in Figure 70. The same general trends can be seen for both nozzles where the amount of pressure required to achieve a detonation was minimized at equivalence ratios between 1.1-1.2 as indicated by the curve fit lines. What was notably different was the range of equivalence ratios where detonation occurred. The

$\epsilon = 0.14$, P_{cmin} curve has a much steeper gradient when compared to the $\epsilon = 0.40$ curve, encompassing a smaller range of equivalence ratios. The $\epsilon = 0.14$ nozzle, also produced more channel pressure for a given mass flow rate when compared to the $\epsilon = 0.40$ nozzle. This could indicate that increased channel pressure influenced the range of equivalence ratios where detonation could be achieved. The increased channel pressure could also be influencing injection performance, which is discussed in Section 4.4.

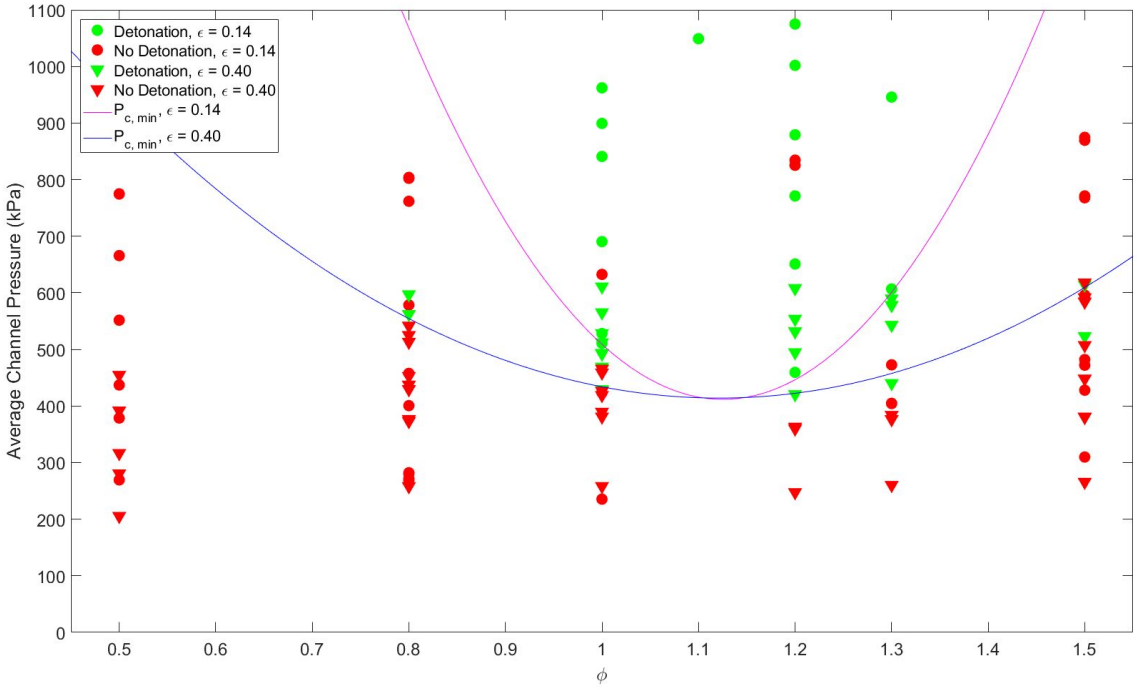

Figure 70. Channel pressure influence on detonability for both $\epsilon = 0.14$ and $\epsilon = 0.40$ nozzles

4.3 Detonation Wave Behavior Analysis

The high-speed imagery was used to analyze the detonation wave's behavior after the incorporation of the aerospike nozzles. With this configuration, the entire annulus was now visible and the detonation wave could be observed travelling around the

entire circumference of channel. However, wave stability did not appear to improve with the use of the nozzles. The detonation waves exhibited similar behavior to tests with the washer/back plate configuration. As shown in Figure 71 during a test run at $\dot{m} = 0.05$ kg/s, $\phi = 1.2$, a detonation wave was seen forming in Frame 1 at the 6 o'clock position. The intensity continued to increase in Frames 2-4 in the same location. In Frame 5, the wave began to rotate in a counterclockwise direction and continued to do so until Frame 8. In Frames 8-12, the wave dissipated at approximately the 2 o'clock position. This behavior was not unique to this nozzle or test condition. Additionally, this behavior appeared to be purely a result of wave instability and not due to the protrusion of the spark plug into the channel as seen in other instances.

A more common operating mode is shown in Figure 72 where two counter rotating waves were present. In Frame 1, two waves were seen at the 12 o'clock and 7 o'clock locations where they were both travelling towards the 9 o'clock position. The waves continue in this manner until Frame 6 where they collided at the 8-9 o'clock location which corresponds to the position of the spark plug shown on Frame 5. Following the collision, the waves either passed through each other or reflected and began rotating in the opposite direction.

The unstable wave behavior was likely attributed to a combination of channel radius, mixing, and the protrusion of the spark plug into the channel. This RDE was likely on the fringe of being able to achieve a stable detonation due to its small channel radius. According to Kudo et al. r_i/λ needs to be greater than 14 to produce a marginally stable detonation in curved rectangular tubes [8]. With an estimated cell size of 0.5-1.75 mm and $r_i = 12$, r_i/λ was found to be between 7-24 for this RDE. Based on the observed detonation behavior, the engine was likely operating in the lower end of this range where it was unstable.

The second concern was the limited amount of time available for mixing. With

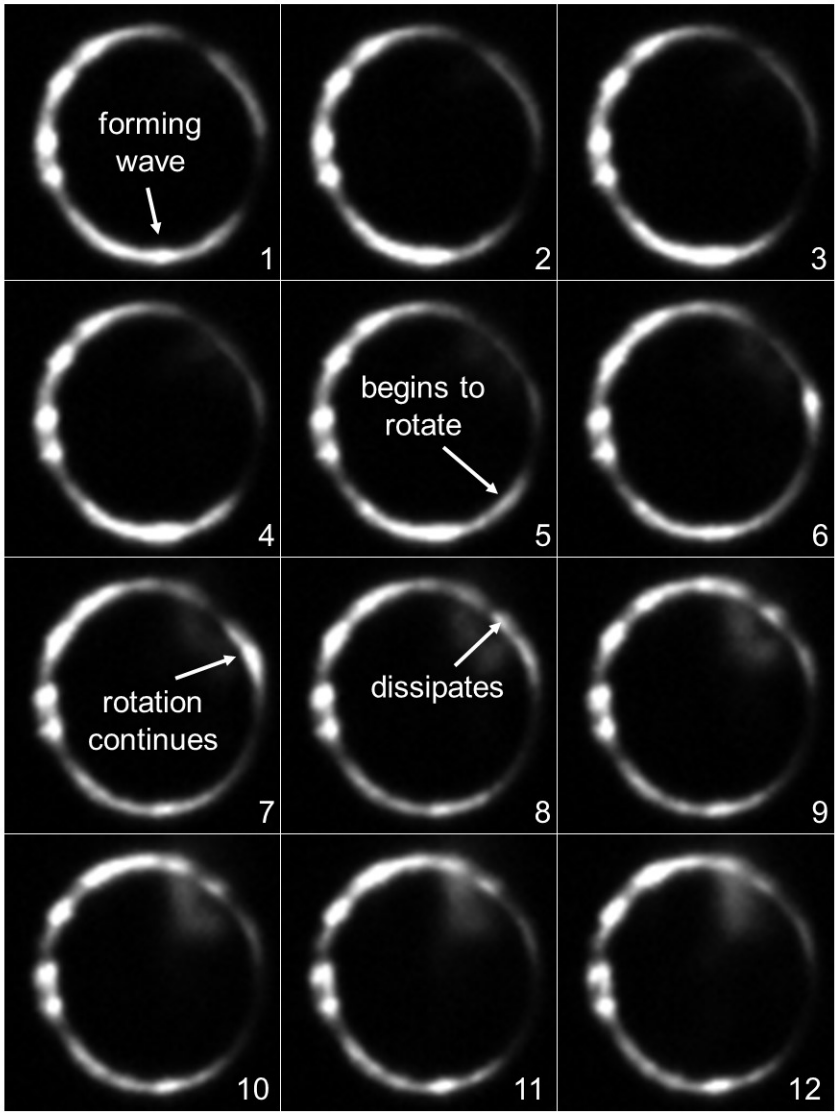

Figure 71. Detonation wave behavior at $\dot{m}$ = 0.05 kg/s, ϕ 1.2 using a ϵ = 0.14 nozzle

as little as 50 μs between passing detonation waves, the reactants were likely poorly mixed which contributed to the instability. Finally, the relatively large, 8 mm diameter spark plug that protruded into the 30 mm long and 2 mm wide channel gap interfered with the detonation wave's progression around the channel as previously discussed. Although these challenges remain, the use of the aerospike nozzle ensured

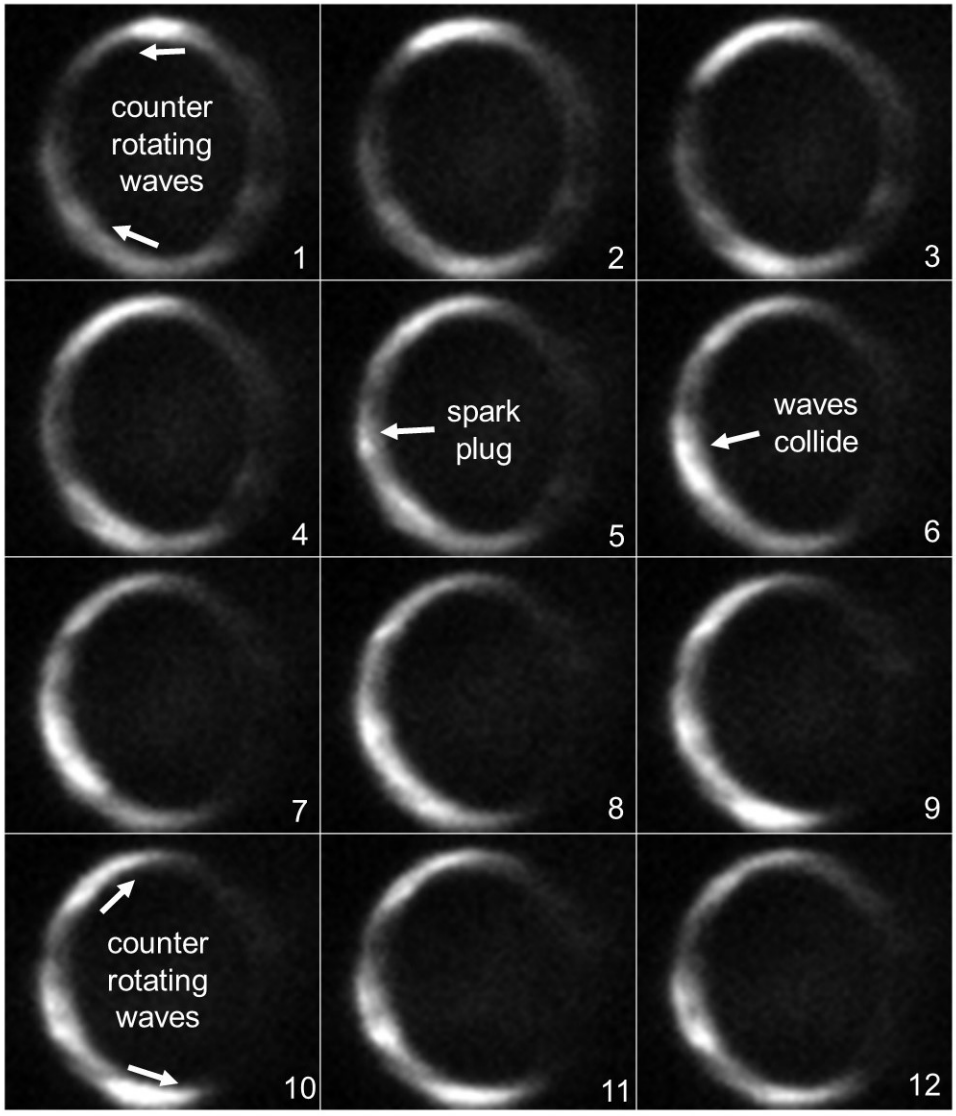

Figure 72. Detonation wave behavior at $\dot{m}$ = 0.075 kg/s, ϕ 1.2 using a ϵ = 0.40 nozzle

constant channel gap around the entire circumference of the detonation channel which eliminated a possible source of instability caused by the misaligned centerbody.

The effect of detonation wave interference from the spark plug was reinforced by examining its condition after a test run as shown in Figure 73. The new, pre-test spark plug had an intact metal strap and electrode tip, and the post-test spark plug's electrode tip was completely eroded away from the detonation wave (this spark

plug was inoperable after one run). The spark plug had a lifespan that could range between 1-10 runs. However, even in the eroded condition, the spark plug could remain operational as long as the ceramic insulation was not damaged. The spark plug was replaced when a spark signal was commanded, but no evidence of combustion was observed or heard. Even in cases that did not detonate, a short "click" or "pop" sound was audible when the spark plug was working. If detonation was not achieved and the noted sounds were not heard, the spark plug was replaced.

The longevity of the spark plug seemed to be dependent on how well a new spark plug survived it's first detonation. During the first run of a new spark plug, the metal shroud would erode away from the detonation wave and cause small metal fragments to impact the ceramic insulation. If the ceramic insulation was damaged as a result of the impact from the metal fragments, the spark plug shorted out and did not create a spark. However, if the ceramic insulation survived the first run, there was less remaining material on the shroud to cause damage, which typically allowed for 5-10 more runs.

4.4 Injection Performance Analysis

Duval et al. noted that the manner in which the injection system recovered from a passing detonation wave could affect engine performance. If the local fuel injector flow recovered more quickly from the momentary increase in pressure from the detonation wave in comparison to the oxidizer (or vice versa), there could be a momentary change in local equivalence ratio that could affect detonability [7]. The effects of recovery time for this research were analyzed by investigating the ratio of P_f/P_c to P_{ox}/P_c as shown in Figure 74. The data shown in this figure and the remainder of this section (unless otherwise noted) was taken immediately before the ignition sequence (average of 100 data points/0.1 s of data). The trend line indicates the ratio of P_f/P_c to P_{ox}/P_c

Figure 73. Spark plug condition pre and post testing

for test runs that achieved detonation, which was found to be 0.87. Exceptions to this trend existed, but 29 out of the 33 cases that detonated (88%) fell within 25% of the trend line value, and 49 of the 71 cases that did not detonate were outside of these bounds (69%).

As shown in Figure 74, two distinct regions of data points were observed, where each region contained values from only one of the two nozzles. For data from the ϵ = 0.14, values for P_f/P_c and P_{ox}/P_c were both less than 2.0. Alternatively, the ϵ =

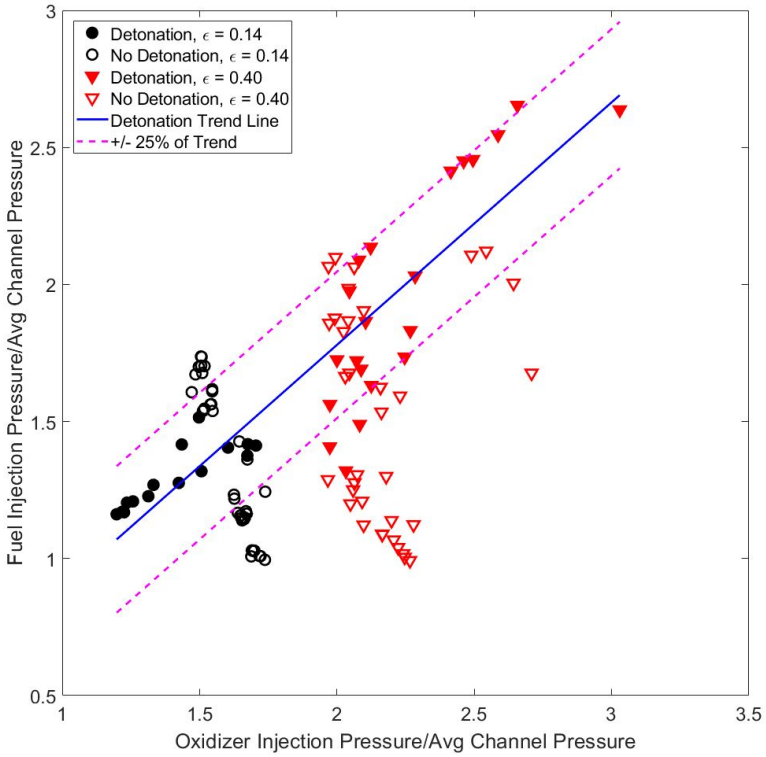

Figure 74. Ratio of injection pressure to channel pressure and the effect on detonability

0.40 nozzle had values above 2.0 for P_f/P_c and P_{ox}/P_c. If the injector was choked, the value of P_f/p_c or P_{ox}/P_c would be expected to be approximately 2.0 or greater. Analyzing the two regions of data points for each nozzle, the injection system for the $\epsilon = 0.40$ nozzle appeared to have choked flow and the injection system for the $\epsilon = 0.14$ nozzle was unchoked.

The difference in choked/unchoked injectors may have influenced the engine's operability range for each nozzle. Research by Druss [31], found that injector "stiffness" (i.e. pressure relative to minimum choking requirements) can affect detonabilty if the relative injection stiffness was not at the proper ratio. The stiffness of the injector can change the flow characteristics as the fuel or oxidizer leaves the injection hole. The $\epsilon = 0.40$ nozzle allowed for a choked injection system and thus a "stiffer" injector when compared to the injection performance of the $\epsilon = 0.14$ nozzle's unchoked injectors.

The stiffer injectors may have allowed the $\epsilon = 0.40$ nozzle to achieve detonation over a wider range of equivalence ratios due to the injection system's ability recover in a more favorable manner from a passing detonation wave.

Duval et al. also studied different injection schemes in an effort to understand what parameters made them most effective [7]. As discussed in Section 3.1, the injection scheme used in the engine's design was jets-in-crossflow. Duval et al's. research found that a momentum ratio, $J = p_f \gamma_f M / p_{ox} \gamma_{ox} M$, between 0.5-0.6 was most effective for jets-in-crossflow in terms of detonabilty [7]. The operating map for the current research in terms of momentum ratio and equivalence ratio is shown in Figure 75. A trend towards an increasing momentum ratio from 0.5-1.1 was visible as equivalence ratio was increased from 0.5 to 1.5. This was expected as more fuel was required relative to the oxidizer when equivalence ratio was increased.

As shown in Figure 75, the most amount of successful detonations was found to occur with momentum ratios between 0.9-1.0 and at equivalence ratios of 1.0-1.5, with 15 occurring in this range. These values for momentum ratio did not agree with Duval et al's. research, but it should be noted that this data was collected from only one set of injectors. To fully explore the effects of momentum ratio, another set of injectors with different hole diameters would be needed so that momentum ratio could be changed independent of equivalence ratio.

Figures 76 and 77 investigate the effects of channel pressure on momentum ratio for each equivalence ratio tested. As shown in Figure 76, momentum ratio remained generally stable as channel pressure was increased for a given equivalence ratio using the ϵ=0.14 nozzle. Alternatively, with the ϵ=0.40 nozzle, momentum ratio tended to increase as channel pressure increased as shown in Figure 77. This indicated that either fuel pressure was increasing relative to the oxidizer or oxidizer pressure was decreasing relative to the fuel.

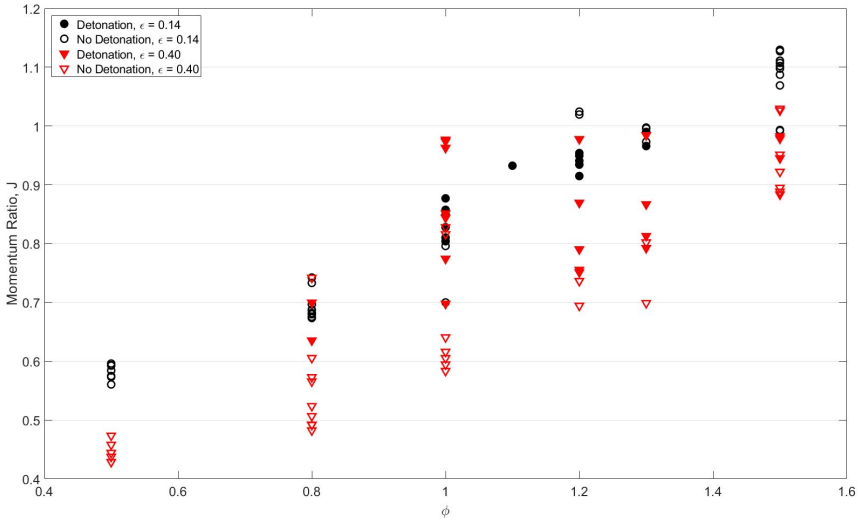

Figure 75. Momentum ratio vs. equivalence ratio and the effect on detonability

The difference in choked and unchoked injectors could be indicative of the momentum ratio trends shown in Figures 76 and 77. When the injection system was unchoked, momentum ratio remained relatively constant as channel pressure increased for a given equivalence ratio as shown in Figure 76. Alternatively, when the injection system was choked momentum ratio tended to increase as channel pressure increased as shown in Figure 77.

A conclusion about the injection system's mixing performance can be made based on the the equivalence ratio associated with the minimum average channel pressure and the minimum mass flow rates required to achieve detonation as shown in Figures 66, 68, and 70. As discussed in Section 2.4, cell size was minimized when the equivalence ratio was near 1.0. It was expected that minimized cell size would enhance the detonability of the engine. Therefore, an equivalence ratio of 1.0 was the expected value where minimum pressure and mass flow rate could produce a detonation.

The lowest mass flow rate where detonation was achieved occurred at an equivalence ratio of approximately 1.2 for both nozzles as shown in Figures 66 and 68. Additionally, the $P_{c,min}$ curve shown in Figure 70, indicated that the minimum equiv-

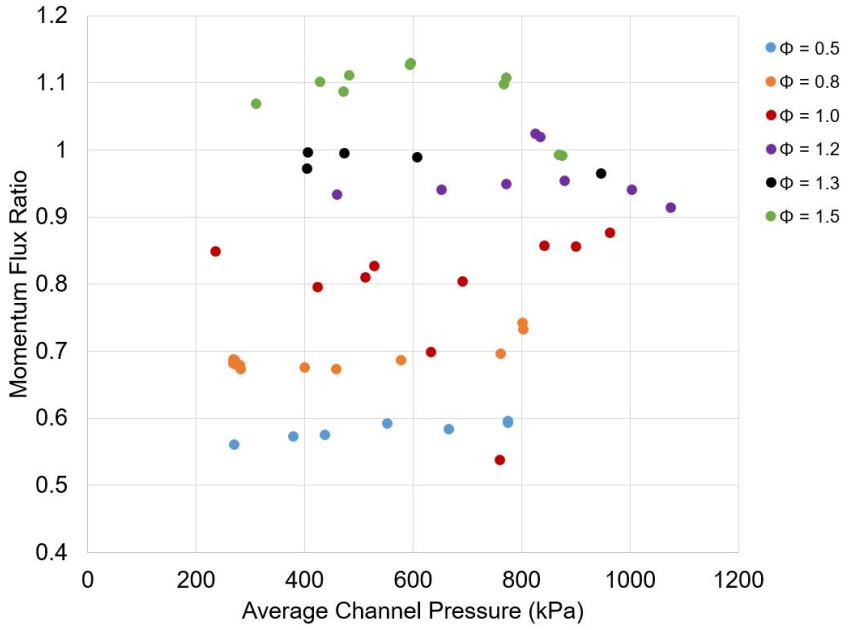

Figure 76. Momentum flux ratio vs. average channel pressure using the ϵ=0.14 nozzle with varying equivalence ratio

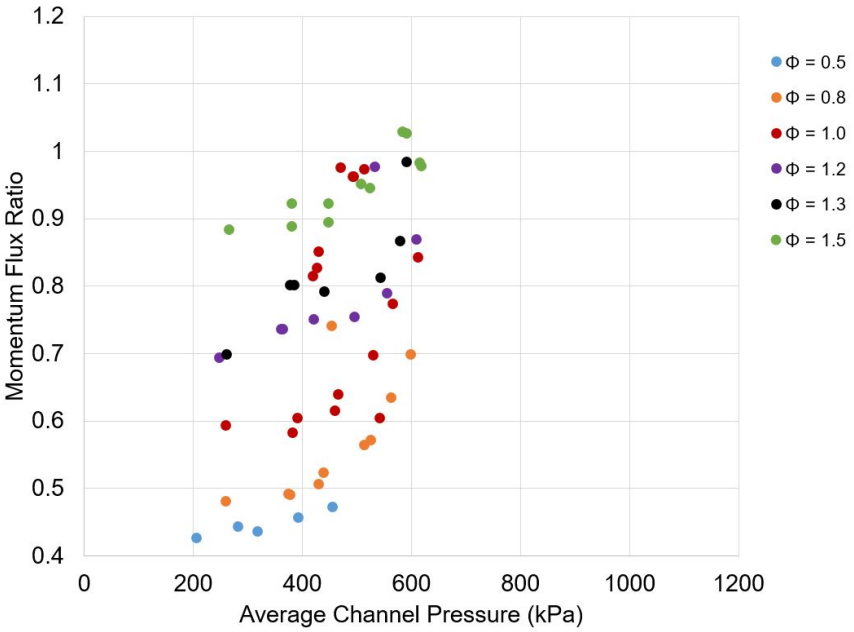

Figure 77. Momentum flux ratio vs. average channel pressure using the ϵ=0.40 nozzle with varying equivalence ratio

alence ratio where detonation could occur was between 1.1-1.2. With minimum mass flow and pressure values that occurred above the expected equivalence ratio value of 1.0 indicated the reactants may not have been fully mixed in the detonation channel. Although the "global" equivalence ratio delivered to the engine was 1.2, the local equivalence ratio of the mixed reactants in the channel may have actually been closer to 1.0 prior to the detonation wave consuming them. In other words, not all of the fuel was mixed with the oxidizer prior to the detonation wave's arrival. In future research, modifications to the injection system such as different diameter injection holes or adding more injection holes could be made to enhance mixing. Additionally, alternate injection schemes such as pintle or semi-impinging jets could be implemented as researched by Duval et al. [7].

The fill height of the engine was of interest because a reduced fill height would result in a reduced mass flow rate. Based on research from Bykovskii et al., the estimated fill height was found to be between 3.5-12 mm [5]. With a cell size of 0.5-1.75 mm for ethylene and nitrous-oxide, the fill height in terms of the number of cells was between 2-24. To estimate the actual achieved fill height in the channel, the ideal gas law was used to calculate the volume the reactants filled prior to being consumed by the passing detonation wave. However, using this method required some assumptions: 1) there was no pre-burning of the reactants, 2) the pressure experienced by the reactants as they entered the channel was the same around the entire circumference, and 3) the temperature of the reactants was the same as the plenum temperature ($\approx$ 290 K) assuming that the reactants would be cooled as they expanded flowing into the channel, but also heated by the nearby detonation wave. The pressure of the reactants entering the channel needed to be calculated since the average channel pressure would not be equivalent to the local pressure near the injection manifolds. Bykovskii et al. estimated that the average channel pressure was

2-3 times the pressure in front of the detonation wave [5], which was the approximate pressure the reactants would experience as they entered the detonation channel.

Using these approximations, the fill height in terms of cell size was calculated as shown in Figures 78 and 79 below, where the pressure used to calculate volume/fill height was the average channel pressure after the detonation had been initiated. Figure 78 shows the maximum expected fill height for each test point using the lowest detonation frequency (11.7 kHz). At this condition, the fill height values ranged between 3.8-9.7 mm, which equated to 7.6-19.4 cells, assuming a "worst-case" minimum cell size of 0.5 mm. Figure 79 shows the minimum expected fill height for each test point using the highest observed detonation frequency (14.0 kHz). Here, fill height values ranged between 3.2-8.1 mm, which equated to 2.2-4.6 cells assuming the "best-case" maximum estimated cell size of 1.75 mm. These fill height values were in agreement with the fill height correlation developed by Bykovskii et al. [5].

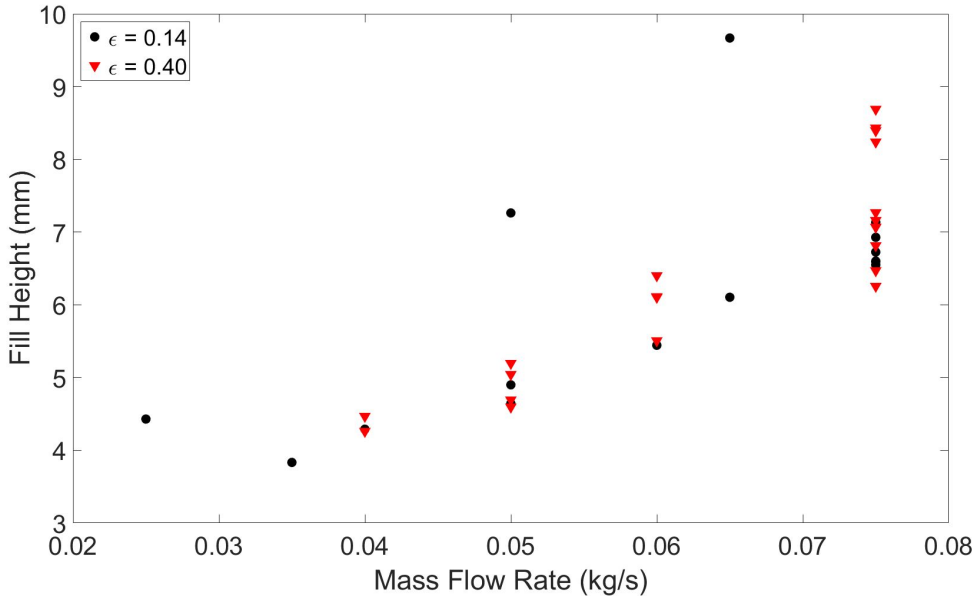

Figure 78. Maximum estimated fill heights with a detonation frequency of 11.7 kHz

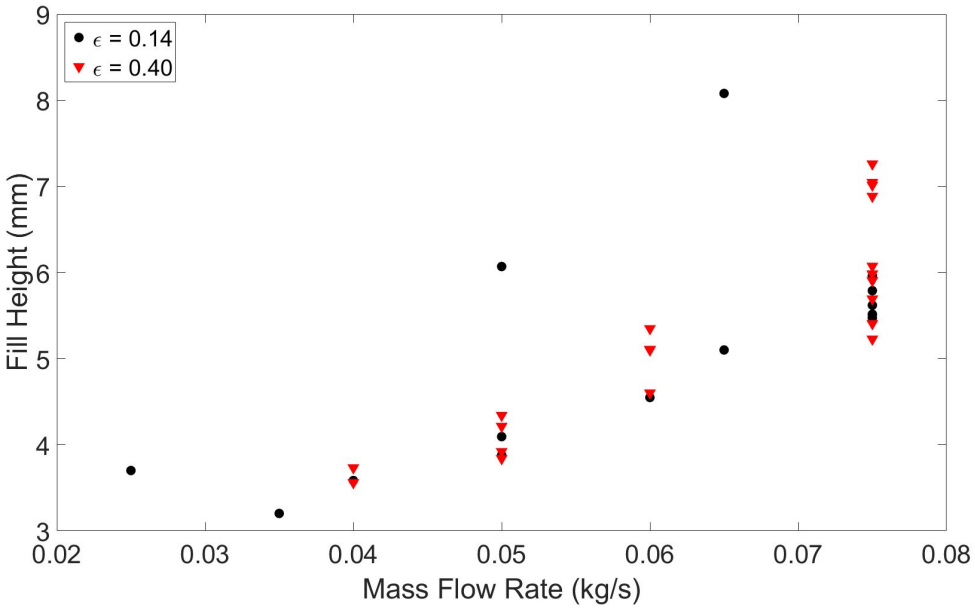

Figure 79. Minimum estimated fill heights with a detonation frequency of 14.0 kHz

4.5 Detonation Frequency Analysis

One of the primary objectives of this research was to build an RDE that could operate at a 20 kHz on a single detonation wave. During the design process, it was assumed that the detonation wave speed of ethylene and nitrous-oxide would be approximately 80% of the CJ velocity of 2200 m/s which equated to 1760 m/s. At 1760 m/s, the diameter of the RDE would need to be 28 mm for the detonation wave to travel around the circumference of the RDE 20,000 times in one second to produce the desired frequency. At these frequencies, traditional instrumentation such as ITP's or ion probes were not able to provide a fast enough sampling rate. Therefore, high speed imaging was used to observe detonation wave speed and extract a frequency. Additionally, a microphone captured acoustic data, where the peak amplitudes were assumed to be a result of the detonation wave.

Capturing the frequency data was more challenging than initially expected due to wave instability. When analyzing the high-speed camera data, it was difficult to find

consecutive images of steady wave behavior that could be used to calculate a wave frequency. In some cases, a visibly steady wave formation did not exist and the video was unusable for determining a wave speed/frequency. This created significant problems for coding software to automatically identify and track the detonation wave. A code was designed to identify the area with the most light intensity, which was assumed to be the detonation wave and track its rate of movement frame-by-frame. However, as shown in Figures 71 and 72, there was not necessarily a confined area of significantly higher intensity. Additionally, if the wave dissipated, an automated code may interpret the wrong region of the image as the detonation wave causing the calculated wave speed to be highly inaccurate. Therefore, the plan to use an automated code was abandoned and the wave speed was tracked and calculated manually.

Using a microphone to capture detonation frequencies also proved to be difficult. There was a narrow range of settings for which the microphone and amplifier was able to capture usable data. The amplifier was sensitive to signal gain settings, where if the gain was too low, it did not capture the acoustics of the engine. An example of this is shown in Figure 80 where the amplitude of the signal remained nearly constant through the duration of the recording. If the microphone had captured acoustic data, there would have been a higher amplitude signal during the first portion of the test run for approximately 0.5-1.0 s, and then taper off as the test sequence ended and flow through the engine subsided.

Alternatively, if the gain was too high the microphone/amplifier would become saturated, clip the signal, and only provide noise to the data acquisitions system as shown in Figure 81. The amplitude of the signal tapered from 0.05V to 0.02V as expected, but the point where the amplitude began to reduce was too late. The recording began when the spark was initiated, and therefore the signal amplitude should have begun to taper in under 1.0 s (valves close 0.5 s after spark). In this

example, the peak amplitudes extended to approximately 1.2 s before they began to taper. This was an indication that the signal was being clipped until the acoustics subsided, which was likely after the detonation and when nearly all of the flow through the engine had stopped. The lower voltage peaks of 0.05V in comparison to 0.8V as shown in Figure 49 were a result of trying to adjust the interface device to determine if a lower output level setting could help mitigate signal clipping. However, the interface's output setting did not appear to have any impact the microphone's performance.

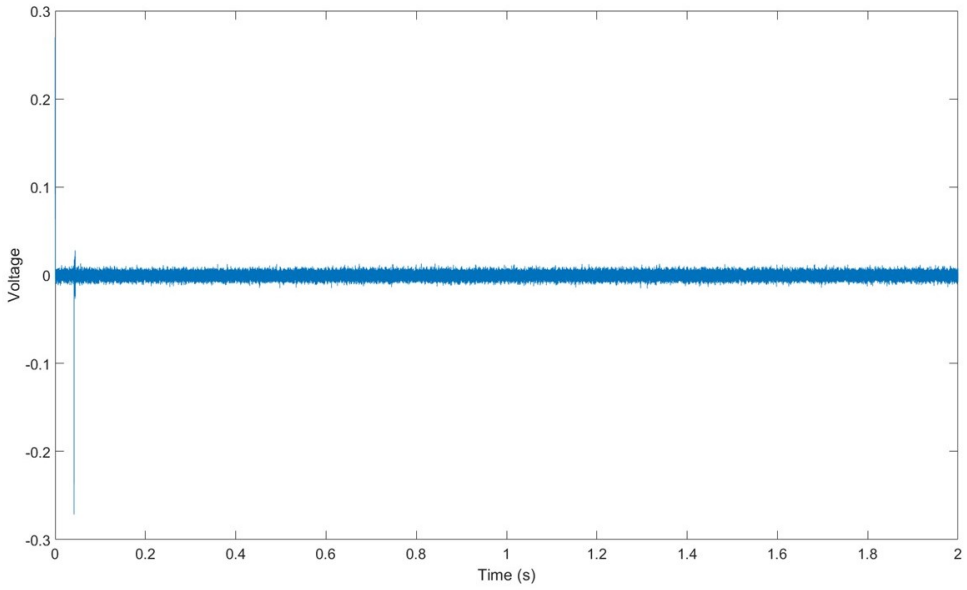

Figure 80. Example of acoustic signal when gain was set too low

Only two instances were observed where the microphone successfully captured data. However, there was no apparent reason why data was able to be captured during these test runs. Tests immediately following these instances did not provide usable acoustic data with the same test conditions and microphone settings. Slight variations in the decibel levels produced by the engine may have randomly allowed for successful data capture. A maximum sound pressure level, SPL, specification was not listed for the microphone, but similar measurement-condenser style microphones

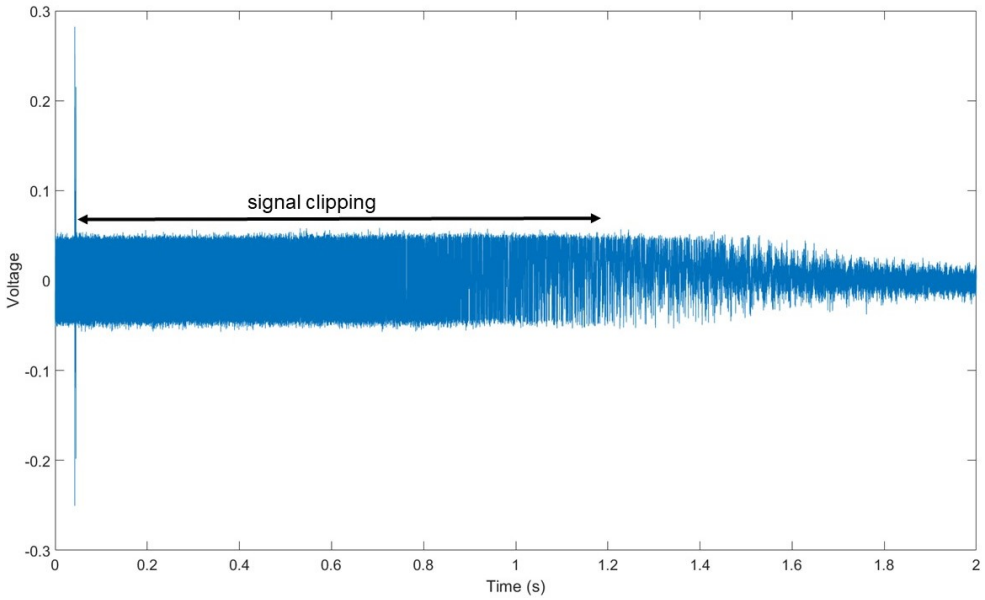

Figure 81. Example of signal clipping of acoustic data

listed a maximum SPL of 120 decibels. The decibel level of the RDE was found to be at or above 130 decibels during detonation, which was the maximum value the decibel meter could measure. The microphone used for this research was likely not well suited for the high decibel environment of RDE testing, which resulted in the lack of usable data and sensitivity to position and gain settings. Attempts to properly tune the microphone were abandoned after approximately 20 test runs failed to produce consistently usable data.

Despite the challenges encountered using the high-speed camera, frequency data captured is shown in Table 3. The frequency was determined by manually counting the number of frames required for the detonation wave to make a revolution from the high speed camera. With a known time interval between frames, the wave speed could be calculated using the RDE's diameter. The ranges provided represents the uncertainty associated with the manual frame counting technique.

As shown in Table 3, the operating frequency of the engine ranged between 11.7-14.0 kHz, which was approximately 30-40% lower than anticipated. As discussed in

Table 3. Engine frequency data

ϕ	$\dot{m}$	P_c (kPa)	ϵ	Wave Speed (m/s)	Frequency (kHz)
0.8	0.06	557	0.4	1030-1090	11.7-12.4
0.8	0.075	591	0.4	1030-1090	11.7-12.4
1	0.06	561	0.4	1030-1090	11.7-12.4
1	0.075	485	0.4	1160-1230	13.1-14.0
1	0.075	830	0.14	1090-1160	12.4-13.1
1.2	0.025	444	0.14	1160-1230	13.1-14.0
1.2	0.035	362	0.4	1160-1230	13.1-14.0
1.2	0.035	652	0.14	1160-1230	13.1-14.0
1.2	0.05	513	0.4	1160-1230	13.1-14.0
1.2	0.05	867	0.14	1160-1230	13.1-14.0
1.2	0.06	545	0.4	1160-1230	13.1-14.0
1.2	0.075	625	0.4	1090-1160	12.4-13.1
1.2	0.075	1053	0.14	1030-1090	11.7-12.4
1.3	0.04	462	0.4	1160-1230	13.1-14.0
1.3	0.05	520	0.4	1160-1230	13.1-14.0
1.3	0.06	577	0.4	1090-1160	12.4-13.1
1.3	0.075	573	0.4	1090-1160	12.4-13.1
1.3	0.075	939	0.14	1160-1230	13.1-14.0
1.5	0.05	497	0.4	1160-1230	13.1-14.0
1.5	0.075	605	0.4	1160-1230	13.1-14.0

Section 2.5, Fernelius et al's. research on detonation wave speed in detonation tubes found that with increasing equivalence ratio, detonation wave speed also increased for various fuel and oxidizer mixtures between $\phi = 0.6$-1.4 [19]. Chang et al. also looked at channel pressure and its effects on detonation wave speed in an RDE and found that increasing channel pressure can reduce the detonation's wave speed [32]. For the current research, equivalence ratio, mass flow rate, channel pressure, and area ratio did not appear to have an independent influence on detonation frequency. However, if uncertainty in the wave speed calculation could be reduced, a trend following Fernelius et al's. or Chang et al's. work might be revealed. The resulting wave speeds were only 47-56% of CJ wave speed, which was lower than the estimated 80%. Assuming that the relationship between detonation wave speed and channel diameter was linear, the diameter would need to be reduced 16-20 mm to achieve the desired 20 kHz frequency.

However, further reducing the diameter could cause more instabilities and cause even greater reduction in wave speed, or the radius could reach a point where detonation was not achievable.

The reduced wave speeds observed for this research may have been a function of several factors to include: 1) channel curvature 2) reactant mixing 3) pre-burning and 4) expansion of an unconfined detonation. As discussed in Section 2.5, reduced channel curvature can cause the detonation wave to become unstable and reduce detonation velocity. Kudo et al. found that if r_i/λ in detonation tube was less than 14, the detonation wave can become unstable [8]. With an inner channel radius of 12 mm and a cell size ranging between 0.5-1.75 mm, r_i/λ was found to be 7-24, which was partially within the unstable regime and could lead to reduced detonation velocity. As researched by Duval et al., poor mixing can reduce also reduce detonation stability [7], and as discussed in Section 4.4, the injectors may not have been optimally mixing the reactants. The poorly mixed reactants may have reduced the detonation wave's stability resulting in a lower detonation wave speed.

Reactant pre-burning was another phenomenon that may have affected detonation stability and wave speed. At the interface between fresh reactants and the hot exhaust gases in the detonation channel exists a deflagration zone where the temperature of the exhaust gases cause the fresh reactants to combust prior to the arrival of the detonation wave. In high-speed imagery, pre-burning may be indicated by light of less intensity ahead of the higher intensity light associated with the detonation wave as shown in Figures 71 and 72. However, due to the instability associated with the detonation waves in this RDE, it was indiscernible whether the light observed ahead of the detonation wave was a result of pre-burning or deflagration behind a previous wave. In either case, pre-burning could reduce the fill height of the reactants, and if enough reactants were not present, the detonation wave's stability and ultimately

speed could have been negatively impacted. Since the RDE in this research was operating at minimum mass flow rates and thus minimal fill heights, the wave speed may have been affected by pre-burning.

Paxson found that the unconfined space associated with an RDE detonation channel was a factor that could have reduced detonation wave speed when compared to detonation velocities observed in detonation tubes [9]. The idealized detonation occurs under constant volume, and the confined space associated with a detonation tube allows for this to occur. Therefore, CJ velocity can often be achieved in a detonation tube. However, geometries in an RDE channel allow for expansion and the detonation no longer occurs in a constant volume environment. The increased volume reduces the peak temperature and pressure associated with the detonation which reduces the shock strength and can be directly correlated with wave speed [9]. Although this phenomenon was not unique to this research, it should still be noted that RDE detonation velocities can only achieve a fraction of those observed in detonation tubes.

In terms of operating frequency, the current research did not meet the design objective of 20 kHz, but this RDE was able to offer a starting point for future small scale RDE development. Regardless, the research objectives of achieving a detonation in a small scale RDE that operated at low mass flow rates were successfully completed. Detonation was achieved in an RDE that had a diameter five times smaller than previous RDE's tested at the DERF, and the total mass flow rate through the engine was reduced by an order of magnitude. It should also be noted that the small scale RDE developed for this research was 30% smaller in diameter than the previously known smallest RDE built by Popov et al. [33]. The additional objective of characterizing the performance of the engine was also achieved, and the engine was able to produce detonations between equivalence ratios of 0.8-1.5 and at a mass flow rate as low as 0.025 kg/s.

V. Conclusion

A small scale RDE was designed to both reduce the hazards associated with RDE testing as well as establish an understanding of operating characteristics of an RDE with a small diameter. Current RDE research facilities such as the AFRL's DERF require reinforced structure, noise abatement, and the storage of large quantities of hazardous materials. The DERF was previously used to test 150 kN class jet engines and was uniquely qualified to safely test potentially dangerous machinery. The number of facilities similar to the DERF are likely few, and the capital required to build such a facility would be prohibitive to many institutions. If a smaller RDE could be developed that reduced some of the operating risks, RDE research could potentially be completed in common lab environments. With the availability of additional research facilities, novel diagnostic tools could be used for RDE research, where they may have been previously inaccessible.

The desire to reduce hazards associated with RDE testing led to the development of an engine that was 25-30 mm in diameter, had a channel gap of 2 mm, and operated on a mass flow rate of 0.05 kg/s. This mass flow rate was an order of magnitude lower than previous RDE test rigs at the DERF and the engine was approximately five times smaller in diameter. The engine's small size would not completely eliminate, but could possibly reduce the need for a reinforced structure, protective barricades, stand-off distance, etc. in the event of catastrophic engine failure. Additionally, the low mass flow rates would reduce the need to store large quantities of hazardous materials in comparison to a larger RDE assuming a similar run time. Additionally, lower mass flow rates would reduce the amount of jet noise produced by the engine and alleviate some of the acoustic concerns. The small diameter of the engine and reduced mass flow rate could increase the detonation frequency and reduce the amplitude of the resulting acoustics, which would reduce vibration. The reduced vibration, could also

enable the use of sensitive lab equipment such as laser diagnostics.

5.1 Methodology

The small scale RDE was developed using geometric criteria researched by Bykovskii et al. Their research revealed sizing requirements for an RDE's detonation channel that needed to be met in order to achieve stable detonation. The dimensions researched were the fill height of reactants in the detonation channel, channel length, channel gap, and channel diameter. Bykovskii et al's. research provided equations to calculate these parameters, where the geometries are based on the cell size of the reactants [5]. In order to reduce the mass flow rate through the engine, the minimum range for fill height was used, which also affected the calculation for channel gap and channel length. The detonation channel diameter was sized based on the desired operating frequency of 20 kHz and the detonation wave speed of the reactants. Bykovskii et al's. design criteria resulted in a fill height of 3.5-12 mm, a channel length of 30 mm, channel gap of 2 mm, and a channel diameter of 28 mm.

The RDE's reactant injection and mixing was a concern for successful operation. At an operating frequency of 20 kHz, the reactants would need to be injected to achieve the needed fill height and mixed in the detonation channel in as little as 50 μs; four times shorter than a typical RDE. Due to the confined geometries of the RDE developed for this research, a Jets-in-Crossflow injection scheme was implemented in the design.

To operate the RDE, a control system needed to be developed as part of this research. The flow of fuel and oxidizer was governed by isolation valves in addition to Alicat® mass flow controllers, where the controllers were set to achieve the desired flow rates of 0.025-0.075 kg/s and equivalence ratios of 0.5-1.5 necessary for testing. A simple spark controller/spark plug was used to ignite the engine. However, testing

later proved that the spark plug needed to be moved from the exit plane of the engine to inside of the detonation channel in order to achieve detonation. The test sequence was automated, which required control software to accurately time the opening of the isolation valves, spark, and valve closure when the sequence was complete. The control software also provided timing signals for high-speed imaging and acoustic monitoring.

The RDE was instrumented with pressure transducers and thermocouples in the fuel and oxidizer plenums as well as a CTAP in the detonation channel. Instrumentation access was limited due to the small size of the RDE. A high-speed camera in combination with a microphone were used to monitor detonation wave behavior and frequency. Automated methods to determine detonation frequency proved to be a challenge due to wave instability, and difficulties capturing usable acoustic data were also encountered.

5.2 Results

The engine was tested over an operating regime of 0.025-0.075 kg/s and at equivalence ratios of 0.5-1.5 to build an operating map of where detonation could be achieved. Using the original configuration of the engine, detonation was not achieved. In this configuration, the spark plug was positioned at the exit plane of the engine and there was no mechanism to increase the static pressure in the channel. In this configuration, the flow velocity far exceeded the flame speed of the reactants. To reduce the flow velocity, a back plate at the exhaust plane of the engine was added to increase the static pressure in the detonation channel and reduce the flow velocity. The spark plug was also repositioned inside the detonation channel to take advantage of the reduced flow velocity in the channel. With this configuration, detonation was achieved at four operating conditions. However, the back plate used had a tendency

to become misaligned which affected testing consistency, and it also obstructed the view of the high speed camera.

In order to rectify the issues encountered with the back plate, the centerbody of the engine was replaced with an aerospike nozzle which would also serve to increase the static pressure in the channel, which appeared to be strongly correlated with the ability to achieve detonation. Two different diameter nozzles were manufactured, which allowed for the channel pressure to be altered independent of flow rate. The resulting area ratios for the nozzles were 0.14 and 0.40. The aerospike nozzles also allowed the detonation wave to be visible around the entire circumference of the detonation channel.

Using the 0.14 area ratio nozzle, detonation was achieved at 13 points at equivalence ratios between 1.0 and 1.3. The lowest flow rate where detonation was achieved was at 0.025 kg/s, and at an equivalence ratio of 1.2. Channel pressure also had an influence on detonability, where the lowest observed pressure where detonation occurred at 460 kPa at an equivalence ratio of 1.2. As equivalence ratio was increased or decreased from 1.2, additional channel pressure was required to achieve detonation.

With the 0.40 area ratio nozzle, the same general trends were observed as the 0.14 nozzle. Detonation was achieved between equivalence ratios of 0.8 and 1.5. However, the lowest flow rate where detonation was achieved was 0.04 kg/s. This was expected since the larger area ratio nozzle would not provide as high of a channel pressure for a given mass flow rate when compared to the 0.14 nozzle. The lowest pressure where detonation occurred was at 421 kPa and at an equivalence ratio of 1.2. The 0.40 area ratio nozzle was able to produce a detonation over a larger range of equivalence ratios when compared to the 0.14 area ratio nozzle, and this may have been a result of reduced channel pressure for a given mass flow rate.

The injection system was also analyzed to understand its affects on detonability.

Injection pressures were investigated in relationship to channel pressure to determine a ratio that produced the most detonations. The data revealed that when the ratio of $\frac{P_f}{P_c}$ to $\frac{P_{ox}}{P_c}$ was approximately 0.87, detonation was more likely to occur. It was also noted that the nozzle area ratio and resulting channel pressure could affect the stiffness of the injectors and may have had an impact on the range of equivalence ratios where detonation occured. Additionally, the injector momentum flux ratio, $\frac{P_f \gamma_f}{P_{ox} \gamma_{ox}}$, was examined, and test data indicated that detonation was more likely at a momentum flux ratio between 0.9-1.0.

Detonation wave stability, wave speed, and detonation frequency were also researched. In all test cases, the detonation wave appeared to be unstable. In some cases the wave was seen momentarily dissipating, but the most common mode was counter-rotating waves that were colliding with the spark plug. Through manual observation of high-speed imagery, the detonation wave speed and resulting detonation wave frequency was determined. Wave speeds ranged between 1020-1230 m/s which produced detonation frequencies of 11.7-14 kHz. Wave speeds were 30-40% lower than expected, which produced frequencies lower than the desired 20 kHz.

5.3 Recommendations for Future Work

This RDE design provided an initial starting point for small scale RDE research, but many opportunities still exist. Particularly, there are several design changes that could be implemented to improve its operability. As previously discussed, the wave speeds and resulting detonation frequencies were below the desired value of 20 kHz. The RDE channel dimensions could be reduced to see if this value can be achieved. Assuming that the detonation frequency scales linearly, the channel diameter would need to be reduced to 16-20 mm.

A contributing source of instability appeared to be the spark plug positioned in

the detonation channel. To remedy this, a new ignition system should be considered. The most straightforward approach would be to modify a spark plug so that the electrode tip was flush with the outer body wall. This would allow the detonation wave to travel around the entire circumference of the channel with minimal obstructions. Considerations for relocating the axial position of the spark plug should also be made. If the spark plug was moved to the base of the channel, near the oxidizer injection plate, it could allow the detonation wave to pass above it without interference. Alternatively, the spark plug could be moved near the aft end of the channel (still in the channel) and possibly allow the detonation wave to pass below.

Another ignition method would be to implement a pre-detonation device (pre-det). A pre-det operates by injecting small amounts of fuel and oxidizer into a detonation tube. A spark plug would ignite these reactants, and the mixture would undergo a Deflagration to Detonation Transition (DDT) event inside the detonation tube before entering the RDE's detonation channel. The pre-det would still require a small hole in detonation channel, but the hole would be reduced to 4.5 mm in diameter instead of the existing 8 mm for the spark plug. However, the main advantage of this approach is that there would be nothing protruding into the channel.

Further testing and modifications to the injection system could be made. During this research, the injection holes directly impinged on each other and were oriented at a 90° angle (i.e. classic Jets-in-Crossflow). A simple alteration would be rotate the fuel injection manifold so that the jets were no longer directly impinging, but were offset circumferentially to the oxidizer injection holes (similar to Semi-Impinging Jets scheme). Additionally, multiple injection manifolds could be made with various injection hole sizes. This would allow for manipulation of injection pressures independent of equivalence ratio and mass flow rate. By adjusting injection pressures, the effects injection pressure ratio and momentum flux ratio could be further investigated.

Either of these modifications would allow for a further understanding of injection performance on detonability.

A handful of challenges were encountered with instrumentation during testing that could also be improved upon. The microphone was intended to capture acoustic data from the engine, but it proved to be incapable of producing usable data. The microphone was likely not capable of handling the level of noise produced by the engine. This was unfortunate, because a microphone could potentially offer a technique to unobtrusively capture detonation wave speed and frequency. Other traditional methods such as ITP's or ion probes require ports into the detonation channel which could affect detonation wave behavior. More capable microphones are available that can handle higher decibel levels and should be implemented in future RDE testing.

After analyzing run data, temperature influenced the detonability of the engine. The influence of temperature could be seen in the channel pressure data, and channel pressure impacted detonability. However, no thermocouple was present to measure channel temperature. The flow was likely susceptible to relatively large amounts of heat transfer from the channel walls due to the narrow channel gap. The actual flow temperature would be desired, but a detonation wave can produce temperatures of over 3000 K which would quickly destroy a thermocouple if inserted directly into the flow. At a minimum, a thermocouple could be embedded in the outer channel wall which could at least provide some insight into relative channel temperatures from test to test.

Improvements to the data acquisitions and control system are also recommended. Particularly, the mass flow rate control software should be incorporated into the main control/acquisitions software. A second operator was required to manually set and observe the flow controllers, which added unnecessary complexity to engine operation. Additionally, the data from the flow controllers was not able to be saved in a manner

that could be synchronized with the pressure, temperature, and timing data from the main control program. This allowed for additional error in equivalence ratio calculations and also made it difficult to study equivalence ratio while the actual detonation was occurring. For future testing, it is recommended that the the main control/acquisition software be programmed to also operate and record data from the mass flow controllers.

In addition to improvements to the test rig, the small scale RDE could be used for expanded research opportunities. Testing of more common fuels, such as propane could allow even more institutions to complete RDE work since this fuel is widely available. The wide availability of propane would also make the small scale RDE more portable since it could potentially be run off of a 450 g bottle made for camping. Propane is also less reactive than ethylene and would be safer to store and operate. However, to incorporate additional fuels an investigation into the fuel and oxidizer's cell size would be needed to ensure operability which could result in some adjustments to the small scale RDE's design.

The small scale RDE was also designed to incorporate thrust vectoring via equivalence ratio manipulation. The connection plate had provisions for three oxidizer connection ports so that the oxidizer plenum could be isolated into three individual sectors; with one oxidizer port in each sector. Using three separate mass flow controllers, the equivalence ratio in one sector of the injection scheme could be changed independently of the other two. The difference in equivalence ratios around the circumference of the detonation channel could affect the thrust in a portion of the channel and create thrust vectoring. The DERF has a small six axis thrust stand available that would be capable of measuring thrust independently in each sector. Groundwork for this type of thrust vectoring was completed by Falempin et al. by altering the mass flow rate in half of the circumference of the injection scheme [34].

The significance of this capability is that no moving parts are required to achieve this effect.

Appendix A. Recommended Design Improvements

Throughout the test campaign, the engine needed to be disassembled and reassembled occasionally, and a couple of minor design changes were noted to make the this process easier. These recommended changes had no impact on testing or results, but they would have been "nice to have" in a future design iteration.

The first suggested change would be at the interface of the fuel and oxidizer manifold. As shown in Figure 82, the fuel manifold was secured to the RDE using a 3/8" socket cap screw. While tightening this screw there was no easy method to counteract the torque imparted on the screw and fuel manifold, and the fuel manifold would rotate while trying to tighten the screw. The rotation of the fuel manifold was also troublesome because the injection holes on the fuel manifold needed to be aligned with the injection holes on the oxidizer manifold. Additionally, if the centerbody or aerospike nozzle was over-tightened upon installation, it could cause the fuel manifold to rotate and move the injection holes out of alignment.

To rectify this, an axial notch or protrusion could be added to the fuel and oxidizer manifold to inhibit rotation, with the male notch on the fuel manifold and female notch on the oxidizer manifold. An additional "offset" notch could also be incorporated to allow for the injection holes to be aligned between each other circumferentially instead of direct impingement.

The second suggested modification would be to resize the bolt holes on the outer body to accommodate a shoulder bolt as shown in Figure 83. There was a small gap between the bolt holes and the standard 1/4" bolt used to fasten the outer body to the remainder of the RDE assembly. This small gap could allow the outer body to be slightly misaligned and required the use of a shimming tool to ensure that the exit gap of the detonation channel was consistent around the entire circumference of the exit plane.

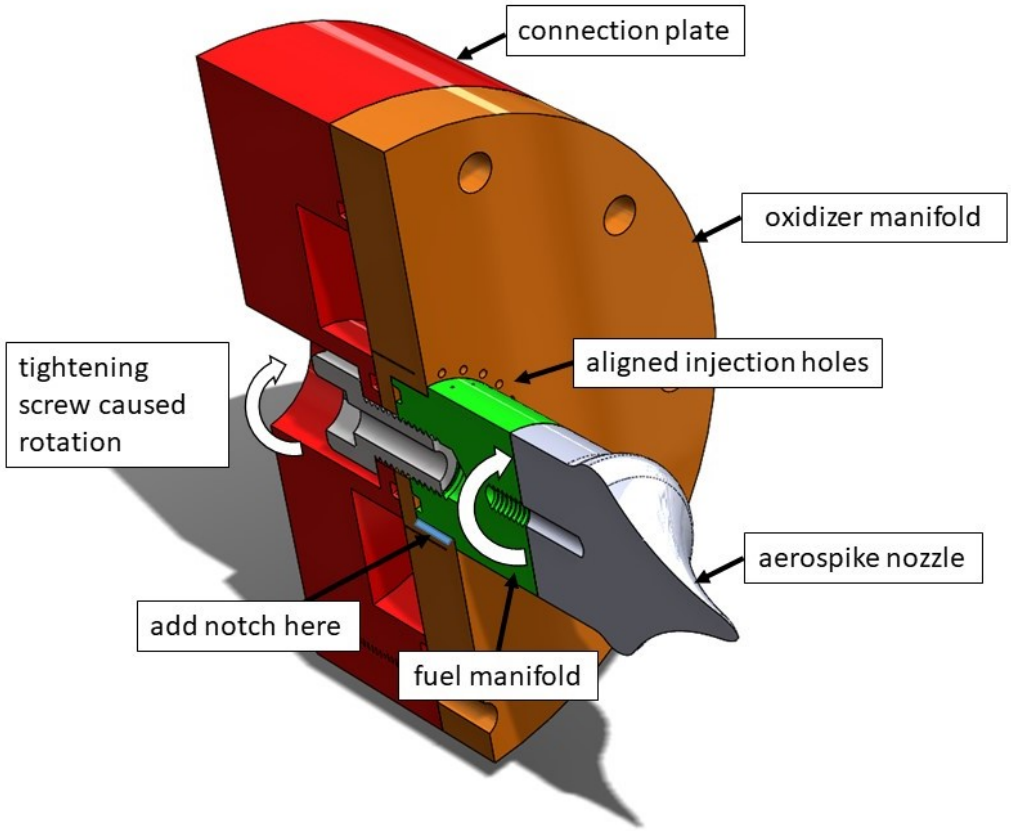

Figure 82. Recommended modifications to injection manifolds to reduce assembly challenges

The outer body alignment issue could be corrected by using a shoulder bolt in place of a standard bold (with modifications to outer body) as shown in Figure 84. A shoulder bolt is manufactured with tight tolerances at the shank. The tighter tolerances in comparison to a standard bolt would allow the bolt holes on the outer body to be machined with a minimal gap between the hole and bolt shank which would eliminate the alignment concern.

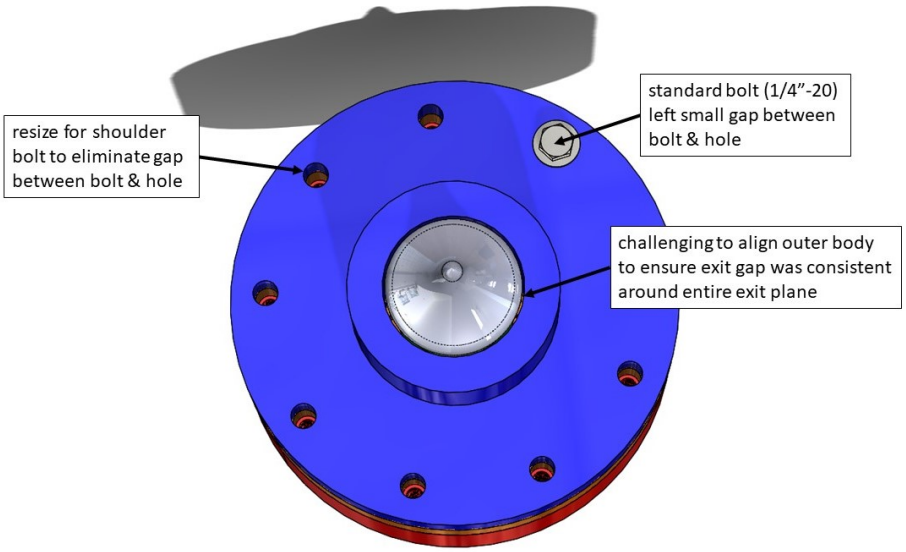

Figure 83. Recommended modification to outer body bolt holes to reduce assembly challenges

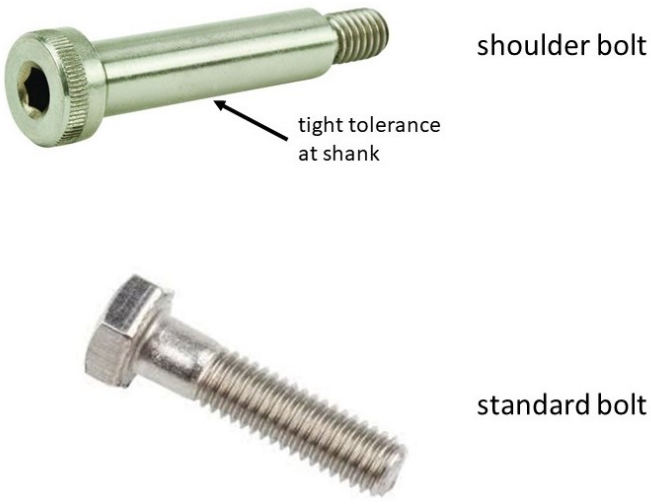

Figure 84. Comparison of shoulder bolt vs. standard bolt

Appendix B. Alternate Method for Detonation Frequency Determination

As discussed in Section 3.3, a code that tracked the detonation wave frame-by-frame to determine detonation wave speed and frequency was not able to be used due to the unstable nature of the detonation wave. However, late in this research effort an alternate method to determine a detonation frequency using high-speed imagery was discovered in work by Bennewitz et al. As shown in Figure 85, their method used fluctuations in pixel intensity over equally spaced, stationary "buckets" around the circumference of the detonation channel in lieu of trying to track the detonation wave frame-by-frame. By analyzing the changing pixel intensity over time for each of these buckets, a detonation frequency could be determined by performing an FFT [35]. A more thorough explanation of their frequency analysis technique can be found in their paper titled "Characterization of Detonation Wave Propagation in a Rotating Detonation Rocket Engine using Direct High-Speed Imaging." Their method was adapted for this research using the following general process:

1. An excerpt of 1000-5000 frames was selected from the high speed imagery

2. The average of the selected images was found and then the average image was subtracted from each individual image

3. The detonation channel location was found by summing of all images to determine the area of greatest pixel intensity (filtered to only include the top 80-95% of intensities). This area roughly represented the detonation channel. Bennewitz et al. used a slightly different technique here, but the code used in the current research had provisions for their method as well

4. Using the area of greatest pixel intensity, an equation for a circle was calculated to represent the detonation channel's location using a Taubin fit method

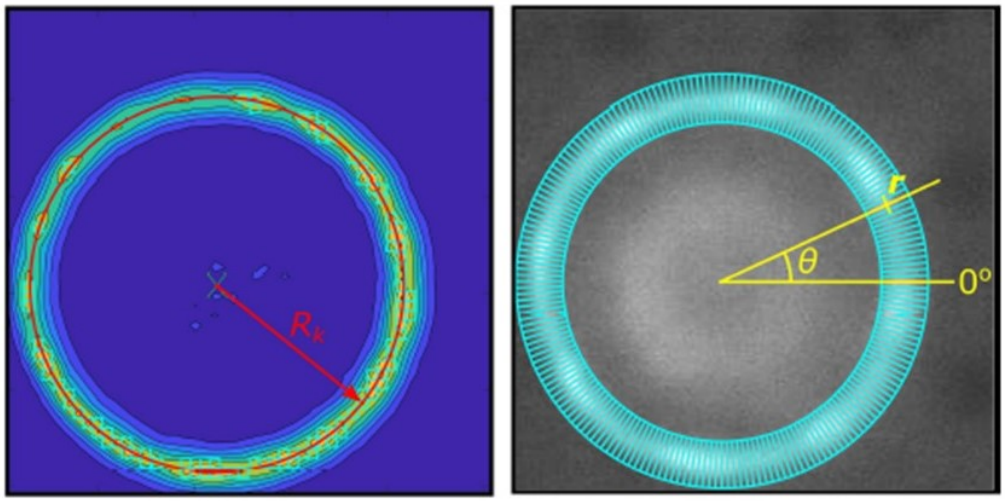

Figure 85. Alternate method for determining detonation frequency [35]

(MATLAB function files for this were available online)

5. The circle/detonation channel was divided into 50-200 sections around the circumference of channel. Each section represented a single bucket, and the pixels contained within the boundaries each bucket were then summed at each time step

6. An FFT was performed on each bucket to determine an operating frequency of the engine. The use of multiple buckets allowed for frequency analysis around the entire circumference of the channel

Results from the code developed for this research are shown in Figure 86. Fifty buckets were used in this example to analyze the frequency around the entire detonation channel. The operating mode was found to be approximately 12 kHz, which agreed with the frequency determined by the manual counting method discussed in Section 3.3. Other regions with high pixel intensities were observed, but this par-

ticular region had relatively high intensities around the entire circumference of the channel which would indicate the presence of a detonation wave travelling around the detonation channel. Another area of high pixel intensity can be seen between 1-5 kHz between 70-240°. This area corresponds to the general position of the spark plug as shown in Figure 87, and the fluctuating pixel intensity was a result of the detonation wave colliding with the spark plug. The frequency at this location was lower because the spark plug would tend to "glow" for 3-4 frames after the collision. This prolonged span of elevated pixel intensity reduced rate of fluctuation and resulting frequency.

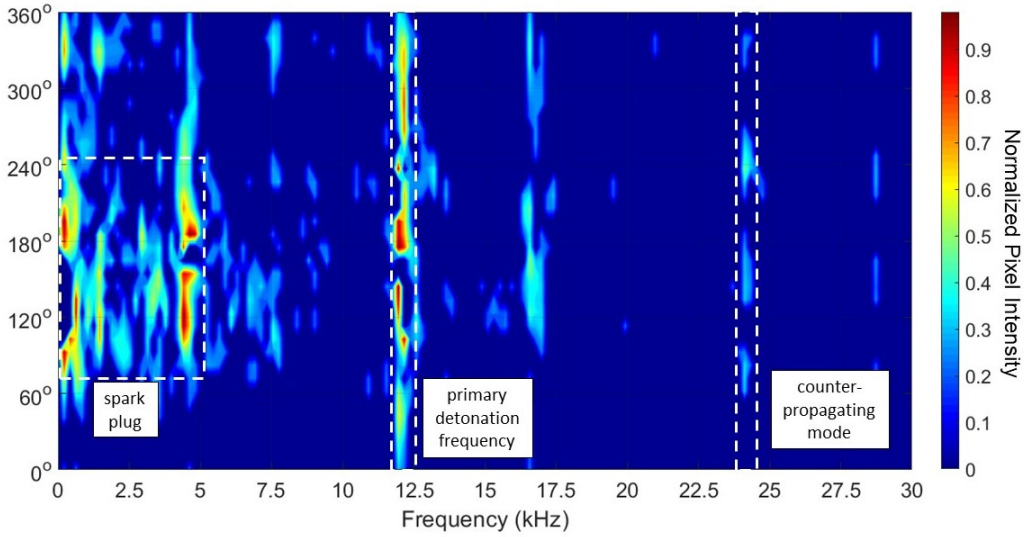

Figure 86. Example of detonation frequency analysis using alternate method

A region of elevated pixel intensity can be seen at approximately 24 kHz that traverses nearly the entire channel circumference. The pixel intensity here was not a high as the region that represented the primary detonation frequency, which indicates that the cause of the fluctuations were not as intense or persistent. However, the frequency was approximately twice that of the primary detonation frequency observed, which could represent the clapping/counter-propagating mode discussed in Section 4.3.

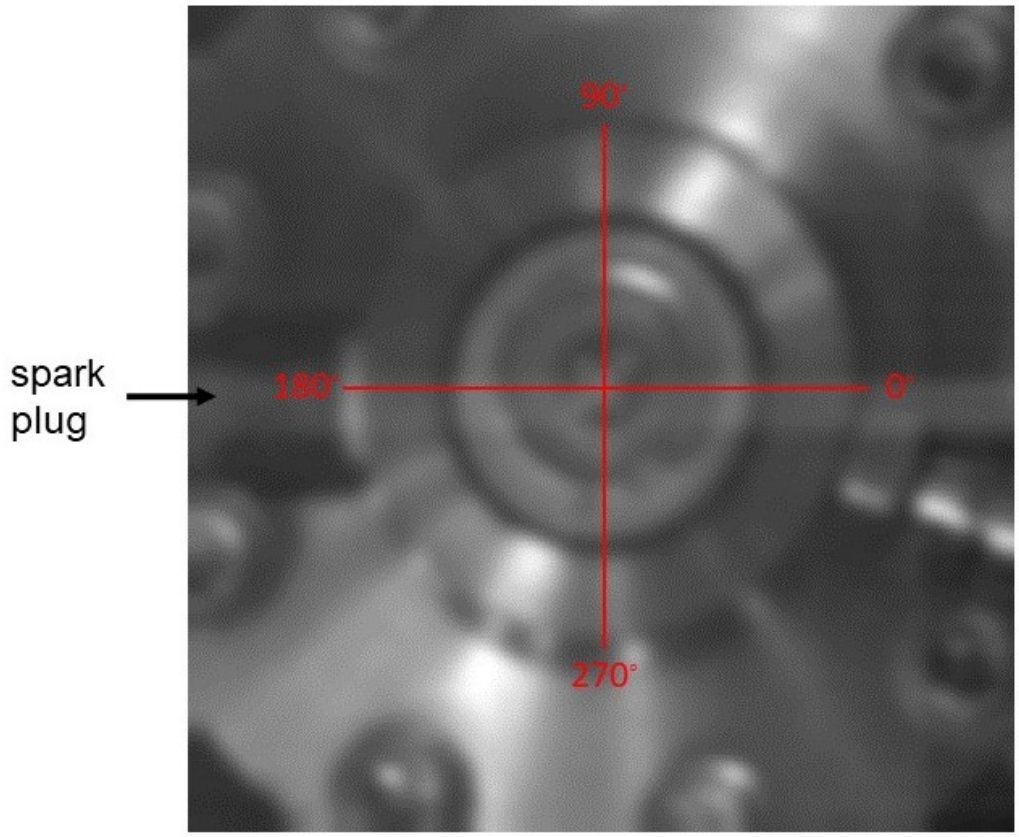

Figure 87. Angular position of the spark plug

This frequency analysis method proved to be robust. In some instances the exhaust of the RDE would cause the overhead mirror to shift, which would cut-off part of the view of the detonation channel. Even when only about half of the channel was visible, this method was still able to determine an operating frequency. Bennewitz at al. demonstrated that this method can also be used to calculate the number of detonation waves, wave direction, and track the detonation wave's position over time if a stable detonation wave can be achieved [35]. This method is recommended for future frequency analysis using high speed imagery and the code developed for this research is available on the AFIT and AFRL share drives.

Appendix C. Machine Shop Drawings

The machine shop drawings are listed in Figures 88 through 95 for the RDE built during this research effort. Figure 88 shows the connection plate, Figure 89 shows the oxidizer manifold, Figure 90 shows the fuel manifold, Figure 91 shows the original centerbody, Figure 92 shows the $\epsilon = 0.14$ nozzle, Figure 93 shows the $\epsilon = 0.40$ nozzle, Figure 94 shows the outer body, and Figure 95 shows the tapping locations for the spark plug and CTAP ports. All dimensions are in inches.

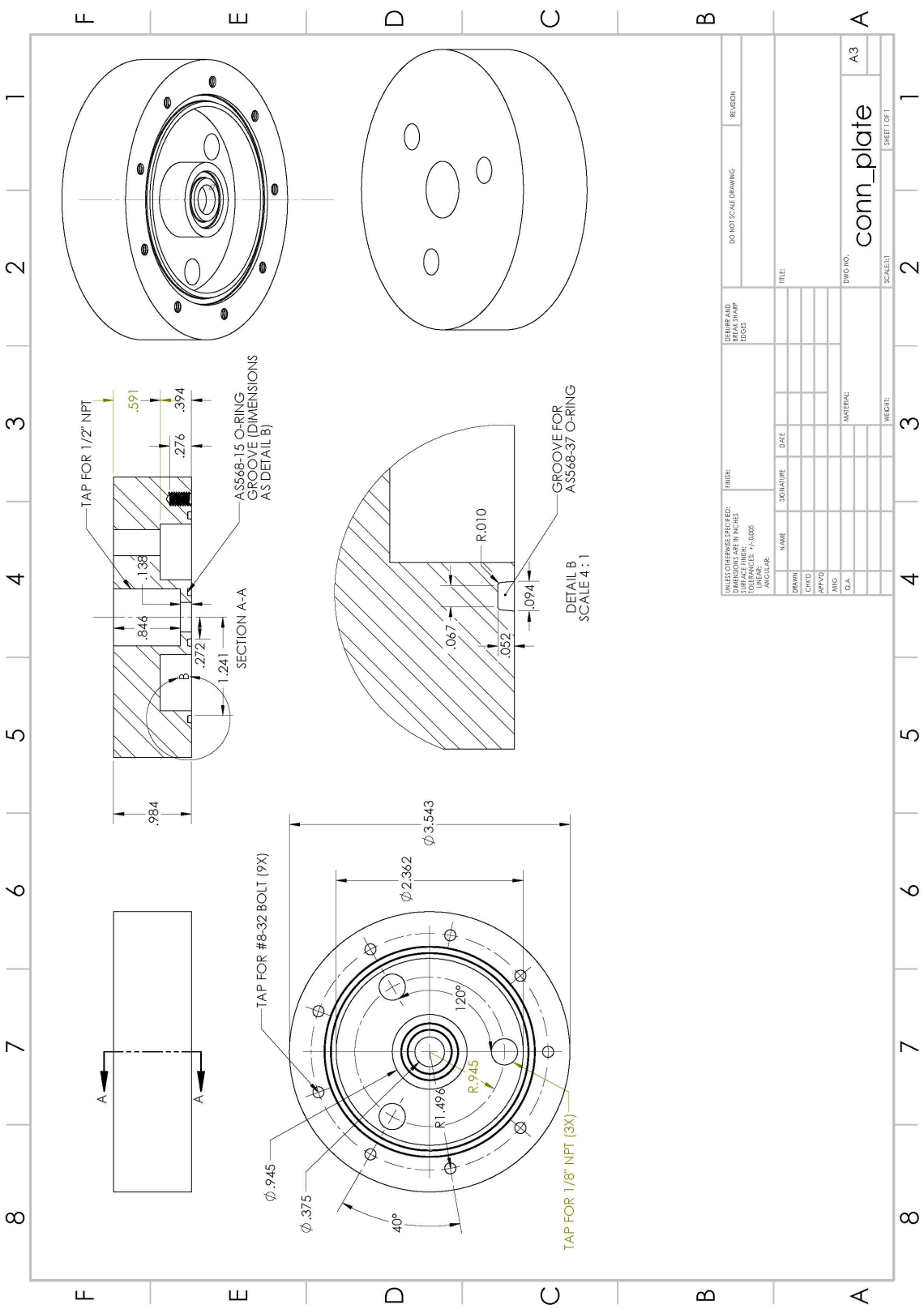

Figure 88. Machine shop drawing for the connection plate

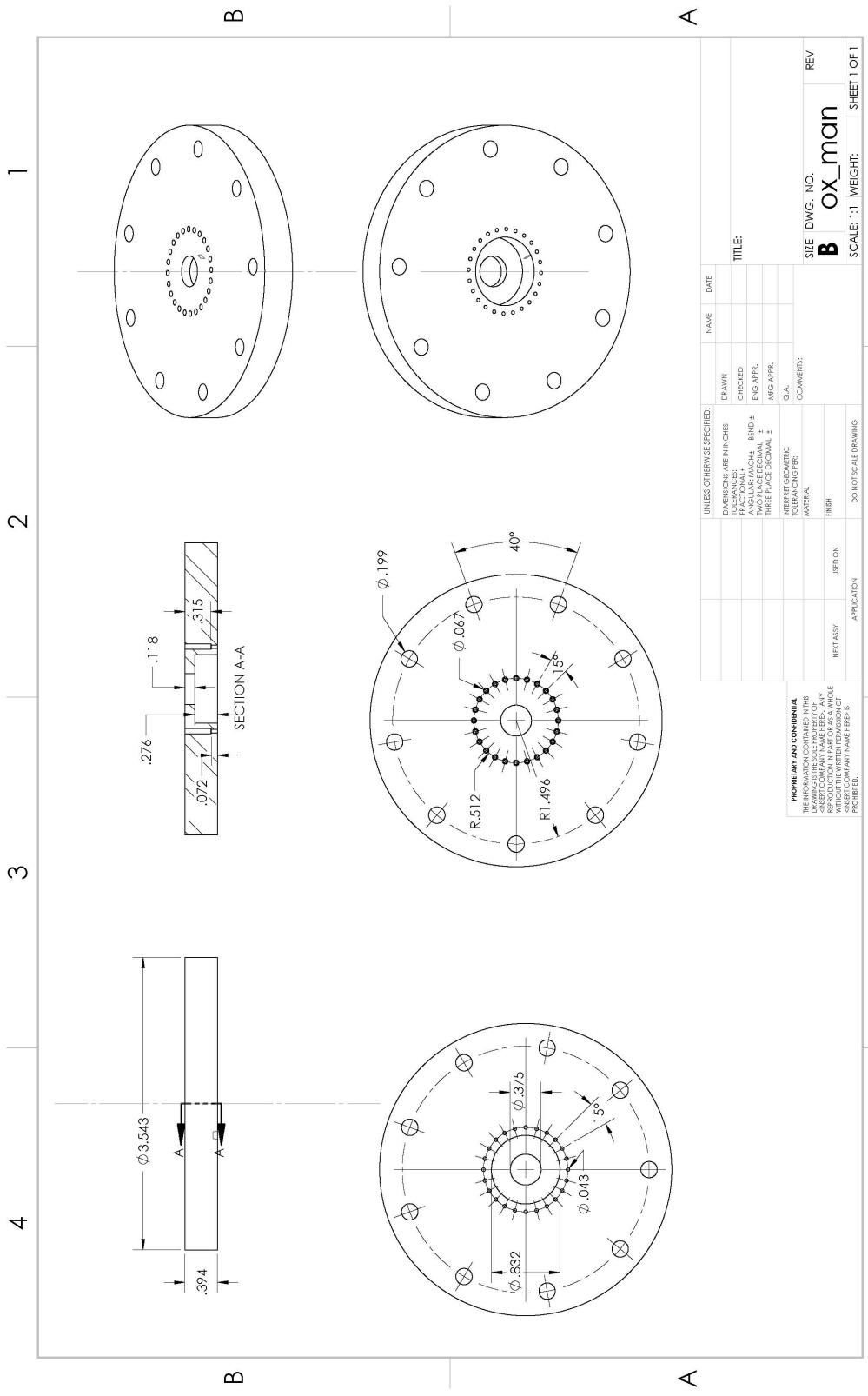

Figure 89. Machine shop drawing for the oxidizer manifold

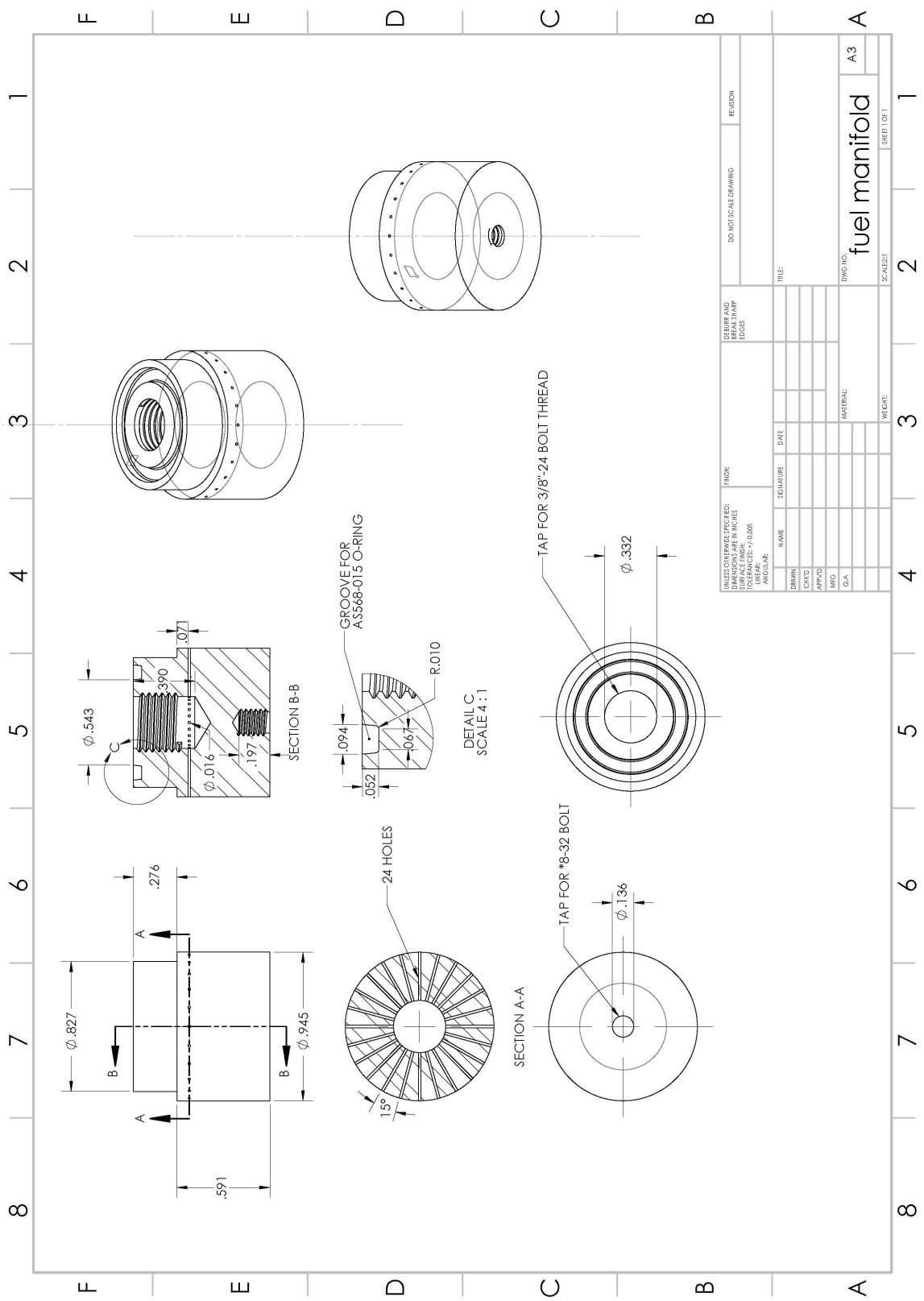

Figure 90. Machine shop drawing for the fuel manifold

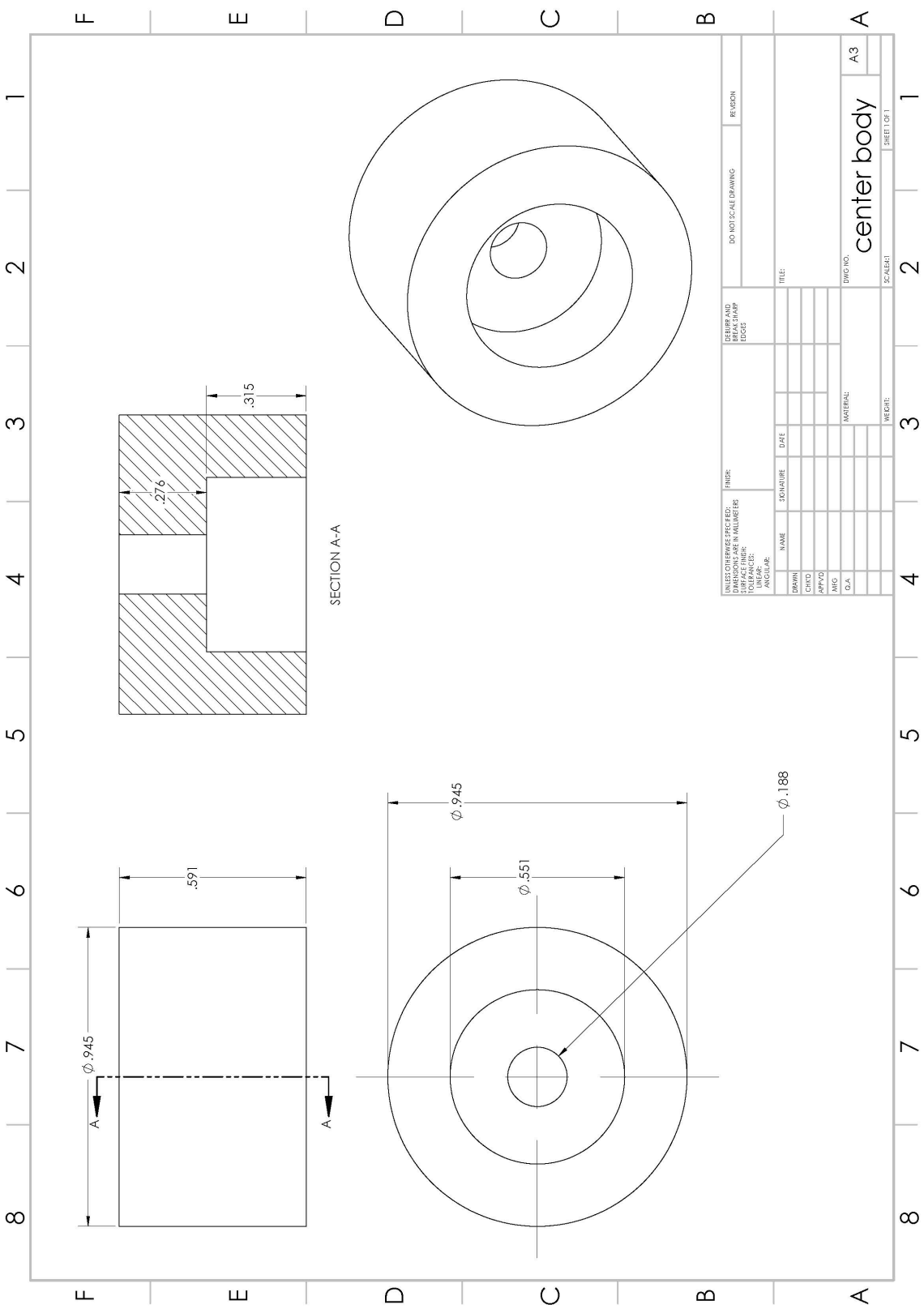

Figure 91. Machine shop drawing for the centerbody

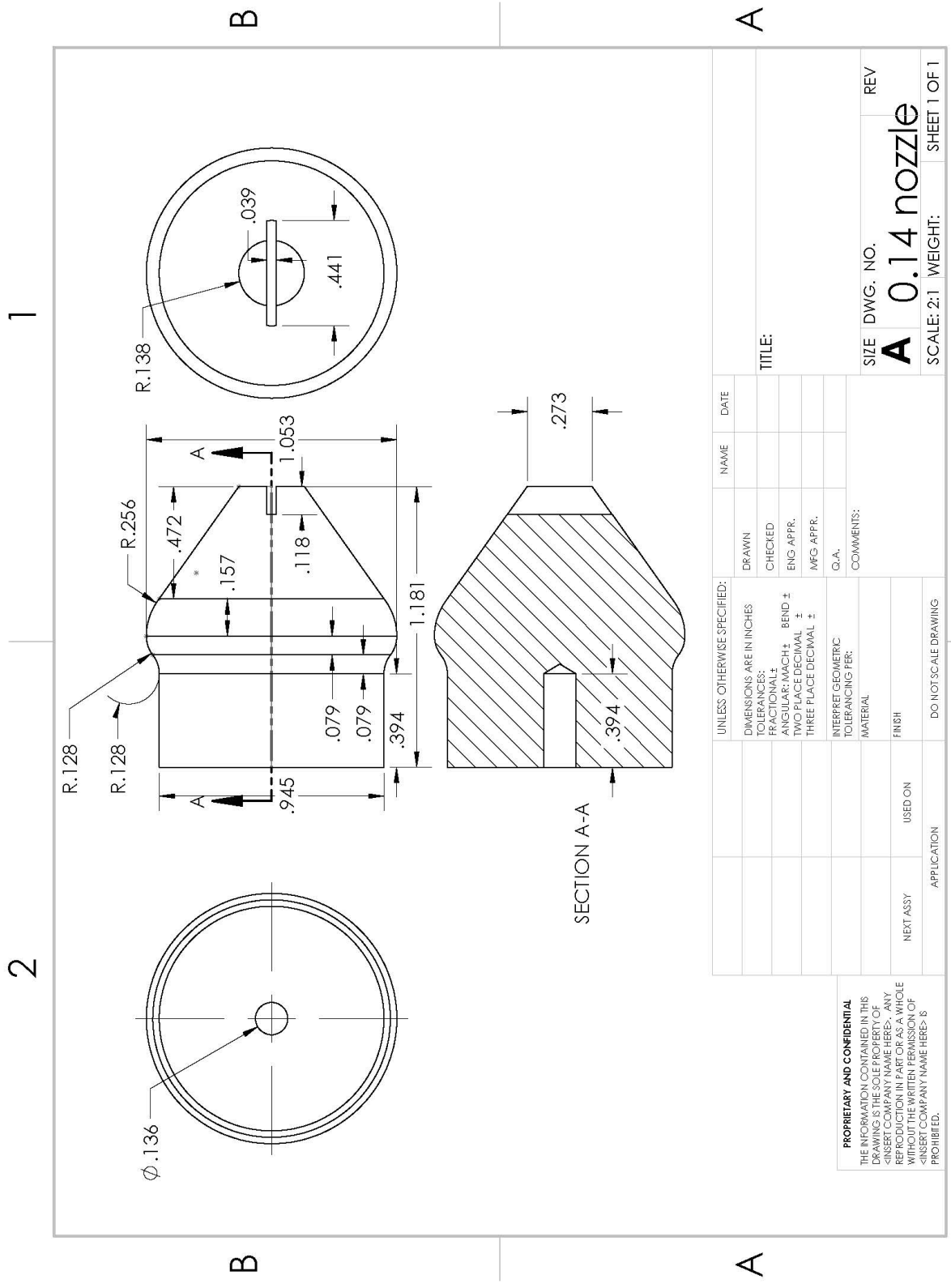

Figure 92. Machine shop drawing for the $\epsilon = 0.14$ nozzle

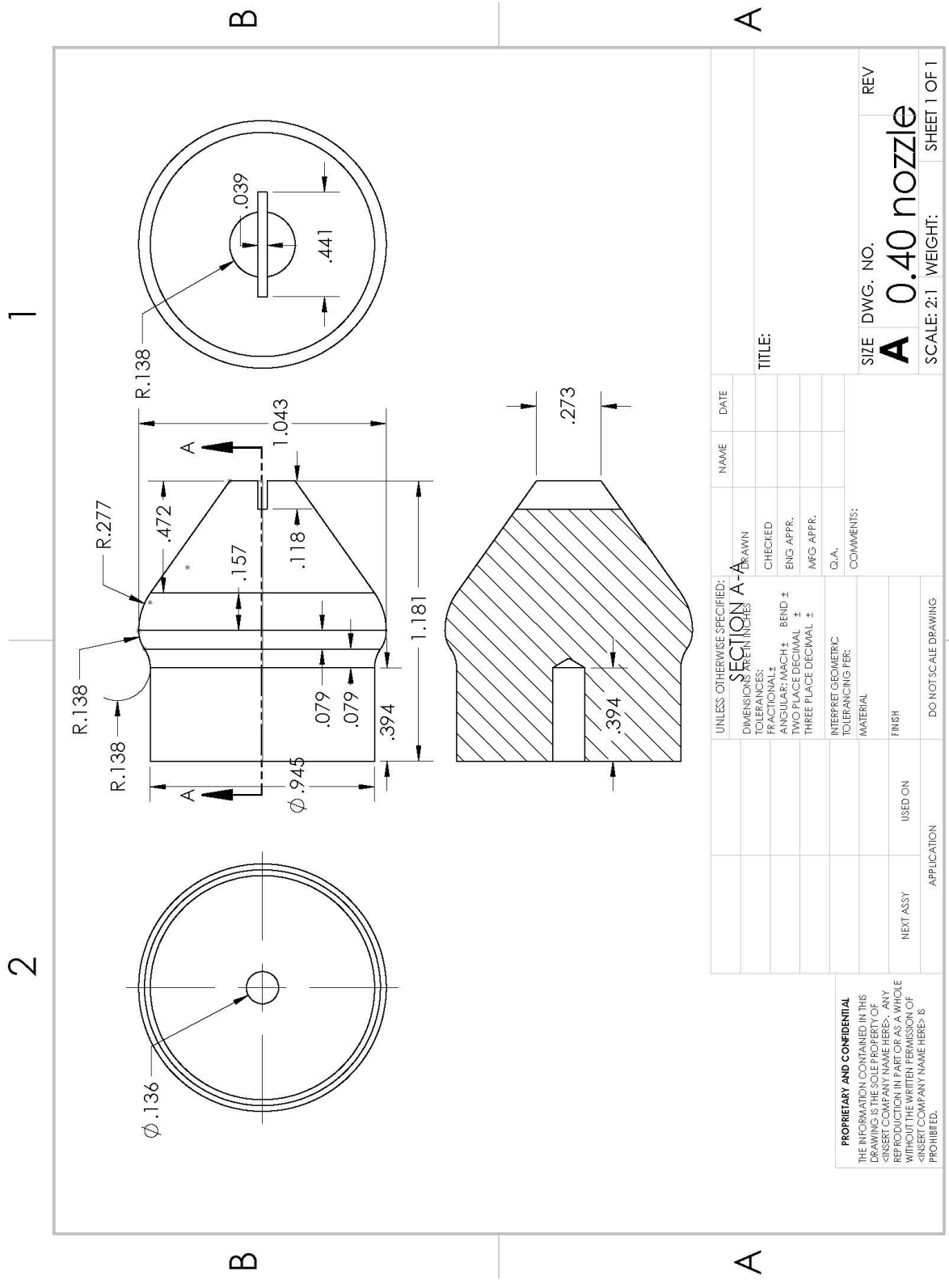

Figure 93. Machine shop drawing for the $\epsilon = 0.40$ nozzle

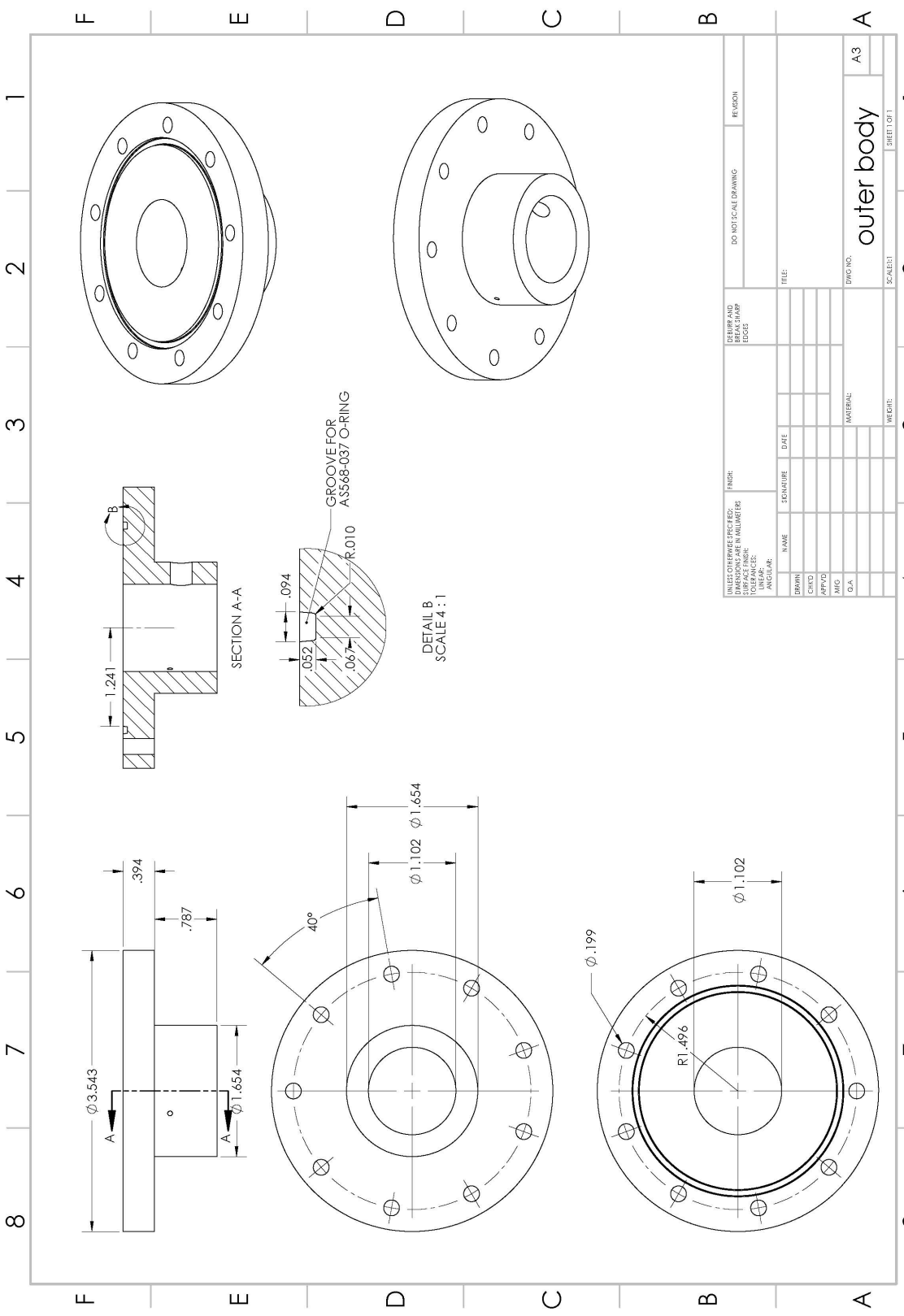

Figure 94. Machine shop drawing for the outer body

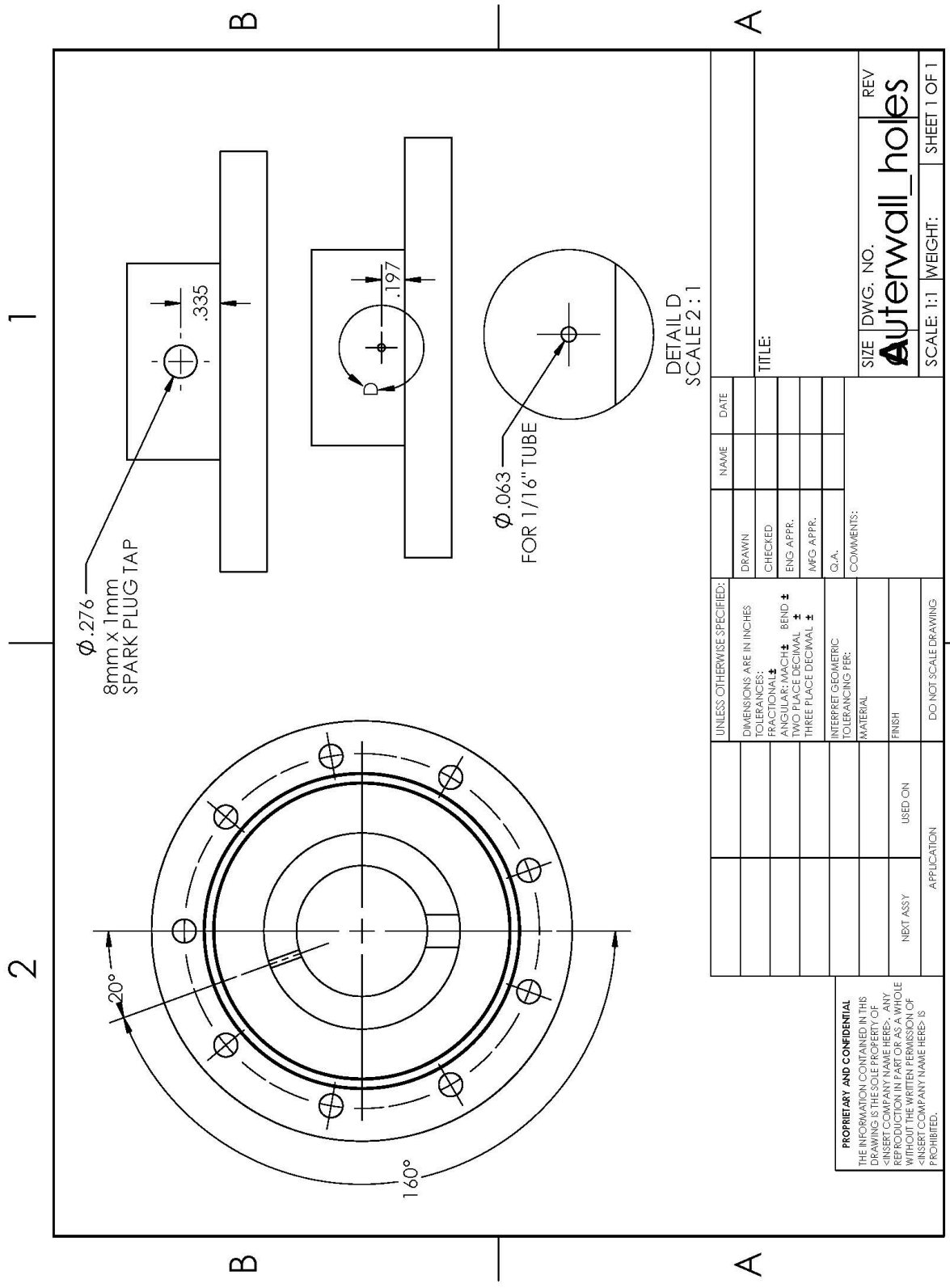

Figure 95. Machine shop drawing for the spark plug and CTAP ports on the outer body

Bibliography

1. Lu, F. K. and Braun, E. M., "Rotating Detonation Wave Propulsion: Experimental Challenges, Modeling, and Engine Concepts," *Journal of Propulsion and Power*, Vol. 30, No. 5, 2014, pp. 1125–1142.

2. Turns, S. R., *An Introduction to Combustion: Concepts and Applications*, WCB/McGraw-Hill, Boston, 3rd ed., 2012.

3. Bussing, T. R. A. and Pappas, G., "An Introduction to Pulse Detonation Engines," *32nd Aerospace Sciences Meeting and Exhibit*, AIAA 1994-0263, Reno, Nevada, 1994.

4. Fotia, M. L., Kaemming, T. A., Hoke, J. L., and Schauer, F. R., "Study of the Experimental Performance of a Rotating Detonation Engine with Nozzled Exhaust Flow," *53rd AIAA Aerospace Sciences Meeting*, AIAA 2015-0631, Kissimmee, Florida, 2015.

5. Bykovskii, F. A., Zhdan, S. A., and Vedernikov, E. F., "Continuous Spin Detonations," *Doklady Physics*, Vol. 22, No. 6, 2006, pp. 1204–1216.

6. Yu, K. H., Burr, J. R., and Fievisohn, R. T., "Fundamental Structure of High-Speed Reacting Flows: Detonation," Tech. rep., Air Force Research Laboratory, AF Office Of Scientific Research (AFOSR), Arlington, Virginia, 2016.

7. Duvall, J., Chacon, F., Harvey, C., and Gamba, M., "Study of the Effects of Various Injection Geometries on the Operation of a Rotating Detonation Engine," *2018 AIAA Aerospace Sciences Meeting*, AIAA 2018-0631, Kissimmee, Florida, 2018.

8. Kudo, Y., Nagura, Y., Kasahara, J., Sasamoto, Y., and Matsuo, A., "Oblique Detonation Waves Stabilized in Rectangular-Cross-Section Bent Tubes," *Proceedings of the Combustion Institute*, Vol. 33, No. 2, 2011, pp. 2319–2326.

9. Paxson, D. E., "Examination of Wave Speed in Rotating Detonation Engines Using Simplified Computational Fluid Dynamics," *2018 AIAA Aerospace Sciences Meeting*, AIAA 2018-1883, Kissimmee, Florida, 2018.

10. Lee, J. H. S., *The Detonation Phenomenon*, Cambridge University Press, Cambridge, 2008.

11. Wintenberger, E. and Shepherd, J. E., "Thermodynamic Cycle Analysis for Propagating Detonations," *Journal of Propulsion and Power*, Vol. 22, No. 3, 2006, pp. 694–698.

12. Vutthivithayarak, R., Braun, E. M., and Lu, F. K., "Examination of the Various Cycles for Pulse Detonation Engines," *47th AIAA/ASME/SAE/ASEE Joint Propulsion Conference & Exhibit*, Joint Propulsion Conferences, AIAA 2011-6064, San Diego, California, 2011.

13. Tieszen, S. R., Sherman, M. P., Benedick, W. B., and Berman, M., "Detonability of H2-Air-Diluent Mixtures," Tech. rep., 1987.

14. Meyers, J. M., Lu, F. K., and Wilson, D. R., "Performance Enhancements on a Pulsed Detonation Rocket Engine," *41st Aerospace Sciences Meeting and Exhibit*, AIAA 2003-1173, Reno, Nevada, 2003.

15. Babbie, C. A., King, P. I., Hoke, J. L., and Schauer, F. R., "Effect of Elevated Mixture Pressure and Equivalence Ratio on Hydrogen-Air Detonation Cell Size," *54th AIAA Aerospace Sciences Meeting*, AIAA 2016-0442, San Diego, California, 2016.

16. Kaneshige, M. J. and Shepherd, J. E., "Detonation Database," Tech. rep., Graduate Aeronautical Laboratories California Institute of Technology, Pasadena, CA, 1997.

17. Ciccarelli, G., Ginsburg, T., Boccio, J., Economos, C., Finfrock, C., Gerlach, L., Sato, K., and Kinoshita, M., "High-Temperature Hydrogen-Air-Steam Detonation Experiments in the BNL Small-Scale Development Apparatus," Tech. rep., Brookhaven National Laboratory & Nuclear Power Engineering Corporation, Upton, NY, 1994.

18. Mitrofanov, V. V. and Soloukhin, R. I., "The Diffraction of Multifront Detonation Waves," *Soviet Physics Doklady*, Vol. 9, 6 1965, pp. 1055.

19. Fernelius, M. H., Sell, B. C., Moosmann, K. J., Andrus, I. Q., Hoke, J. L., and Schauer, F. R., "Characterization of a Premixed Laboratory Scale Pulsed Detonation Burner," *2018 AIAA Aerospace Sciences Meeting*, AIAA 2018-1610, Kissimmee, Florida, 2018.

20. Sutton, G. P. and Biblarz, O., *Rocket Propulsion Elements*, John Wiley & Sons, Incorporated, Somerset, 9th ed., 2017.

21. Thomas, L. M., Schauer, F. R., Hoke, J. L., and Naples, A. G., "Buildup and Operation of a Rotating Detonation Engine," *49th AIAA Aerospace Sciences Meeting including the New Horizons Forum and Aerospace Exposition*, AIAA 2011-602, Orlando, Florida, 2011.

22. Gaillard, T., Davidenko, D., and Dupoirieux, F., "Numerical Optimisation in Non Reacting Conditions of the Injector Geometry for a Continuous Detonation Wave Rocket Engine," *Acta Astronautica*, Vol. 111, 2015, pp. 334–344.

23. Stevens, C. A., Fotia, M. L., Hoke, J. L., and Schauer, F. R., "Comparison of Transient Response of Pressure Measurement Techniques with Application to Detonation Waves," *53rd AIAA Aerospace Sciences Meeting*, AIAA 2015-1102, Kissimmee, Florida, 2015.

24. Kowalkowski, M., Matsutomi, Y., and Heister, S., "Flame Sensing in Pulsed Combustion Using Ion Probes, Diodes and Visual Indications," *45th AIAA/ASME/SAE/ASEE Joint Propulsion Conference & Exhibit*, AIAA 2009-4945, Denver, Colorado, 2009.

25. Pandiya, N., St. George, A. C., Driscoll, R. B., Anand, V., Malla, B., and Gutmark, E. J., "Efficacy of Acoustics in Determining the Operating Mode of a Rotating Detonation Engine," *54th AIAA Aerospace Sciences Meeting*, AIAA 2016-1649, San Diego, California, 2016.

26. Engineering ToolBox, "Flow Coefficients - Cv - and Formulas for Liquids, Steam and Gases - Online Calculators," https://www.engineeringtoolbox.com/flow-coefficients-d_277.html, 2019.

27. Boller, S. A., Polanka, M. D., Huff, R., Schauer, F. R., Fotia, M. L., and Hoke, J. L., "Experimental Flow Visualization in a Radial Rotating Detonation Engine," *AIAA Scitech 2019 Forum*, AIAA SciTech Forum, AIAA 2019-1253, San Diego, California, 2019.

28. Moffat, R. J., "Describing the uncertainties in experimental results," *Experimental Thermal and Fluid Science*, Vol. 1, No. 1, 1988, pp. 3–17.

29. Wang, W. and Zhang, H., "Laminar Burning Velocities of C2H4/N2O flames: Experimental Study and Its Chemical Kinetics Mechanism," *Combustion and Flame*, Vol. 202, 4 2019, pp. 362–375.

30. Fotia, M. L., Schauer, F. R., and Hoke, J. L., "Experimental Study of Performance Scaling in Rotating Detonation Engines Operated on Hydrogen and Gaseous Hydrocarbon Fuel," *20th AIAA International Space Planes and Hypersonic Systems and Technologies Conference*, AIAA 2015-3626, Glasgow, Scotland, 2015.

31. Druss, R. I., "Low Mass Flow RDE Operating on Gaseous Air and Ethylene for Future Scramjet Integration," Master's Thesis, Air Force Institute of Technology, 2019, pp. 79–114.

32. Chang, P.-H., Leong, W. K., Li, J.-M., Teo, C. J., and Khoo, B. C., "Investigation of Channel Pressure Effect on Rotating Detonation Engine," *AIAA Scitech 2019 Forum*, AIAA 2019-2020, San Diego, California, 2019.

33. Popov, E. L., Samsonov, A. N., Bykovskii, F. A., and Vedernikov, E. F., "MHD Effects in Continuous Spin Detonation," *Doklady Physics*, Vol. 64, No. 2, 2019, pp. 77–79.

34. Falempin, F., "Continuous Detonation Wave Engine," *Advances on Propulsion Technology for High-Speed Aircraft*, Vol. RTO-EN-AVT, No. 8, 2008, pp. 1–9.

35. Bennewitz, J. W., Bigler, B. R., Hargus, W. A., Danczyk, S. A., and Smith, R. D., "Characterization of Detonation Wave Propagation in a Rotating Detonation Rocket Engine using Direct High-Speed Imaging," *2018 Joint Propulsion Conference*, AIAA Propulsion and Energy Forum, American Institute of Aeronautics and Astronautics, 7 2018.

REPORT DOCUMENTATION PAGE

Form Approved
OMB No. 0704–0188

1. REPORT DATE *(DD–MM–YYYY)*	2. REPORT TYPE	3. DATES COVERED *(From — To)*
26-03-2020	Master's Thesis	Oct 2018 — Mar 2020

4. TITLE AND SUBTITLE

Development of a Small Scale Rotating Detonation Engine

5a. CONTRACT NUMBER

5b. GRANT NUMBER

5c. PROGRAM ELEMENT NUMBER

6. AUTHOR(S)

Dechert, Joseph R., Capt

5d. PROJECT NUMBER

5e. TASK NUMBER

5f. WORK UNIT NUMBER

7. PERFORMING ORGANIZATION NAME(S) AND ADDRESS(ES)

Air Force Institute of Technology
Graduate School of Engineering and Management (AFIT/EN)
2950 Hobson Way
WPAFB OH 45433-7765

8. PERFORMING ORGANIZATION REPORT NUMBER

AFIT-ENY-MS-20-M-257

9. SPONSORING / MONITORING AGENCY NAME(S) AND ADDRESS(ES)

Air Force Research Lab Aerospace Directorate
Combustion Branch, Turbine Engine Division
1790 Loop Road North
WPAFB OH 45433-7765

10. SPONSOR/MONITOR'S ACRONYM(S)

AFRL/RQTC

11. SPONSOR/MONITOR'S REPORT NUMBER(S)

AFIT-ENY-MS-20-M-257

12. DISTRIBUTION / AVAILABILITY STATEMENT

DISTRIBUTION STATEMENT A:
APPROVED FOR PUBLIC RELEASE; DISTRIBUTION UNLIMITED.

13. SUPPLEMENTARY NOTES

14. ABSTRACT

The Rotating Detonation Engine (RDE) has been researched extensively in recent years, but the minimum size limits of an RDE have not been well investigated. The goal of this research was to build an RDE small enough to produce a detonation frequency above 20 kHz with a single detonation wave while also reducing the engine's mass flow rate. An engine with these design characteristics would reduce hazards associated with previous RDE testing. This research objective resulted in the design of an RDE with an outer diameter sized at 28 mm using ethylene and nitrous oxide as a fuel and oxidizer. The engine was tested over a range of equivalence ratios between 0.5-1.5 and at mass flow rates of 0.025-0.075 kg/s to characterize its operation. Key design parameters were the injection hole diameter, detonation channel gap, detonation channel length, and detonation channel diameter. Detonation was achieved in an RDE of this scale, which proved operability of an engine with these design characteristics was possible.

15. SUBJECT TERMS

Rotating Detonation Engine, Small Scale, Pressure-Gain Combustion, Detonation Combustion, Detonation Frequency

16. SECURITY CLASSIFICATION OF:			17. LIMITATION OF ABSTRACT	18. NUMBER OF PAGES	19a. NAME OF RESPONSIBLE PERSON
a. REPORT	b. ABSTRACT	c. THIS PAGE			Dr. Fred R. Schauer, AFIT/ENY
U	U	U	UU	164	19b. TELEPHONE NUMBER *(include area code)* (937) 255-6565, x4204; fschauer@afit.edu